POLITECNICO
MILANO 1863

SCUOLA DI INGEGNERIA INDUSTRIALE
E DELL'INFORMAZIONE

Characterisation of Battery Electric Buses by means of a Lumped Parameters Modelling approach

TESI DI LAUREA MAGISTRALE IN
ENERGY ENGINEERING
INGEGNERIA ENERGETICA

Author: **Simone Di Mauro**

Student ID: 940580
Advisor: Riccardo Mereu
Co-advisor: Francesco Davide Sanvito
Academic Year: 2021-22

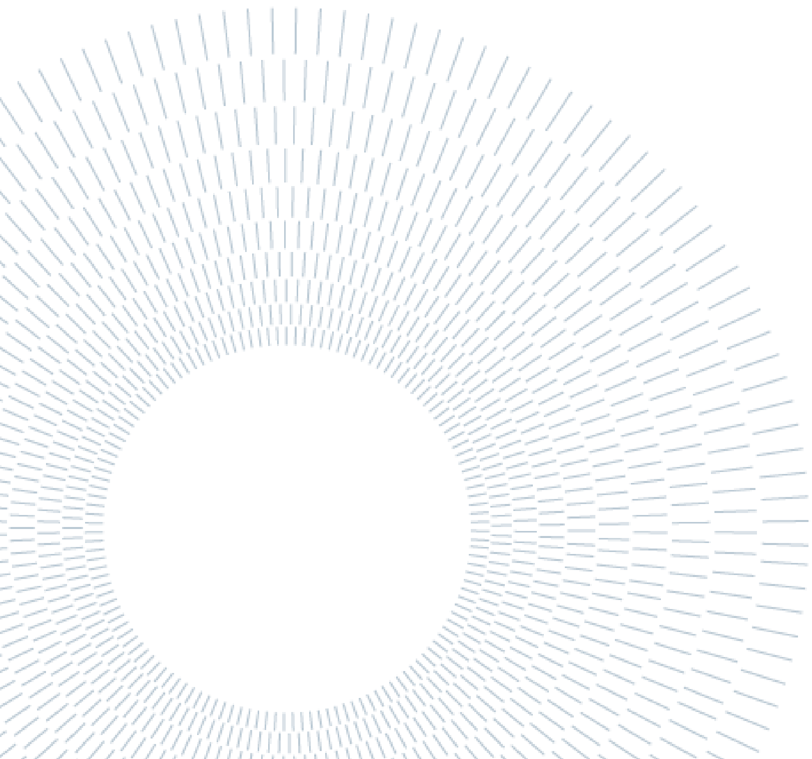

Abstract

Transportation consumes one quarter of world's energy use resulting in one of the most energy intensive sectors in the global economy. Furthermore, the reliance of this segment on fossil fuels makes it account for 37% of the global CO_2 direct emissions coming from the end-use sector. Buses are responsible for 6% of greenhouse gases emissions in the European Union and cleaner solutions in the public transport sector might help curbing the above-mentioned emissions. In this context, many European cities have switched to completely electric buses fleets following transports' decarbonization's direction. This choice raises the need for a precise assessment of buses' energy request to better include them in the cities' energy systems and strategies. The simulation tools for e-buses consumption available in literature lack of detailed definitions of the additional units characterizing their operations. The purpose of this thesis is to extend to electric buses an existing Lumped Parameters' Model (LPM) designed for the estimation of car consumption. The proposed model is enriched with the components buses are equipped with and powertrain, air conditioning unit, battery thermal management system and auxiliaries are the four different blocks composing the model. Among the aspects that the model takes as an input there are the bus dimensions and its components' specifications, the external temperature and the desired comfort one, the geographical and temporal collocation and the driving conditions. The outcome consists in the energy consumption of the analysed bus specific to the travelled route. Validation is performed comparing the output of the tool with the results of another model and percentage error found is lower than 10% for all the tested driving cycles. In the end, the validated model is utilized to simulate an impact analysis on different scenarios changing the input parameters, which results are partially reported here. The total consumption at -10 °C is two times higher than the mild temperature one. Increasing passengers' occupancy at 40 °C reflects in the highest worsening in the consumption compared to mild and cold temperature scenarios. The driving cycles' aggressiveness has a clear correlation with both traction and auxiliaries consumption. Seasonal effects on radiation thermal load as well as the impact of coordinates on the total consumption are negligible.

Keywords: lumped-parameter approach, electric consumption simulation tool, battery electric bus, HVAC, BTMS, auxiliaries

Abstract in italiano

Il trasporto consuma un quarto dell'energia mondiale risultando uno dei settori più energivori dell'economia globale. Inoltre, l'affidamento di questo settore nei combustibili fossili fa sì che renda conto del 37% delle emissioni dirette globali provenienti dall'end-use. Gli autobus sono responsabili del 6% delle emissioni di gas serra nell'Unione Europea e delle soluzioni più pulite nel settore dei trasporti potrebbero aiutare a limitare le sopramenzionate emissioni. In questo senso, molte città europee hanno cambiato le loro flotte di autobus in completamente elettriche seguendo la direzione della decarbonizzazione dei trasporti. Questa scelta solleva la necessità di una precisa definizione della richiesta energetica degli autobus per includerli meglio nei sistemi energetici e nelle strategie delle città. Gli strumenti per la simulazione del consumo degli e-bus disponibili in letteratura mancano di definizioni dettagliate riguardo le unità addizionali che caratterizzano le loro operazioni. Lo scopo di questa tesi è di estendere ai bus elettrici un modello a parametri concentrati (LPM) esistente e progettato per la stima del consumo delle auto. Il modello proposto è arricchito con i componenti con cui i bus sono equipaggiati e la catena cinematica, l'aria condizionata, il sistema di gestione termica della batteria e gli ausiliari sono i quattro blocchi che compongono il modello. Tra gli aspetti che il modello prende in input ci sono le dimensioni del bus e le specifiche dei suoi componenti, la temperatura esterna e quella desiderata di comfort, la collocazione geografica e temporale e le condizioni di guida. L'output consiste nel consumo energetico del bus analizzato, specifico alla strada percorsa. La validazione è svolta comparando l'output dello strumento con i risultati di un altro modello e la percentuale di errore è minore del 10% per tutti i cicli di guida testati. Alla fine, il modello validato viene utilizzato per simulare un'analisi di impatto su diversi scenari cambiando i parametri in ingresso, i cui risultati sono di seguito parzialmente elencati. Il consumo totale a -10 °C è due volte più alto rispetto al caso a temperatura mite. Aumentare il numero dei passeggeri a 40 °C si riflette nel più alto peggioramento nel consumo rispetto ai casi a temperature miti e fredde. L'aggressività dei cicli di guida ha una chiara correlazione sia con il consumo della trazione che degli ausiliari. Gli effetti stagionali sul carico termico di radiazione, così come l'impatto delle coordinate sul consumo totale sono trascurabili.

Parole chiave: approccio a parametri concentrati, strumento per la simulazione di consumo elettrico , autobus elettrici a batteria, HVAC, BTMS, ausiliari

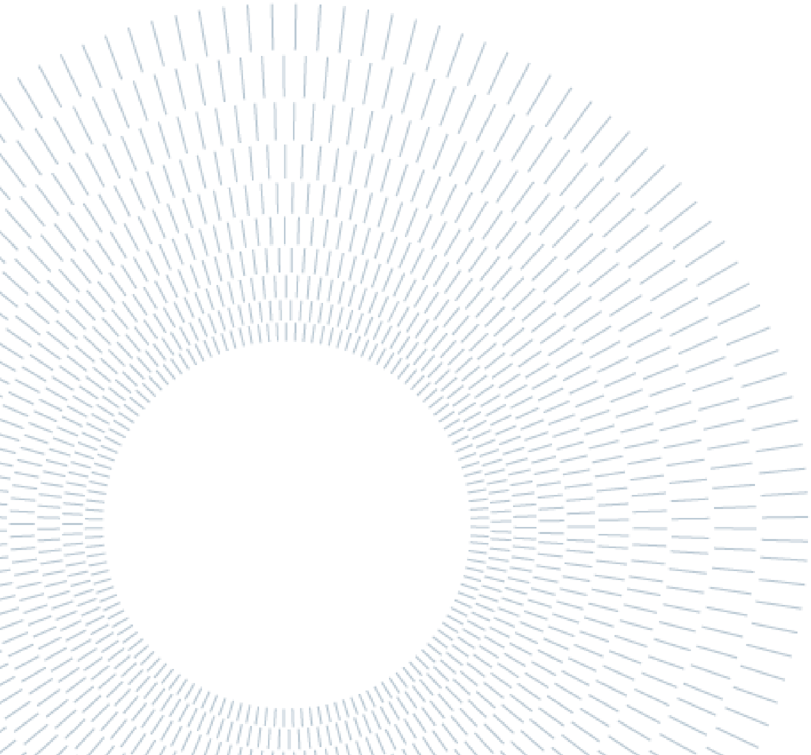

Contents

Abstract .... **iii**

Abstract in italiano .... **iv**

Contents .... **vii**

Introduction **1**

1 Transport sector focus **3**

1.1. Transport sector overview and future scenarios 4

1.2. The importance of public transport: EU case study 9

2 Literature review **13**

2.1. Driving cycles 13

2.2. Vehicle longitudinal dynamics 15

2.3. Powertrain specifications 17

2.4. Additional components 19

2.5. Proposed modelling approach 20

3 Methods and models **23**

3.1. Vehicle specifications 24

3.2. Longitudinal Dynamics 26

3.3. Auxiliaries 31

3.3.1. Electric auxiliaries 31

3.3.2. Hydraulic auxiliaries 33

3.3.3. Pneumatic auxiliaries 35

3.4. Heat and Ventilation Air Conditioning 36

3.4.1. Thermal Loads 40

3.5. Battery thermal management system 47

4 Results **51**

4.1. Validation process 51

4.1.1. Validation on HVAC and BTMS 53
4.1.2. Total consumption validation 54
4.1.3. Total consumption validation for different external conditions .. 56
4.1.4. Infeasibility computation 59
4.2. Scenario and sensitivity analysis 61
4.2.1. External temperature 62
4.2.2. Passengers’ occupancy 65
4.2.3. Comfort temperature 69
4.2.4. Road grade 72
4.2.5. Aggressiveness 75
4.2.6. Auxiliaries consumption composition 78
4.2.7. Geographical and temporal collocation 82
5 Conclusions 91
Acronyms 95
Bibliography 97
List of Figures 101
List of Tables 105

Introduction

Many human activities are responsible for climate change. Among them, the transport sector appears to be one of the most energy-intensive and polluting. This segment entails both freight and passengers' mobility and accounts for almost one quarter of world's energy use [1].

The reliance on conventional fuels for this sector is massive, with transportation asking for the 61.5% of all the oil used each year [1]. This aspect results in a very much polluting behaviour with transports responsible for 37% of the CO_2 direct emissions coming from the end-use sectors [2].

Cities are particularly affected by transports-related pollution. Since the world is experiencing an urbanization process, and cities will have an even more central role in future, adopting cleaner solutions in this sector is crucial.

Public transports contribute to the 6% of the greenhouse gases (GHG) emissions for the European Union [3] and choosing battery electric buses (BEB), could be an interesting way to reduce them. The effectiveness of this choice depends on the origin of the electricity used as a "fuel". Nevertheless, the employment of BEB using electricity coming from a clean energy mix could truly help a city to reduce its pollution.

In fact, the European Union's Net Zero Emissions goal for 2050 relies also on the switching of public transports from existing diesel fleets to BEBs and new alternative powertrains. The public transit company of Milan has recently announced the Full Electric plan for 2030 which aims at providing its service with a complete electric buses fleet.

At the same time, these plans require an improvement on BEBs' driving range, battery sizing and smarter charging strategies and infrastructures. The supporting ground for all these objectives is a more precise definition of BEBs operations and consumption in different working conditions.

The purpose of this study is the development and testing of a Lumped Parameters' Model (LPM) capable of simulating the consumption of the BEBs. The model takes into account the consumption coming from the powertrain of the vehicle, the air conditioning and ventilation unit, the battery thermal management system and the auxiliary components. This model is essential to perform an analysis on the electricity request coming from public transport's buses and how they can be included in the Energy Systems Model of a city. A second phase of the work consists in validating the proposed model in different driving conditions and testing also different levels of external temperature and passengers' occupancy. The validated LPM is then used to perform an impact analysis for its input parameters. The results collected in the impact analyses allow to understand the different specific weight of each of the contribution to the final consumption and how they are affected by input variables like external temperature and passengers' occupancy.

The structure of the thesis is composed of five different chapters addressing the different parts of the work. Chapter 1 provides an overview on the transport sector, focusing its attention on public transport buses in Europe. Chapter 2 dives into the existing literature on the predictive models for electric buses consumption. Chapter 3 provides details on how the modelling is conducted and the thoughts behind all the methodological choices undertaken. Chapter 4 presents the validation phase of the proposed model and the impact analysis of all the possible varying inputs for the tool. In the end, chapter 5 draws some conclusions and underlines possible further improvements and future utilization for the LPM developed.

1 Transport sector focus

Means of transport are essential in the current global economy and being able to move across the planet is crucial for the development of ideas and the trading of goods and services.

The mobility of passengers and freight is a fundamental building block of the modern society, which is more interconnected than ever and seems to be willing to push this concept even further. Transports' importance has grown consistently and now contribute to one fourth of the global energy consumption. Unfortunately, this growth has not been free of charge, since transports' energy consumption produces dangerous side effects: pollution coming from fossil fuels combustion. In facts, transports still strongly rely on traditional fuels and there is the urge for a huge shift of paradigm in this sector economy, moving towards cleaner solutions and diminishing its impact on the global energy consumption.

Climate change has become a critical issue, and today it is fundamental to consider new paths of development which increase the global population's wealth without sacrificing Earth's resources.

Besides, emerging challenges and circumstances have already encouraged extensive adjustments in the history of transportation. During the late 19th century, the spread of horses as main means of transportation led to an enormous problem in urban areas with manure disposal. The difficulties risen in the management of this issue pushed rapidly towards one of the last breakthrough inventions of the modern times: the internal combustion engine. In this way, cars took the place of horses and manure problems were overcome. With a similar urgency, climate change is advancing as a communal global concern to policy makers, to the scientific community and to citizens. The electrification of the transport sector may be a possible step towards a more sustainable direction.

The purpose of this chapter is to underline how much transports impact the energy sector globally and in Europe, what are its perspective and what is the role of public transports, in particular buses.

1.1. Transport sector overview and future scenarios

According to the World Energy Outlook 2021 [2], the transport sector is responsible for 37% of CO_2 direct emissions from the end-use sectors. Moreover, this parameter is experiencing the fastest growth between all of these segments. This is the result of two parallel trends that are negatively influencing the quantity of CO_2 emitted:

- The increase in the demand for cars in countries with none zero pledges policies in place
- The limited diffusion of alternative fuels

The International Energy Agency (IEA) have developed different scenarios in order to forecast and monitor the future level of CO_2 emissions according to the actions and policies announced or in place worldwide.

- The Net Zero Emissions (NZE): “A scenario which sets out a narrow but achievable pathway for the global energy sector to achieve net zero CO_2 emissions by 2050. It doesn’t rely on emissions reductions from outside the energy sector to achieve its goals.” [4]
- The Stated Policies Scenario (STEPS): “A scenario which reflects current policy settings based on a sector-by-sector assessment of the specific policies that are in place, as well as those that have been announced by governments around the world.”
- The Announced Pledges Scenario (APS): “A scenario which assumes that all climate commitments made by governments around the world, including Nationally Determined Contributions (NDCs) and longer-term net zero targets, will be met in full and on time.”

By 2030 the emissions for the transport sector are expected to define a 2.5 Gt gap [2] between the APS and NZE scenarios’ ambition for 2030. Three-quarters of this difference is due to the different objectives in the road transport subsector for these two scenarios. The road transport is nowadays responsible for 15% of all the energy-related CO_2 emissions in the world and this percentage is expected to grow in the APS prevision because of a global increase in the demand for it. On the contrary, an NZE scenario would require a reduction in its current level by one quarter and this explains the big difference in the goals for 2030. This opposite trend can be seen in Figure 1 that reports also the behaviour of the other contributions to transportation sector.

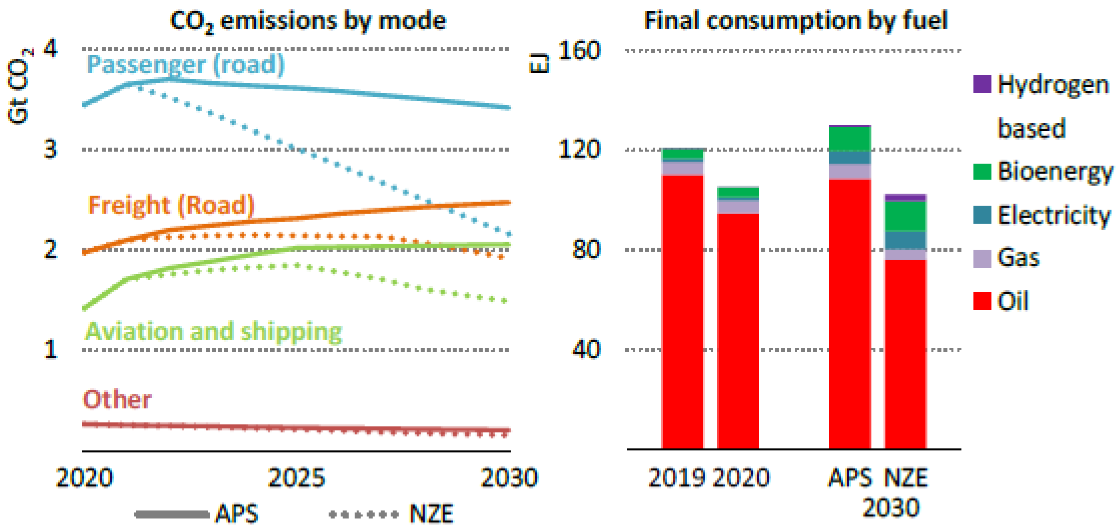

Figure 1: CO2 emissions trend by mode and final consumption prevision by fuel. [2]

The reduction in the CO_2 emissions should be fostered by a reduction in the final consumption of the sector compared to the pre-pandemic levels, in order to reach the NZE objectives for 2030. This decrease in the consumption should also be accompanied by a decrease in the fossil fuels' reliance in favor of electricity, bioenergy and hydrogen as energy sources.

In the Announced Pledges Scenario, an increase in the consumption is experienced while still keeping the same level of oil dependency and filling the energy gap with the alternative fuels spreading.

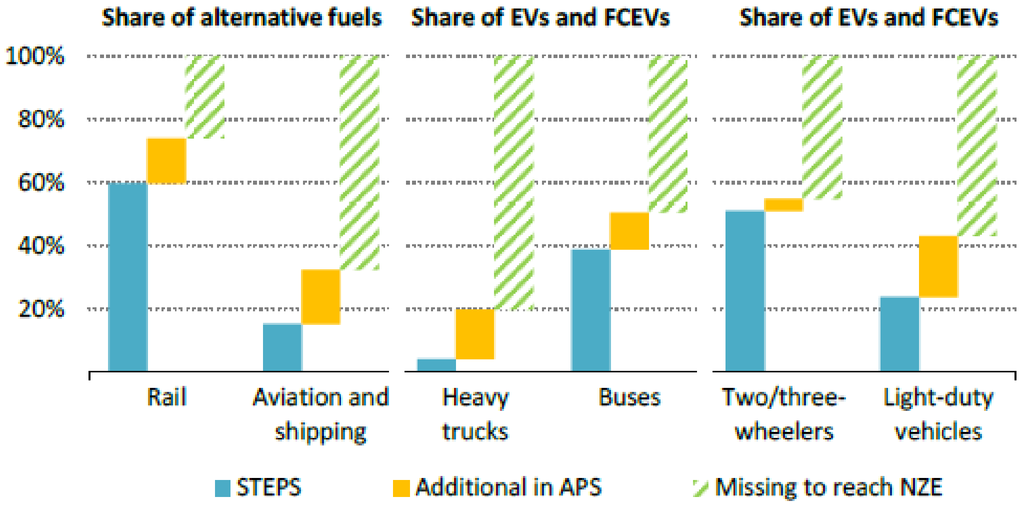

Figure 2: Share of alternative fuels and electric vehicles in the subsectors. [2]

Figure 2 shows how far the 2030 objectives for the means of transportation of the single scenarios are. The rail, aviation and shipping are monitored in terms of the share of the alternative fuels, including electricity. It can be seen that, according to the STEPS, rail will reach 60% of the NZE objectives just respecting the actual policies in place. On the other hand, aviation and shipping are very difficult sectors to be electrified or to perform a switch towards cleaner fuels. This happens because of the highly energy-consuming nature of their service and step forwards the reliability of the alternative technological solutions available need to be done. The distance from the NZE objective is very deep and it will be arduously reached.

The other four stacked columns report the shares of electric and fuel cell vehicles in the global market in terms of sales. The heavy trucks are the ones where the lower share will be reached according to the STEPS, because there is a lack of infrastructures and limited driving range. In the two/three-wheelers market there is a very little distance between the STEPS and APS, and the electric vehicles in this field are already widespread also in emerging economies because of their lower additional cost compared to cars. In addition to that, less charge is required for their operations. More than 50% of the share in the light duty vehicles market must be covered by Net Zero Emissions policies, and this goal will be achieved by introducing pledges on the conventionally fueled cars in the emerging economies.

In the end, the condition of the bus market, which is the reference field for this thesis, is analyzed. The STEPS prevision underlines that 40% of the NZE shares' objective in this market will be achieved just by putting in place the stated policies. The bus market is easier to be controlled by national governments since many of the companies providing collective transport services are partially or totally owned by public entities. Despite the rising number of electric buses in public transport fleets, issues related to the optimization of the charging infrastructure and scheduling as the provision of clean electricity are still debated.

Overall, there is still room for improvement in the electric bus sector, and their diffusion and competitiveness can be enhanced, investing in the public transports' sector and helping to overcome the above-mentioned problems.

This kind of growth in the alternative mobility market requires important investments in order to reach the stated goals, and that is the reason why money allocation is part of the policies' objectives for the scenarios.

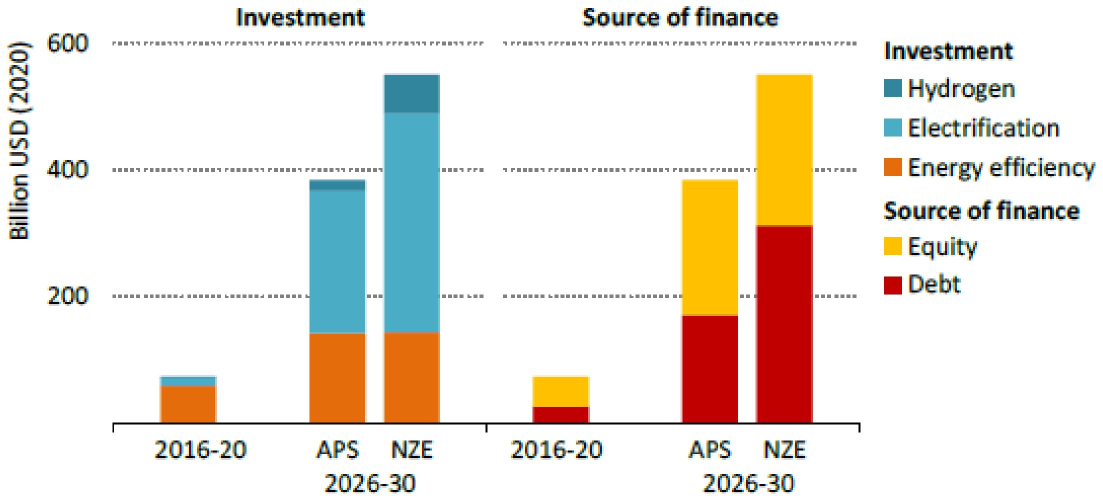

Figure 3: Share of investments in transports in 2016-2020 period and future scenarios. [2]

Figure 3 shows that the money invested between 2016 and 2020 were insufficient to support the transition outlined by the projections of IEA. The investments, in this period, were mainly made in the energy efficiency field of the more widespread solutions, instead of pushing towards newer solutions like hydrogen and electrification of the transport sector. The past four-year-period levels should increase by fifteen times almost reaching 400 billion dollars in the period 2026-2030 in the APS. The prevision for the NZE scenario is even higher, with 570 billion dollars investments for the same years. The future scenarios are equal in terms of energy efficiency investments, but the difference emerges when looking at electrification and hydrogen ones, with NZE particularly betting on these technologies as key solutions for transition. Investments in the hydrogen sector were almost null in the past few years while play an important role in the definition of NZE total investments.

Concerning the source of the investments, contributions of both low interest debt and risk capital equity should grow and finance the acquisition of zero-emission vehicles and foster the creation of new charging infrastructures. The debt percentage should grow even more in the APS and NZE scenarios, and particularly in the second one should even become preponderant on the overall amount of money invested. Government and state-owned companies have an important task in this transition, since they have to make the newborn sectors appealing for investors, and push for innovation in their countries to reach clear targets in the domestic transports market.

The investments will help to improve the cost-competitiveness of the electric vehicles in the future, and the desired reduction of the CO_2 emissions in the road transport sector will be achieved as in Figure 4.

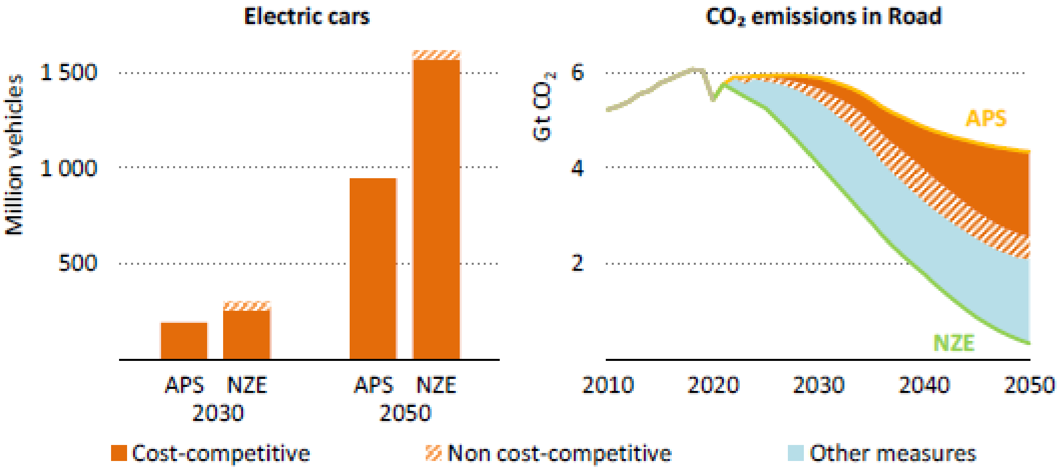

Figure 4: Cost-competitiveness in the road transport sector. [2]

In the APS and NZE scenarios investments are so massive in the electric cars sector that the vast majority of the millions of electric cars in the market will be cost-competitive. This means that choosing an electric car over a traditional one will be as much convenient thanks to similar total cost of ownership that includes running costs like fuel and maintenance.

The Net Zero Emissions goal will be reached with the contribution of the spread of electric vehicles, both cost and non-cost competitive (in a minor share) and also relying on other measures. This very last contribution contains different solution:

- Increasing energy efficiency of the vehicles
- Switch to other alternative fuels like bioenergy and hydrogen-based ones
- Avoiding part of the demand

1.2. The importance of public transport: EU case study

Between the measures that allows to reduce the gap between the APS and the NZE CO_2 emissions levels for 2050, is listed: "avoiding part of the demand". This statement allows to infer considerations about what this could mean in the transport sector analysing the actual situation of the European Union.

The transport sector energy consumption in the EU for the 2000-2019 period had some ups and downs due to the 2008 world economic crisis but has always kept being above the 250 Mtoe threshold [5]. There is a peak for 2007 at 290 Mtoe and the lowest point is reached in 2000 with 262 Mtoe. This means that the economy affects this data but it exists a solid core of the total consumption which is hard to avoid without important behavioural and structural changes. The values are extracted from Figure 5.

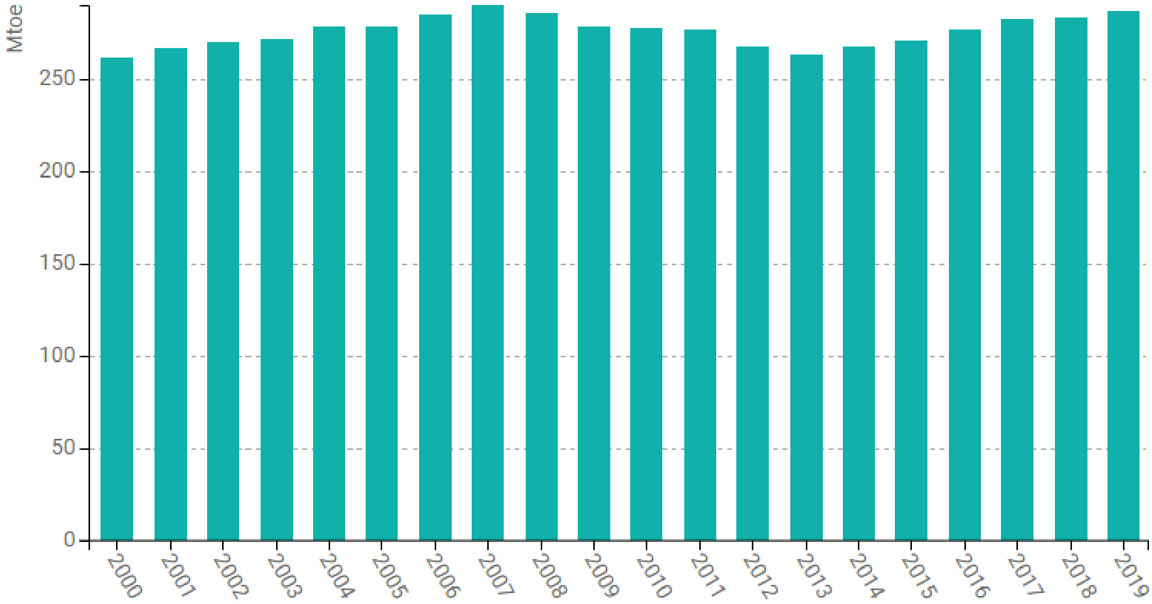

Figure 5: Transport sector overall energy consumption trend in the EU. [5]

The most impactful type of transport is once again road transport and its prevalence on the other solutions is very impressive. It can be also noticed that in the 20-years-span the contribution of the other transports is almost constant independently on the level of consumption, while the increase of total consumption always corresponds to an increase of road transport one. This means that when the economy is wealthier the additional amount of transport of freight or passengers is taken care by the on-wheel subsector. In 2007 road transport accounted for 270 Mtoe over the total as reported in Figure 6.

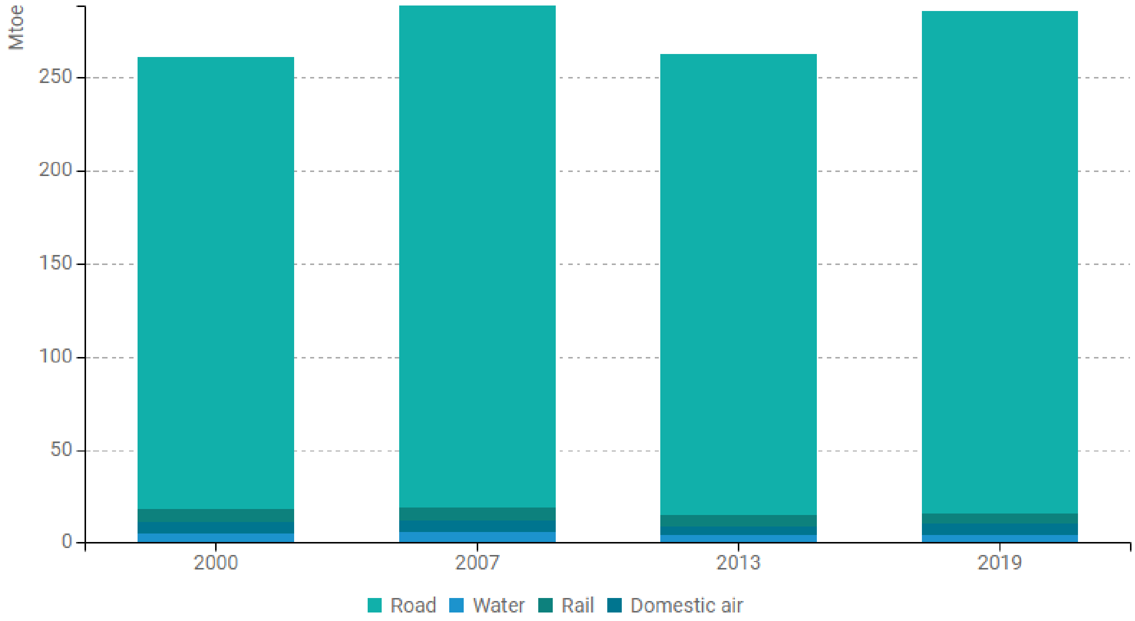

Figure 6: : Transport sector energy consumption by mode in the EU. [5]

Road transport deals with passengers and freight, and both of these contributions has grown between 2000 and 2019. Focusing the attention on the passengers' portion it can be noticed how the increase was composed in the graph of Figure 7.

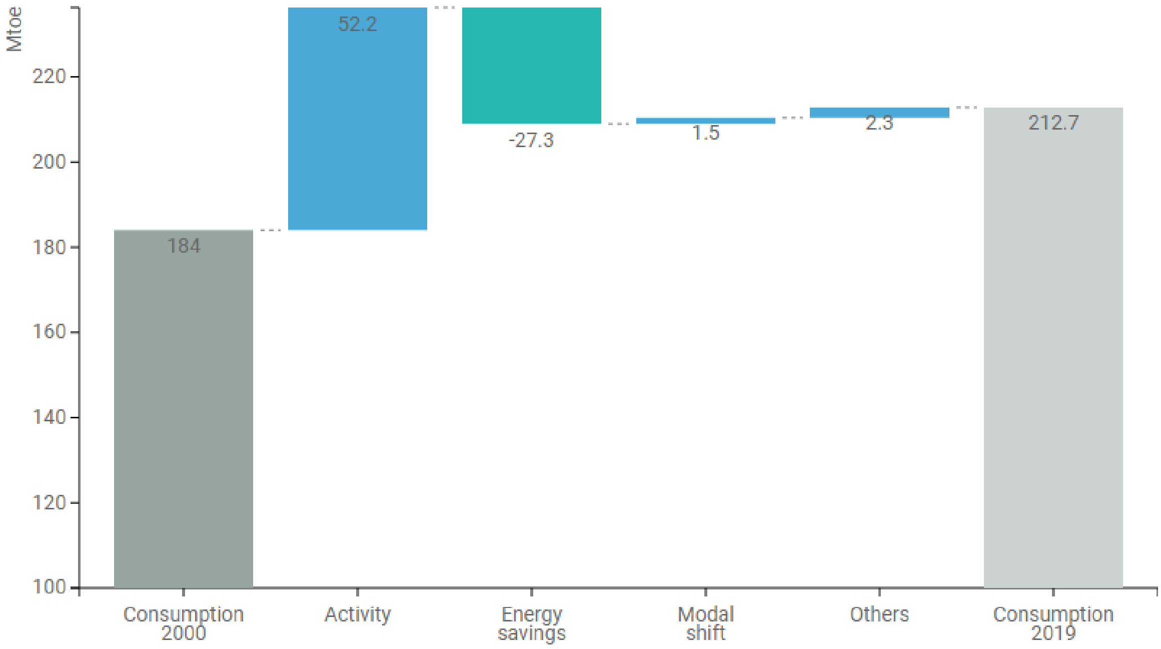

Figure 7: Passengers' transport consumption growth composition. [5]

The switch from 184 Mtoe to 212.7 Mtoe is the resultant of four different contributions: an increase because of higher traffic, a gain due to energy savings and two negligible increases because of modal shift and other behavioral and operational effects. The modal shift accounted for only 1.5 Mtoe and depended on the decrease by 1.1% of the public transport share over the total traffic.

This is where the starting point of these considerations comes in. A little shift in the direction of cars over public transport resulted in a 1.5 Mtoe change. Moreover, the share of public transport in 2019 for EU is 19% and this tells that a behavioral shift in this sense could really help diminishing the impact of road transport and consequently the one of transports in the overall energy consumption of the EU.

In facts, public transport and, in this case, buses, have a very low impact if compared on their intensities of consumption over the passengers' kilometers provided. In Figure 8 the main source of transport for passengers' mobility consumptions are confronted on the basis of the service that they grant.

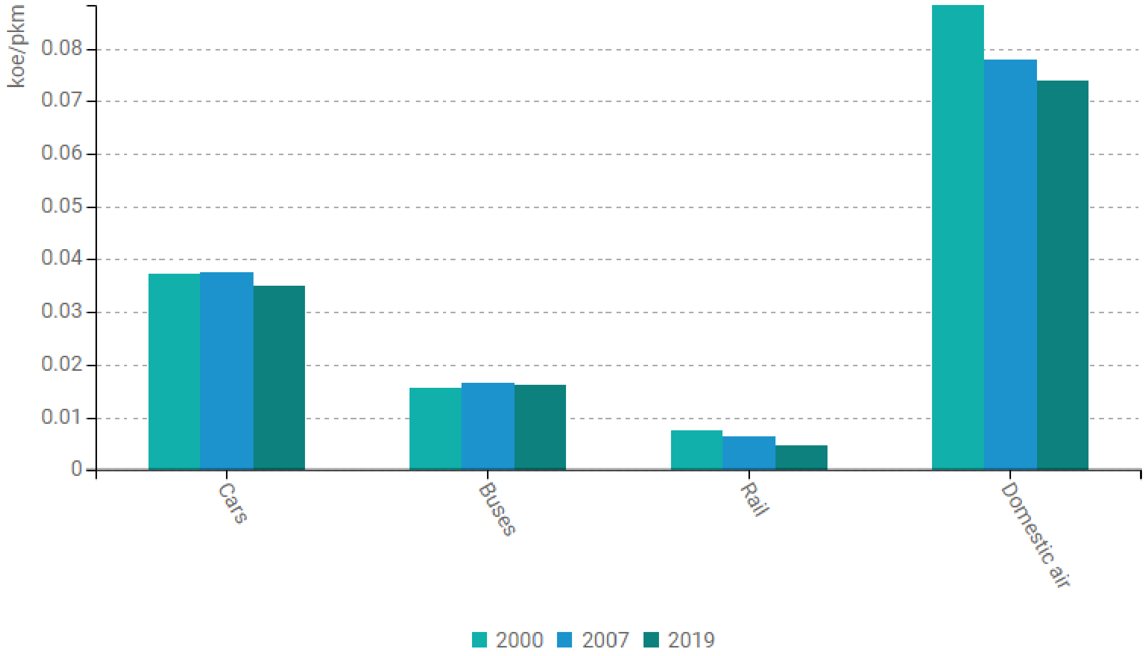

Figure 8: Intensity of consumption for the main transports. [5]

The most intensive consumption in terms of kilos of oil equivalent (koe) over the total passengers' kilometers (pkm) is the domestic air travelling that, even if it is decreasing, have still the highest specific consumption.

Rail is the best solution with the lowest index while cars have an intensity of consumption between 0.03 and 0.04 koe/pkm, that if compared to the buses' one is more than double.

Buses proves to be a good intermediate solution between cars and rail especially for urban surface where the infrastructures for trains and its working conditions are difficult to be developed. Buses are a good alternative for surface travelling instead of cars because they allow a higher number of passengers' kilometers for the same amount of energy since they move more passengers contemporaneously.

For this reason, moving towards public transport and particularly buses instead of cars could be a way to avoid part of the total energy consumption for road transport. Moreover, these buses should be electric in order to keep up with the ongoing electrification of the transport sector.

In this context the development of a tool able to assess the electric buses consumption would fit in well with both a reduction in the overall energy consumption in the sector and the shift of the actual public transports' fleet to electric.

2 Literature review

This section introduces an overview on the state of the art in bus energy consumption's simulations, focusing on the modelling approaches and the different levels of detail available in literature to define the objective of the developed model.

2.1. Driving cycles

In order to test the performance of the vehicles in terms of fuel or energy consumption and pollutants emitted, a series of data linking timestep with speed, acceleration and road grade were collected: the driving cycles.

These datasets are exploited to show how different driving conditions can impact on the fuel economy or on the polluting footprint of the analysed vehicle. This practice was started for cars but found its application also in larger vehicles like buses for public transport and many driving cycles were designed by researchers starting from existing bus routes. The different sequence of speed and acceleration over time can lead to the simulation of very different driving conditions like the fragmented route with low speed and frequent accelerations of the city buses and the high-speed constant extra-urban paths.

The datasets can be found on websites like DieselNet [6] or the one from the National Renewables Energy Laboratory of the U.S. government [7] and a list of the most frequently utilised ones is here reported together with their more recognisable initials:

- New York Bus-NYB
- Manhattan Bus-MB
- New York Composite-NYC
- Orange County Transit Authority-OCTA
- Central Business District-CBD
- City Suburban Heavy Vehicle-CSHV
- Braunschweig-BRAU
- Urban Dynamometer Driving Schedule-UDDS

Figure 9 and Figure 10 show two different driving cycles above-mentioned, where the vehicle speed trend, expressed in miles per hour, is reported with a 1 second resolution timestep.

From these images, took from NREL website, it can be seen that driving conditions can be very different and hence testing the same vehicle on two different driving cycle can lead to clearly distinguishable results in terms of consumption.

BRAU is characterised by frequent stop and very much intensive acceleration, while UDDS has long idle time and slighter variation in velocity.

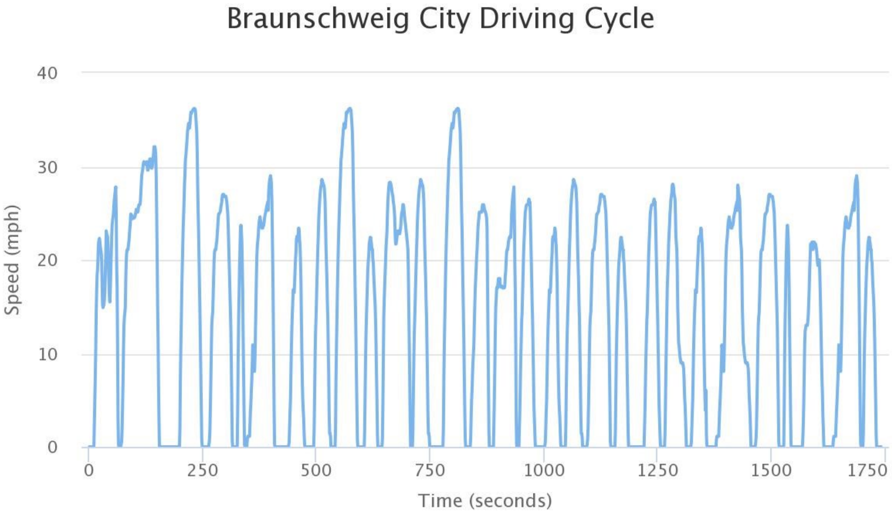

Figure 9: BRAU driving cycle. [7]

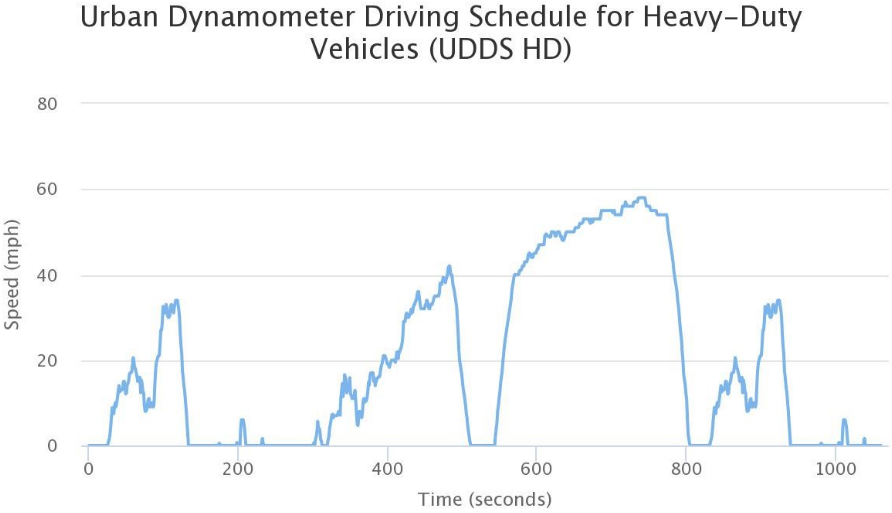

Figure 10: UDDS driving cycle. [7]

2.2. Vehicle longitudinal dynamics

The first step of each type of vehicle testing is the definition of the longitudinal dynamics, in other words, understand the way the bus, in this case, interacts with road and air.

The determination of the energy consumption of the traction unit is common to all vehicle testing tools and, for buses, the most common approach is the backward facing one as can be found in H. Basma et al. [8], O. Hjelkrem et al. [9] and D. Goehlich et al. [10]. In this type of modelling the traction force is the resultant of four different contribution applied to the vehicle, accounting for the effect of: drag friction, rolling friction, gravity, and inertia.

Driving cycles provide the speed and sometimes the acceleration of the vehicle coupled with each timestep within the bus route's profile. If acceleration is not present it can be derived approximately by dividing by the interval of time the velocity variations between two consecutive instants.

Road grade influences the determination of some of the forces composing the traction force but is generally not specified in the papers.

Vehicle characteristics like weight and dimensions are always made explicit, in the form of curb weight, or total weight, and reporting the frontal area and the length of the bus.

This part of the analysis allows to understand the propulsion power to be furnished to the wheels and the power to be possibly recovered from braking by accounting for the traction power for each timestep.

The main data required for an exhaustive definition of longitudinal dynamics are listed in Table 1 and don't vary that much between different models. In the table is shown whether the data is specified or not in the different paper analysed for the literature review of this thesis. Many of these studies utilized the data without explicitly reporting them in the text, while vehicle weight was clearly defined for all of them. Also bus dimensions, in the form of its length and frontal area is reported in the majority of the papers, since they strongly influence the vehicle longitudinal dynamics. The most complete paper was the reference study for this thesis, Basma et al. [8], where all the parameters except for motor inertia were reported.

Table 1: Longitudinal dynamics parameters.

	Basma et al. (2020) [8]	Hjelkrem et al. (2021) [9]	Czogalla et al. (2019) [11]	Basma et al. (2021) [12]	Kammu-aug-Iue et al. (2019) [13]	Goehlich et al. (2018) [10]	Mallon et al. (2017) [14]	El-Taweel (2021) [15]	Basma et al. (2019) [16]
Vehicle weight	✓	✓	✓	✓	✓	✓	✓	✓	✓
Wheel radius	✓			✓	✓		✓		
Wheel inertia	✓			✓			✓		
Motor inertia							✓		
Drag coefficient	✓	✓		✓	✓		✓	✓	
Rolling coefficient	✓	✓		✓	✓		✓	✓	
Bus dimensions	✓	✓	✓	✓	✓		✓	✓	
Passenger weight	✓	✓	✓			✓			

2.3. Powertrain specifications

After vehicle longitudinal dynamics has been taken care of, attention shifts towards the way power is managed and transported in the bus's traction unit: the powertrain. In the automotive industry exist several types of powertrains, like the internal combustion engine powertrain or the plug-in hybrid ones. During this thesis the focus was on the full electric powertrain that characterizes the battery electric bus (BEB), since it is the most diffused in the alternative transport sector.

Analysing a BEB raises the need to describe transmission system, electric motor characteristics, battery specifications, and regenerative braking operations. In facts, part of the braking's kinetic energy is prevented from wasting by producing electricity to charge the battery.

Transmission system can't be neglected since it is fundamental for the mechanical functioning of the vehicle and allows to understand how the motor is coupled with the wheels in terms of torque and angular speed.

Electric machines are described by some graphs, called characteristic curves, that provide the existing working points of the motor/generator, coupling torques with angular speeds and their efficiencies. Alternatively, the efficiencies can be defined for each partial load over the maximum power of the machine. Most of the papers do not report motor specific behaviour, except for Basma et al. [8], Goehlich et al. [10] and Basma et al. [16].

The level of detail of the battery modelling determines part of the tool's complexity since its charging and discharging process affect the accuracy of the prevision. Most of the papers do not analyse these operations, not taking into consideration also the current intensity, relying only on a generic battery efficiency, like Hjelkrem et al. [9].

Concerning the brake energy recovery there can be a regenerative efficiency for braking, or the quantity of recoverable energy can be determined approximately as in Czogalla et al. [11].

In Table 2 the powertrain's needed data for different modelling are defined.

Table 2: Powertrain specifications.

	Basma et al. (2020) [8]	**Hjelkrem et al. (2021)** [9]	**Czogalla et al. (2019)** [11]	**Basma et al. (2021)** [12]	**Kammu-aug-Iue et al. (2019)** [13]	**Goehlich et al. (2018)** [10]	**Mallon et al. (2017)** [14]	**El-Taweel (2021)** [15]	**Basma et al. (2019)** [16]
Electric motor efficiency	✓				✓	✓			✓
Regenerative brake efficiency		✓						✓	
Motor maximum power			✓			✓			✓
Motor maximum torque	✓		✓	✓		✓			✓
Motor angular speed	✓					✓			✓
Drivetrain efficiency	✓	✓		✓	✓		✓		
Final drive ratio	✓		✓	✓			✓		
Gear ratio	✓		✓	✓			✓		
Battery size	✓	✓				✓			✓
Battery efficiency		✓							
Charge efficiency							✓		
Discharge efficiency							✓	✓	
Battery open circuit voltage	✓		✓	✓			✓		✓
Initial SOC	✓			✓		✓			✓
Cell electric resistance	✓			✓			✓		✓
Battery overall cells	✓						✓		✓

2.4. Additional components

The definition of the other units concurring to the final consumption of the bus plays a major role in determining the researched accuracy of a developed predictive tool. The main units consuming energy during bus operations regards the climatization and ventilation tasks, carried out by the Heat Ventilation Air Conditioning unit; the preservation of battery integrity by thermally managing it, through the Battery Thermal Management System and the fulfilment of the additional functionalities a bus requires thanks to the auxiliaries components.

The consumption of these three units impacts strongly on the overall prediction, especially in the more extreme weather conditions, that can lead HVAC and BTMS to very important request to the battery. Despite this fact, the preponderant part of the models for bus's energy consumption decide to miss the detail of these additional components and assign to all of them, or to a part of them a fixed power requirement.

For example, Czogalla et al. [11] reports an "accessory" power, which contains also HVAC and is set to 5 kW. The same happens also for Kammuang-Iue et al. [13], where this number is 6 kW, and it is equal also for the diesel bus analysed.

In the Goehlich et al. [10] paper instead, two scenarios are analysed where once the sum of the additional components is set to 24 kW and the other time to 8 kW.

Both Mallon et al. [14] and El-Taweel et al. [15] assume an overall auxiliaries' components power of 3 kW.

Hjelkrem et al. [9] has a mixed approach since HVAC requirement is approximately calculated, relying on the temperature difference between the cabin and the exterior, while auxiliaries' one is fixed to 2 kW.

The only papers that provide some specifications on the consumption coming from HVAC, BTMS and auxiliaries splitting them up and not considering them as fixed are the one from H. Basma. The most impactful of these components results to be the HVAC unit although neither of these papers allows to precisely understand how the definition of the thermal loads affecting the bus cabin was carried on. Moreover, no detail on the functioning of the air conditioning cycle and its working conditions were reported.

BTMS was not explicitly mentioned in none of the papers apart from Basma ones and Goehlich et al [10], but it is probably contained in the very broad definition of auxiliaries' consumption that is reported in the other papers. In H. Basma et al. [8] its average power request is shown but there are no calculations proving how it was determined.

2.5. Proposed modelling approach

The model is developed with a specific purpose: provision of BEB's consumption taking into account the relative energy use of other vehicle components.

In facts, HVAC, BTMS and all the auxiliaries are included in the model and their requests are accounted and monitored throughout the driving cycles. Moreover, it is thought in order to simulate different scenarios in terms of external temperature, comfort temperature, passengers' occupancy, driving conditions, temporal and geographical collocation, and vehicles' characteristics. These possibilities are granted thanks to a higher level of complexity than the average one found in literature, with the goal of providing a complete model with multiple switchable input variables. The precision in the definition of additional components, accompanied with the chance to change the input variables in this wide manner, are certainly the missing piece of the puzzle of what is found in literature. These modelling decisions allows for sure a broader assessment of the bus as an energy system and how it interacts with the exterior.

The model is written in Python language, it is open source, not monetizable and aims to be the starting point for analysing different kind of bus's powertrain, different driving cycles and different from Li-Ion battery packs. Moreover, its structure gives the possibility to switch off part of the overall consumption and assess for only part of it.

Like all the reviewed models, a backward facing approach is chosen for the longitudinal dynamics' analysis, both for its intuitiveness and for the sake of simplicity. The approach for HVAC's consumption determination is the Heat Balance Method, a lumped parameter approach borrowed by already existing thermal models for cars and trucks [17], [18]. This allows to have an overview on how different loads affect HVAC consumption. Taking the external temperature, the desired comfort temperature and the radiation parameters (time of the day, day and location) as inputs, it gives back heating or cooling requirements for each timestep. BTMS unit is considered as an additional consumption for the HVAC and setting as a goal the final temperature of the battery surface. Auxiliaries are not set as a constant power request as in most of the literature, instead, their step-by-step consumption for each of the components is assessed.

In conclusion, the model can be applied to provide a precise BEB’s consumption in the public transport sector and how it is entailed in the overall energy system of a city.

3 Methods and models

In this chapter is presented an overview of the BEB's (Battery Electric Bus's) consumption model developed in Python language. The goal of the modeling process is to assess the specific electrical request coming from the four consuming macro-units: Powertrain, Auxiliaries, Heating and Ventilation Air Conditioning (HVAC) and the Battery Thermal Management System (BTMS). The designing process aims at providing a single tool capable of analyzing different consumption scenarios varying the model's input. The main advantage of this model is the ability to compute punctual electrical consumption for each unit without the need to combine it with already existing software such as Advisor for longitudinal dynamics or Dymola for heat pump precise definition.

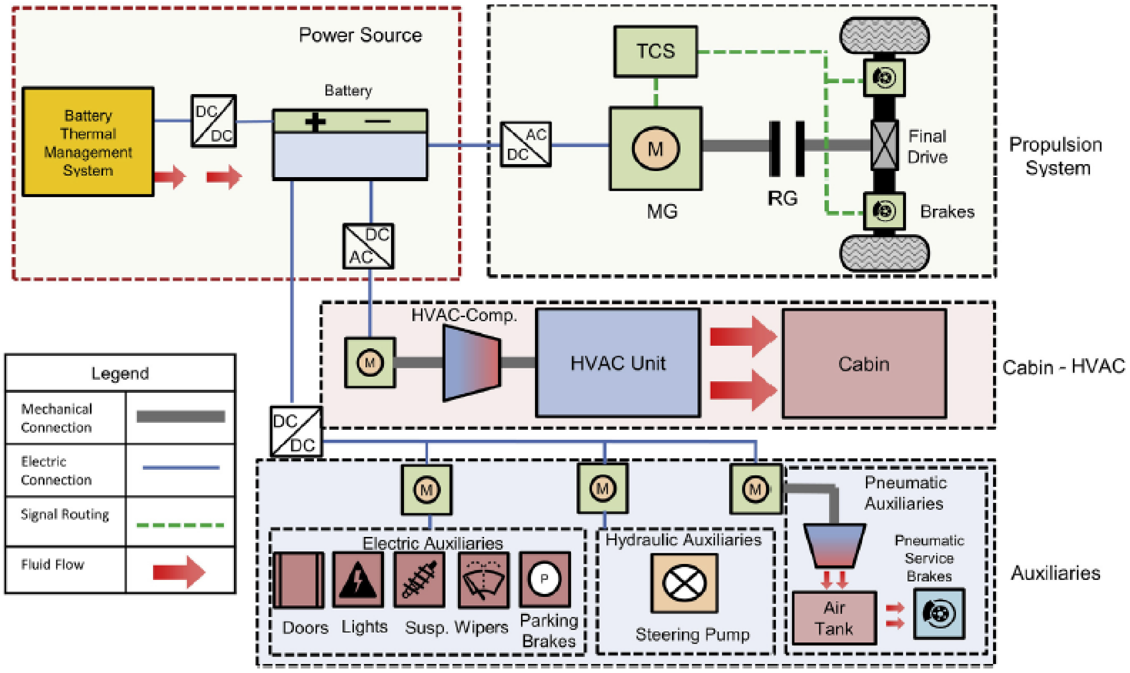
Power Source
Battery
Battery Thermal Management System
DC DC
AC DC
DC AC
TCS
M
MG
RG
Final Drive
Brakes
Propulsion System
HVAC-Comp.
HVAC Unit
Cabin
Cabin - HVAC
Legend
Mechanical Connection
Electric Connection
Signal Routing
Fluid Flow
DC DC
Electric Auxiliaries
Doors
Lights
Susp.
Wipers
Parking Brakes
Hydraulic Auxiliaries
Steering Pump
Pneumatic Auxiliaries
Pneumatic Service Brakes
Air Tank
Auxiliaries

Figure 11: E-bus's units schematization. [8]

3.1. Vehicle specifications

The geometry of the bus as well as its materials' characteristics are important in the definition of the power requested to the battery by the main consumers in the BEB.

The vehicle in exam is a 12-m bus typically operating in the public transport sector, although the tool allows to change bus dimensions analysing different kind of buses. The height and width are respectively equal to 3.3 m and 2.5 m, having a frontal area of 8.25 m^2 [19].

Figure 12: Reference public transport bus. [19]

Vehicles' envelope is thought as composed by two types of materials: one devoted to vehicle body and one to windows, and each side of the bus is considered as fractionally covered by the two of them as reported in Table 3.

Table 3: Surfaces composition.

	Doors	No doors	Floor	Roof	Back	Front
VB	0.4	0.5	1	1	0.75	0.4
W	0.6	0.5	0	0	0.25	0.6

The different areas of the bus are obtained by multiplying the area of a side by its compositional fractions. For example, the vehicle body area of the frontal area is equal to 0.4 multiplied by 8.25 m^2.

Vehicle body's material and windows characteristics used in further dissertation are reported in Table 4.

- Thermal conductivity K
- Density ρ
- Transmissivity τ
- Absorptivity α
- Specific heat c
- Surface thickness λ

Table 4: Materials' properties. [17]

	K [W/mK]	ϱ [kg/m³]	τ [-]	α [-]	c [J/kgK]	λ [mm]
VB	0.2	1500	0	0.4	1000	10
W	1.05	2500	0.5	0.3	840	3

Another important aspect influencing mainly vehicle's longitudinal dynamics is the overall weight of the bus. This is a varying parameter since passengers' load depends on the actual presence of occupants on the bus n_p but is also characterized by some fixed contributions: glider mass g, battery pack mass b and the rotational masses J_w and J_m. Overall weight formula is made explicit in Equation 1 [14] and all the needed parameters [8] are in Table 5. For example, for a 30 passengers' occupancy scenario vehicle mass is 19105.5 kg.

$$m_v = n_p * m_p + g + b + 4 * J_w * (\frac{1}{r_w})^2 + J_m * (\frac{fd * gr}{r_w})^2 \tag{1}$$

Table 5: Vehicle overall weight definition's parameters. [8], [14]

variable	value	u.o.m.
Passenger mass	68	kg/p
Glider mass	11600	kg
Battery mass	4200	kg
Wheel inertia	20.52	kg*m²
Motor inertia	0.277	kg*m²
Wheel's radius	0.48	m
Final drive ratio	5	-
Gear ratio	5.5	-

3.2. Longitudinal Dynamics

A precise definition of power flows involving the electric machine is of key importance to fully understand operations of this rear-wheel driven bus.

The electric machine is reversible working either as a motor to allow traction and as a generator to recover energy from braking, on the basis of the longitudinal dynamics' assessment.

Forces participating in traction power definition are set through a backward facing approach since dynamic data are known from the driving cycle and inertial force is determined from vehicle mass and acceleration [14].

Four different forces are considered to reach instantaneous traction power:

- Drag power that accounts for air resistance to bus movement
$$P_{drag} = 0.5 * \rho_{air} * A_{front} * c_d * v^2 \tag{2}$$

- Rolling power where the resistance of wheels to rotation is taken into account
$$P_{roll} = m_v * g * c_r * \cos(\theta) * v \tag{3}$$

- Body power that is due to gravity
$$P_{body} = m_v * g * \sin(\theta) * v \tag{4}$$

- Inertial power that is inherent with bus movement
$$P_{inertial} = m_v * a * v \tag{5}$$

The traction power for each timestep is then obtained by:

$$P_{res} = P_{drag} + P_{roll} + P_{body} \tag{6}$$

$$P_{trac} = P_{res} + P_{inertial} \tag{7}$$

The operating conditions of the electric machine, torque and angular velocity, are determined starting from vehicle velocity and traction power as follows [14]:

$$T_{em} = \frac{P_{trac} * r_w}{v * fd * gr * \eta_{dt}} \tag{8}$$

$$\omega_{em} = \frac{v}{r_w * fd * gr} \tag{9}$$

The electric machine's torque is expressed in Nm while the angular velocity in rad/s but since efficiency maps for motor/generator are generally in rpm a simple conversion is performed:

$$rpm_{em} = \frac{\omega_{em} * 60}{2\pi} \tag{10}$$

Some parameters need to be fixed in order to complete the electric machine description: the maximum torque is set to 1000 Nm [8] and the maximum power angular velocity to 1500 rpm, from a typical AC induction motor [20], with similar characteristics. The maximum power for the motor is equal to 157 kW, derived from the machine parameters defined:

$$P_{MAX} = T_{MAX} * \omega_{MAX\ POWER} \tag{11}$$

Efficiency is coupled with the fractional load as in [21] but:

- electric machine is considered having exact same performance between generator and motor behaviour
- efficiency values are taken from an efficiency map that already includes inverter efficiency [8]
- the link between efficiencies' range and partial load for this motor is taken from a precedent version of the tool working with battery electric cars [22]. The maximum efficiency is linked with a fractional load between 0.1 and 0.2, hence 0.91 efficiency is assigned to this range

The way ratio is calculated differs from positive and negative traction as shown later and determines an efficiency table made like Table 6:

Table 6: Electric machine' efficiencies.

Ratio range	efficiency
[0;0.02]	0.7
(0.02;0.04]	0.73
(0.04;0.06]	0.79
(0.06;0.08]	0.85
(0.08;0.1]	0.88
(0.1;0.2]	0.91
(0.2;0.4]	0.88
(0.4;0.6]	0.85
(0.6;0.8]	0.82
(0.8;1]	0.79
>1	0.73

The traction power derived from Equation 7 can either be null, positive or negative:

If P_{trac} is equal to 0, no request is delivered from the electric machine to the battery.

If the overall traction power is positive, then the actual request to the motor is higher because of a drivetrain efficiency set to 0.95 [8]:

$$P_{out} = \frac{P_{trac}}{\eta_{dt}} \tag{12}$$

This actual power is divided by the maximum power to obtain ratio and consequently the motor efficiency from Table 6:

$$ratio = \frac{P_{out}}{P_{MAX}} \tag{13}$$

$$\eta_{motor} = f(ratio)$$

Then the request from positive traction to the battery is:

$$P_{motor} = \frac{P_{out}}{\eta_{motor}} \tag{14}$$

If the power request to the battery is higher than the maximum power, then the cycle is considered unfeasible since motor can't supply it to the vehicle.

Braking moments within the driving cycle are accompanied by a negative traction power and since the electric machine is equipped to work as a generator, part of that power is recoverable and can recharge the battery.

The portion of recoverable braking power is half of the total [11] and needs to be multiplied by the drivetrain efficiency to grasp what is the actual power reaching the machine working as a generator.

$$P_{brake} = -\frac{P_{trac}}{2} \tag{15}$$

$$P_{brake\_out} = P_{brake} * \eta_{dt} \tag{16}$$

The determination of the final energy who is going to charge the battery pass through intermediate variable definition and different paths based on their values. First, if the angular velocity of the generator is lower than the maximum power angular velocity of 1500 rpm, then the maximum torque of the generator T_{gm} is equal to the maximum torque available T_{max}.

If this is not true than the auxiliary variable torque power max T_{pm} is defined. The maximum torque of the generator is then calculated as in Equation 17.

$$\begin{cases} T_{pm} = \frac{P_{MAX}}{\omega_{gen}} \\ T_{gm} = T_{MAX}, \quad if\ T_{pm} \geq T_{MAX} \\ T_{gm} = T_{pm}, \quad if\ T_{pm} < T_{MAX} \end{cases} \tag{17}$$

Once the maximum torque is defined, the maximum power that can be produced from the generator is another needed piece of information derived as:

$$P_{gm} = T_{gm} * \omega_{gen} \tag{18}$$

The regenerative power recoverable from braking is dependent on the level of charge of the battery, the so-called state of charge, whose maximum value is fixed to 0.8 [8]. If the SOC value is equal or higher than the SOC maximum, then the regenerative power P_{regen} is null.

Instead, if the level is lower, the ratio of power is found in two different ways with the maximum generator power P_{gm} value as discriminator as follows:

$$\begin{cases} ratio = \frac{P_{gm}}{P_{MAX}}, & if\ P_{brake\_out} \geq P_{gm} \\ ratio = \frac{P_{brake\_out}}{P_{MAX}}, & if\ P_{brake\_out} < P_{gm} \end{cases} \tag{19}$$

The generator efficiency is found as motor's one consulting Table 6 and the regenerative power and energy are then obtained by:

$$P_{regen} = P_{brake\_out} * \eta_{gen} \tag{20}$$

$$E_{regen} = P_{regen} * ts \tag{21}$$

Finally, the charging energy is calculated as the minimum between the battery available capacity and the product between regenerative power, the charging efficiency set to 0.98 and the timestep.

$$E_{ch} = \min\left(P_{regen} * \eta_{charge} * ts, cap_{available}\right) \tag{22}$$

The charging power is then obtained as:

$$P_{ch} = \frac{E_{ch}}{ts} \tag{23}$$

The longitudinal dynamics' energy request and recovery are unavoidable in the definition of the overall consumption of the bus since they are related with the bus's movement. This consumption is very much affected by the characteristics of the driving cycle, for example the aggressiveness of the drive, the number of bus stops and the average velocity of the route.

The parameters adopted in the previous dissertation are summarised in Table 7:

Table 7: Longitudinal dynamics' parameters. [8]

parameter	value	u.o.m.
Air density	1.225	kg/m^3
Frontal area	8.25	m^2
Drag coefficient	0.55	-
Rolling resistance	0.008	-
Wheel radius	0.48	m
Drivetrain efficiency	0.95	-
Timestep	1	s
Charge efficiency	0.98	-
SOC max	0.8	-

3.3. Auxiliaries

The main auxiliaries operating on any kind of bus are:

- Wipers
- Lighting
- Doors' opening system
- Parking brake
- Suspensions
- Steering pump
- Service brakes

They can affect the total electric consumption of a bus during its operations and are strictly dependent on the type of driving cycle tested, the weather conditions and the time of the day in which tests are conducted.

All these sub-systems can be shaped as an additional electric energy request to the battery although they can be divided into electric, hydraulic, and pneumatic auxiliaries.

3.3.1. Electric auxiliaries

The accessories belonging to this category are wipers, lighting, doors' opening system and parking brake. Their modelling can be defined through a binary signal either open or close. When the signal is open the auxiliary requires from the battery an instant power equal to the maximum value for that accessory. Instead, the power flow is null if the signal is close.

Wipers are devoted to the cleaning of the back and front windshield when it is raining. Then it is a weather-dependent demand of 110 W [8], that can be avoided if the sky is clear.

Lighting allows bus driver's night vision and internal cabin illumination for passengers' comfort. The overall system asks for 550 W [8] and it is active only if the natural light is not enough, when the driving cycle is performed at night.

During passengers' get off/on the bus there are two separate auxiliaries working: doors' opening and closing procedure last 3 seconds and receives 90 W [8] while the parking brake to stop the bus is a single second request of 560 W [8]. All the electric auxiliaries' consumptions need to be divided for a 0.8 efficiency to find the actual value. Of course, the number of bus stops of the analyzed driving cycle is the only parameter affecting these consumptions. For example, extra-urban routes' energy consumption with low number of stops will be very little influenced by doors' opening and parking brake.

The main features regarding electric accessories are condensed in Table 8.

Table 8: Electric auxiliaries' parameters. [8]

auxiliary	variable	value	u.o.m.
Wipers	power	110	W
Lighting	power	550	W
Door Opening	power	90	W
Parking brake	power	560	W
Door Opening	duration	3	s
Parking brake	duration	1	s
Electric Aux	efficiency	0.8	-

3.3.2. Hydraulic auxiliaries

Suspension system and steering pump account for the hydraulic auxiliaries and the shaping up of their consumption is a bit more complex than the electric ones.

Suspension system is activated during bus stops just like parking brake and doors' opening and its duration is 3 seconds. The power value, by the way, depends on the weight of the bus since it is defined as in Equation 24:

$$P_{el\_susp} = \frac{M_{front} * g * \Delta h}{\eta_{susp} * \Delta t_{susp}} \tag{24}$$

The hydraulic potential energy needed to lift the 4500 kg frontal mass of the bus [23] by 65 mm [8] is divided by the suspension's operation time and by the suspension system efficiency which is constant and considered to be 70%. The values are summarized in Table 9.

Table 9: Hydraulic suspensions' parameters. [8], [23]

variable	value	u.o.m.
Frontal Mass	4500	kg
Parking Brakes	65	mm
Efficiency	0.7	-
Duration	3	s

The other hydraulic component of the bus is the steering pump, which allows to manoeuvre the vehicle and it is strictly depending on its velocity. The higher the speed is and the lower the power needed will be since steering pump will find less resistance to its operation. When the vehicle is stopped and speed is null, no load on the battery is considered, while there are 3 level of direct power demand from the pump when it is not: low, medium, and high. Low level corresponds to 0.42 kW [23], [24] and is related to velocities higher than 3.5 m/s. The medium request applies for 0.9 kW for speed between 0.5 m/s and a higher limit of 3.5 m/s. The maximum load on the battery comes from speed closer to 0 until 0.5 m/s and accounts for 3.2 kW. The levels of power with reference to their speed window are summed up in Table 10.

Table 10: Steering pump power levels and speed windows. [23], [24]

levels	Power [kW]	Speed [m/s]
No load	0	0
High level	3.2	(0; 0.5]
Medium level	0.9	(0.5; 3.5]
Low level	0.42	>3.5

Although there might be some rectilinear part of the road where the steering pump might not be actually used the effect of the linearity of the driving cycle is not considered. This choice does not affect urban routes where the bus drives into traffic and is continuously forced to steer, also because of frequent bus stops. On the other hand, it can certainly affect rural driving cycles, where long straight roads are covered at high speed, but since power requirements from the pump at high speed are relatively low, the eventual error is considered negligible.

A typical trend of the steering pump power with respect to velocity is reported in Figure 13.

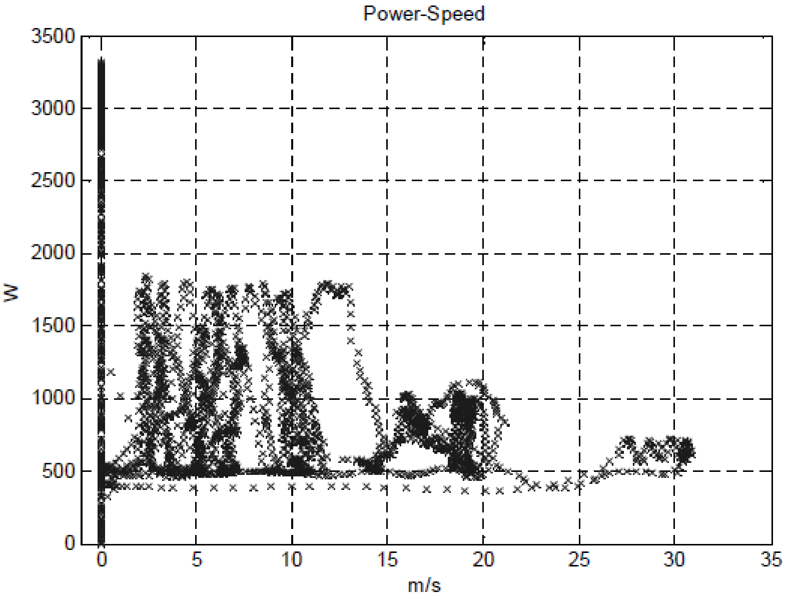

Figure 13: Electric Power-Speed trend for hydraulic steering pump. [23]

3.3.3. Pneumatic auxiliaries

Many of the previously defined part of the bus can be modelled as pneumatic auxiliaries (for example bus doors' opening) but for the sake of simplicity are considered as simply electrically moved.

One of the most important auxiliaries for a vehicle and particularly for a public transport bus, since carrying a larger number of passengers, is the service brake system. As shown in the longitudinal dynamics' chapter, the braking power is divided into two exactly equal fraction: the part devoted to brake energy recovery while the rest is dissipated through the pneumatic brakes at the wheels. The required flow rate of compressed air is coming from a 30 litres tank at 10 bars [8], [23] and it is calculated for each braking instant through a proportion with the intensity of the mechanical braking torque at the rear wheels. The maximum torque has already been defined and it is required to always have at least half the tank full for safety reasons, in case of emergency braking. Hence it is supposed to have a maximum flow rate of air of 13 l/s in case of punctual intensive request. Main formulas are resumed in Equation 26.

$$\begin{cases} P_{brake\_mech} = -0.5 * P_{trac}, \qquad if\ P_{trac} < 0 \\ torque_{brake\_mech} = \dfrac{P_{brake\_mech}}{w_{wheel}} \\ v_{air\_brake} = \dfrac{torque_{brake\_mech}}{torque_{brake\_max}} * v_{air\_brake\_max} \\ V_{air\_tank} = V_{air_{tank},j-1} - v_{air\_brake} + v_{air\_compr} \end{cases} \tag{26}$$

Air tank is filled with pressurized air coming from a compressor which works at full speed when air goes under critical level consuming 2.7 kW with an efficiency of 80%. It stops working only when the tank is full at the rhythm of 4 l/s.

All the reference data for pneumatic brakes' consumption are in Table 11.

Table 11: Pneumatic brakes' parameters. [8], [23]

variable	value	u.o.m.
Max air flow	13	l/s
Air flow to tank	4	l/s
Compressor efficiency	0.8	-
Compressor Power	2.7	kW
Air tank volume (full)	30	l

Pneumatic brakes' consumption is influenced by the intensity and by the number of braking phenomena which characterize the driving cycle. Hence the main parameters affecting compressor's working are average deceleration, the number of stops and traffic congestion that may force to continuous stopping and restarting.

3.4. Heat and Ventilation Air Conditioning

Air conditioning is crucial in the definition of BEB's operations and extreme weather conditions can lead up to double the electric energy consumption of a bus with respect to mild temperatures' ones [8].

Every timestep of the driving cycle is characterised by a different load to be either removed (cooling) or to be introduced (heating), in order to reach and keep the comfort temperature inside the vehicle's cabin.

The main formula governing HVAC procedures [25] are the following ones:

$$Q_{AC\_loads} = -\sum_{i}^{n} Q_i \tag{27}$$

$$Q_{AC\_temp} = -\frac{(m_a * c_a + DTM_{bus}) * (T_i - T_{comf})}{t_c} \tag{28}$$

$$Q_{AC} = Q_{AC\_loads} + Q_{AC\_temp} \tag{29}$$

As can be seen from Equation 29 the instantaneous air conditioning load Q_{AC} is the result of two different contributions: the sum of all the existing thermal loads and the effect of the internal cabin temperature variation. Internal temperature is higher than comfort one in summer, hence temperature related term is positive and the exact opposite in winter. The summatory is positive for summer while it is globally negative for winter. For these reasons they are both preceded by a negative sign in Equation 27 and Equation 28 to be positive during heating and negative during cooling.

Equation 28 depends on different variables and allows to have a transient trend for cabin temperature, starting from the external temperature as initial point for climatization process. It also gets smaller and smaller as long as the transitory moves by and becoming zero once comfort temperature is reached.

The air mass within the cabin is obtained simply by multiplying the bus volume by air density assumed to be 1.225 kg/m^3.

The difference between the internal temperature and comfort one is multiplied by the thermal mass of the bus expressed in kJ/K. Thermal mass definition sets the quantity of energy needed to cool down or heat up the air and the other objects within the cabin (DTM_{bus}). While air mass m_a can be easily found from its density and bus internal volume, an estimation is needed to find the deep thermal mass of the cabin's components other than air. DTM values found in literature are: 10.6 kJ/K for a truck's driver cabin [18] and 5.6 kJ/K for a small electric car [17] and they are esteemed considering driver's dashboard, seats exc. In a large ambient like a bus cabin the most relevant mass, apart from air, is constituted by 28 plastic seats made of polypropylene (PP) [19]. Seat's geometry is modelled as two identical squared pieces of PP with a 0.5 m side and 5 mm thickness. This results in a total 0.07 m^3 volume for the 28 seats. Polypropylene's properties are 900 kg/m^3 density and a 1600 J/kg*K specific heat. These calculations reported in Equation 30 provides a 100.8 kJ/K esteem for the DTM of the bus.

Thermal mass is dimensionally a thermal capacity and bus's one is found with the formulas reported in Equation 30 while the assumptions and properties are made explicit in Table 12.

$$\begin{cases} A_{seat} = 2 * (l_{seat})^2 \\ V_{pp} = n_{seat} * A_{seat} * t_{seat} \\ m_{pp} = V_{pp} * \rho_{pp} \\ DTM_{bus} = c_{pp} * m_{pp} \end{cases} \tag{30}$$

Table 12: Cabin thermal mass' estimation parameters [7].

variable	value	u.o.m.
Seats	28	-
Seats side	0.5	m
Seats thickness	5	mm
PP density	900	kg/m^3
PP specific heat	1600	J/kg*K
DTM$_{bus}$ esteem	100.8	kJ/K

The denominator in Equation 28 is the pull-down constant t_c which is a constant derived from the pull-down time t_p defined as a modelling feature. Pull-down time is the period within the system should reach comfort conditions and it is chosen to be 600 s (10 minutes). Pull-down constant depends on the initial temperature of the cabin, that is set to the external temperature, and from the comfort goal to be achieved as Equation 31 makes explicit.

$$t_c = \frac{t_p}{\ln\left|T_0 - T_{comf}\right|} \tag{31}$$

Comfortable temperature's interval is considered to be within 19°C and 23°C for winter conditions, and 23°C and 27°C for cooling mode [8]. Since thermal modelling needs single comfort temperature values to move towards with an asymptotic behaviour, 21°C for heating mode and 25°C for summer conditions are chosen.

The changing in the internal temperature is obtained thanks to the total load for each timestep as shown in Equation 32:

$$\begin{cases} Q_{tot} = Q_{ac} + Q_{met} + Q_{vent} + Q_{doors} + Q_{eng} + Q_{amb} + Q_{rad} \\ \Delta T_i = \dfrac{Q_{tot} * ts}{DTM_{bus} + m_a * c_a} \\ T_i = T_{i,j-1} + \Delta T_i \end{cases} \tag{32}$$

The power consumed by HVAC is obtained as the sum of fans' needs, that accounts for 1 kW [8] and that are active even when the unit is off, summed with the request from air conditioning system.

The system is thought as composed by an electric heater, to deal with freezing air during winter's rigid temperatures (PTC), a reversible heat pump (HP) and a waste heat recovery to reduce cabin air thermal needs by recuperating heat from the air flow rate expelled during ventilation (WH).

The precise definition of each of this component and their different type of operations would have been complex without the aid of an external software devoted to it. For this reason, HVAC overall power is obtained by dividing the air conditioning load Q_{AC} by a coefficient of performance *COP*, which values are empirically found and dependent on the external temperature in [26] as in Figure 14.

$$P_{HVAC} = P_{vent} + \frac{Q_{AC}}{COP} \tag{33}$$

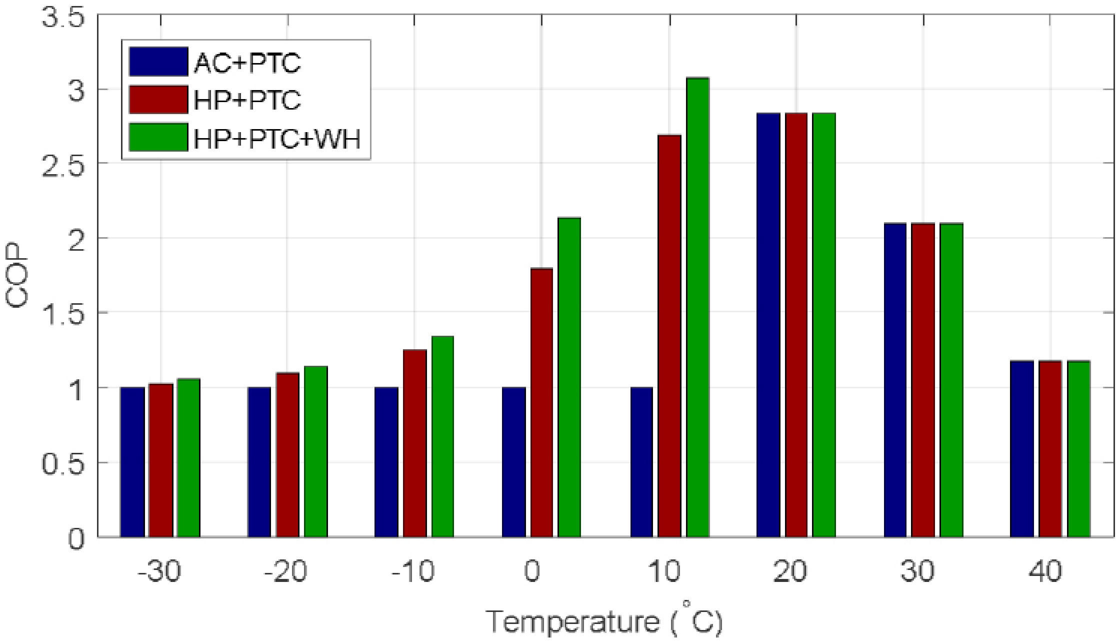

Figure 14: COP values for different external temperatures [26]

The values reported in Table 13 and Table 14 are taken down from Figure 14, for the HP+PTC+WH scenario and the in between temperature's COPs are obtained as an average between previous and succeeding values.

Table 13: COP heating.

T_o	-10	-5	0	5	10
COP	1.33	1.73	2.12	2.60	3.08

Table 14: COP cooling.

T_o	25	30	35	40
COP	2.5	2.11	1.66	1.20

There are no values for 15 °C and 20 °C since the HVAC unit is considered off when these external temperatures occur.

3.4.1. Thermal Loads

In this subheading every single thermal load to the summatory is eviscerated to grasp how they contribute to the definition of the air conditioning load in Equation 27.

The heat released by each passenger while they are on board of the bus is called metabolic load and accounts for 70 W per passenger [27]. It is due to the metabolic activity of the human body which is not negligible even at rest. This unavoidable heat helps reducing the needed input load for winter condition while it is a disadvantage during summer. It has a constant influence once the passenger's occupancy is set, and it can be very impactful for very much-frequented routes.

Air quality within the vehicle need to be taken into serious consideration, the high number of occupants can lead CO_2 and other contaminants concentration to concerning levels. To have a controlled ventilation, 8 complete air recirculation are performed within an hour [9], hence time of recirculation is 450 s. The ventilation air flow rate is obtained by dividing the volume of the cabin by this recirculation time. While the ventilation heat is found as follows, depending on the temperature difference between inside and outside air.

$$Q_{vent} = \frac{V_{bus}}{t_{ric}} * \rho_{air} * c_{air} * (T_o - T_i) \tag{34}$$

Ventilation is always a drawback in terms of air conditioning since it is introducing external air at a different temperature than the cabin comfortable one. This effect tends to become more intensive as long as internal temperature gets closer to comfort, since temperature difference between inside and outside air grows.

When air conditioning is active on cars the cabin is kept closed in order not to interfere negatively on its refreshing/heating function. Unfortunately, this is not possible for buses since doors are frequently opened during stops to allow passengers to exploit the public service. This is particularly detrimental when an accentuated temperature difference with the exterior is present.

The doors' opening heat exchange is taken care off by considering two different air flow rates happening at each bus stop: the one flowing through the orifices (doors) and the one due to human's passage [9].

The flow through the doors depends on an orifice coefficient of 0.5 and on doors' dimensions with 1.2 m width and 3 m height [19]. The formula presented in [9] to account for the air flow rate across the orifice is:

$$q_{orifice} = \frac{k}{3} * A * \sqrt{g * H_{door}} \tag{35}$$

The term A is the total area of doors that are generally 3 for a 12m bus.

The rest of the air flow rate for bus doors' opening rely on two different experimental terms reported in [9] which are: the rate of passenger flowing of 0.25 1/s and the exchanged volume per passage of 0.25 m^3. Hence flow rate contributions due to passengers is calculated as:

$$q_{passage} = n * V_{passage} \tag{36}$$

The heat exchange during stops is then calculated as:

$$Q_{doors} = (q_{orifice} + q_{passage}) * \rho_{air} * c_{air} * (T_o - T_i) \tag{37}$$

This load is null throughout the driving cycle except, of course, when doors are opened for bus stops. Once thermal comfort is achieved in the cabin the heat exchange with external air in extreme condition can give rise to peak thermal load. For this reason, the overall request for this heat exchange needs to be calculated for each different test and then divided between all the single instant as a constant extra load. To manage this request in this way helps avoiding excessive stress on the heat pump, having no peaks but instead a constant demand.

Moreover, this contribution is considered only for heating mode, and it is neglected for cooling. This choice is made to simplify the definition of the AC load for temperatures higher than 25 °C since the maximum temperature difference between the internal cabin temperature and the external one is 15 °C and it is reached only for 40 °C at the end of the transitory.

The parameters are synthetized in Table 15.

Table 15: Ventilation load parameters.

variable	value	u.o.m.
Orifice coefficient	0.5	-
Door height	3	m
Door width	1.2	m
Passenger rate	0.25	1/s
Passage exchange	0.25	m^3

Electric engines tend to heat up less than traditional internal combustion ones but anyway their thermal interaction with the cabin must be taken into consideration.

The heating effect on engine's surface temperature is proportional to the angular velocity of the electric machine expressed in rpm [17] and is calculated in °C as in Equation 38.

$$T_{eng} = -2 * (10^{-6}) * rpm^2 + 0.0355 * rpm + 77.5 \tag{38}$$

The superficial area of the engine' envelope is calculated based on a 150-kW motor dimension is 2.74 m^2 and its heat exchange coefficient is calculated like in Equation 39 without considering external convection. Engine heat exchange coefficient is:

$$U_{eng} = \frac{1}{\frac{1}{h_{int}} + \frac{k_{vb}}{\lambda_{vb}}} \tag{39}$$

Engine load is then found as follows:

$$Q_{eng} = U_{eng} * A_{eng} * (T_{eng} - T_i) \tag{40}$$

Radiation load impacts on bus's temperatures and its value depends on the way rays are split when they get in contact with its outer structure. Part of the solar flux is absorbed by the surfaces increasing their temperature while, for transparent ones only, another significant part is transmitted to the interior of the bus affecting cabin's temperature.

The solar flux intensity, expressed in $W/m^{2,}$ depends on three different aspects of how the driving cycle is performed: geographical location, temporal collocation, and surfaces' orientation [28]. The first characteristic is defined by: longitude, latitude, and the longitude of the central meridian of the reference time zone (ex. for Italy is -15°). Setting the day of the year and the time of the day is enough to take care of the temporal dimension. Normally during bus operations, the exposition to the sun can change due to the nature of the driving cycle and to the shading factor because of clouds or buildings presence. In this study the bus is thought moving in south direction with the side without doors exposed east throughout the route. The floor of the bus is not included in this contention since it is not invested by solar flux. This leads to the angles reported in Table 16 where *csi* is the inclination and *psis* is the azimuth of the surfaces.

Table 16: Surfaces' orientation.

	Doors	**No doors**	**Roof**	**Back**	**Front**
csi	90	90	0	90	90
psis	270	90	0	360	180

Moreover, flux is divided into direct and diffuse radiation where the second term refers to the quantity of flux hitting the bus after an intermediate interaction with atmospheric gases. The contribution due to the flux reflected by the soil and arriving to the vehicle is neglected because of its low intensity [17]. The radiative contribution is considered only in cooling mode since during winter it is generally cloudy [27]. But this assumption can be unlocked if the examined day is sunny and the help from radiation in cabin heating wants to be accounted.

The procedure to find direct and diffuse solar flux is here reported [28] where: *g* is the day of the year, *h* is the hour of the day, *long* is the longitude and *fu* is the time zone reference's meridian.

First, the daily angle is found to derive sun declination, both in radiant:

$$w = g * \pi/180 \tag{41}$$

$$\begin{cases} d = 23.45 * \sin\left((\mathrm{g} + 284) * 360 * \dfrac{\pi}{(180 * 365)}\right) \\ d = d * \pi/180 \end{cases} \tag{42}$$

The time equation *e*, expressed in degrees, keeps into consideration all the anomalies of terrestrial orbit:

$$e = 0.42 * \cos(w) - 3.23 * \cos(2w) - 0.09 * \cos(3w) - 7.35 * \sin(w) - 9.39 * \sin(2w) - 0.34 * \sin(3w) \tag{43}$$

The hourly angle based on coordinate and time of the day the time defines temporal collocation:

$$\begin{cases} \omega = 15 * (12 - h) - 0.25 * (e - 4 * (long - fu)) \\ \omega = \omega * \pi/180 \end{cases} \tag{44}$$

Direct and diffuse solar fluxes are influenced by three different parameters with different physical meanings:

- The virtual extra atmospheric radiation *A* in W/m^2
- The atmospheric extinction coefficient *B*
- The diffused radiation factor *C*

Their values are dependent on the day of the year *g* and the hourly angle *w*:

$$A = 1150.25 + 72.43 * \cos(0.95w) + 34.25 * \sin(0.017w) + 1.5 * \log(g) \tag{45}$$

$$B = 1/(6.74 + 0.026 * g - 5.13 * 10^{-4} * g^2 + 2.24 * 10^{-6} * g^3 - 2.8 * 10^{-9} * g^4) \tag{46}$$

$$C = 1/(16.9 + 0.0001 * g - 8.65 * 10^{-4} * g^2 + 3.93 * 10^{-6} * g^3 - 4.005 * 10^{-9} * g^4) \tag{47}$$

The elevation angle of the sun upon the horizon is calculated in Equation 48 where all the input angles are in radiant:

$$\beta = \text{asin}\,((\sin(lat) * \sin(d) + \cos(lat) * \cos(d) * \cos(\omega)) \tag{48}$$

Then only positive β values are considered while negative ones are set to 0, since it means we are performing the procedure at night.

In the next step the solar azimuth is found, and its value is multiplied by -1 if the time of the day τ is higher than 13, meaning that an afternoon hour is being examined.

$$psi = \operatorname{acos}\left(\frac{(\sin(\beta) * \sin(lat)) - \sin(d)}{\cos(\beta) * \cos(lat)}\right) \tag{49}$$

The incidence angle of the direct solar radiation θ is the resultant of all the different angles defined until this moment and needs to be set to π/2 for values equal or higher than π/2.

$$\theta = \operatorname{acos}\left(\cos(\beta) - \cos\left(psi - psis\right) * \sin(csi) + \sin(\beta) * \cos(csi)\right) \tag{50}$$

The normal direct radiation is null if β is, while has this expression in other cases:

$$I_{dir,n} = \frac{A}{e^{B/\sin(\beta)}} \tag{51}$$

And finally, the direct flux is:

$$I_{dir} = I_{dir,n} * \cos(\theta) \tag{52}$$

The diffuse radiation is derived from the direct flux once the view factor between the surface and the celestial vault *F* is:

$$\begin{cases} F = \dfrac{1 + \cos(\mathrm{csi})}{2} \\ I_{dif} = C * I_{dir,n} * F \end{cases} \tag{53}$$

Radiation load is then defined as in Equation 54 and it is affected by solar fluxes, surface areas and transmittance.

$$Q_{rad} = \left(I_{dir} + I_{dif}\right) * A * \tau \tag{54}$$

The indirect interaction between the internal and the external environment is taken into account in the ambient load expression here presented:

$$Q_{amb} = (T_s - T_i) * A_s * U \tag{55}$$

The surface temperature is reported later in the dissertation while the surface areas' calculations are made explicit in 3.1. The overall heat exchange coefficient is obtained by assessing different contribution from internal/external convection and conduction through the surface:

$$U = \frac{1}{\frac{1}{h_{out}} + \frac{1}{h_{int}} + \frac{\lambda}{k}} \tag{56}$$

The internal convection coefficient is equal to 0.6 W/m^{2}K [17] considering almost still air within the cabin as exchange media with bus's sides. The external convection instead happens with moving air and this aspect reflects in the external convection coefficient which includes also the bus average velocity in its definition [17].

$$h_{out} = h_{int} + 0.64 * \sqrt{v_m} \tag{57}$$

The conduction across the surfaces depends on their conductivity k and their thickness λ, which are different for vehicle body and window type of surfaces.

Every different exterior piece of the bus have its ambient exchange, depending on its geometrical and physical properties and it is not constant throughout the driving cycle. The thermal difference between the two ambient separated by the walls experiences an increase. The closer cabin temperature is to comfort and the higher ambient load for the envelope is.

Both the indirect exchange with external environment and the radiative interaction of the vehicle, contribute to the characterization of each surface temperature [17]. Part of the ambient load is gained by the surface and part of the radiation load is absorbed by cabin walls, resulting in a temperature increase as shown in Equation 58.

This type of ambient load relies on the values of surface and internal temperature calculated in the previous timestep, since the final temperature find in Equation 58 is then used in Equation 55. This was underlined by writing *j-1* subscripts.

The overall exchange coefficient as well as areas are the same as before while wall's absorbance, density and specific heat are defined in Table 4.

$$\begin{cases} Q_{amb,s} = \left(T_o - 2 * T_{s,j-1} + T_{i,j-1}\right) * A * U \\ Q_{rad,s} = \left(I_{dir} + I_{dif}\right) * A * \alpha \\ \Delta T_s = \dfrac{(Q_{rad,s} + Q_{amb,s}) * ts}{A * \rho * k * c} \\ T_s = T_{s,j-1} + \Delta T_s \end{cases} \tag{58}$$

3.5. Battery thermal management system

Battery is the most important component of a full electric vehicle and keeping its temperature monitored and actively intervene to thermally manage it is a very delicate task. Battery performance can drastically diminish when its temperature is not maintained within 20 °C and 35 °C [8]. There are plenty of system exploited for BTMS operations using liquids like water/glycol and mineral oil [29] but air is chosen as thermal media in this work. This choice grants lower complexity and lower costs to the system and allows to avoid potential leaks of liquid that can affect battery integrity.

The temperature of air tends to increase moving from one cell to another during cooling and vice versa during heating. This phenomenon is physically undeniable, but it is neglected for the sake of simplicity and only one temperature for the coolant/heating media is considered.

Battery surface temperature for each timestep is obtained by considering an equivalent simplified thermal circuit of a single battery cell [30] shown in Figure 15. T_{in} is the temperature of the core, T_{surf} is the surface temperature, R_{in} and R_{out} are the thermal resistances, respectively 3.39 K/W and 9.08 K/W [30], while Q is the heat generated within the cell, C_p is the thermal capacity of the cell of 77.7 J/K [31] and T_{amb} is the temperature of the air used for battery thermal management which varies, that will be referred at as T_{BTMS}. All the data refers to a Lithium-Ion battery and are reported in Table 17.

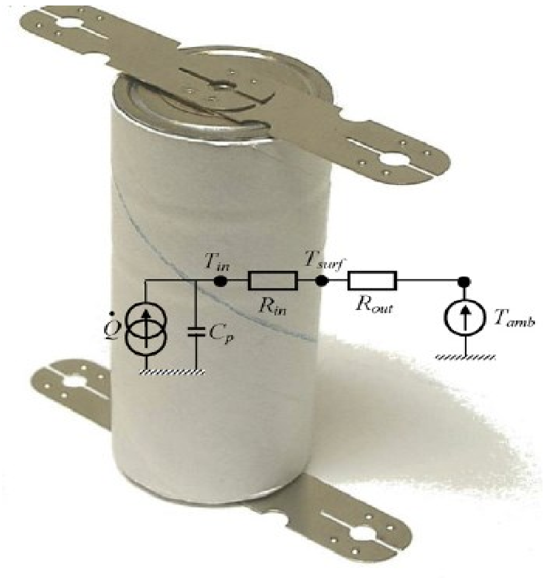

Figure 15: Battery cell's simplified thermal equivalent circuit. [30]

The computation of battery cell's surface temperature is here described starting from the equivalent circuit in Equation 59:

$$\frac{T_{surf,j} - T_{surf,j-1}}{ts} = \frac{T_{BTMS} - T_{surf,j}}{C_p * (R_{in} + R_{out})} + \frac{Q_{int} * R_{out}}{C_p * (R_{in} + R_{out})} \tag{59}$$

Defining a constant the equation can be written as:

$$\begin{cases} a = \dfrac{ts}{C_p * (R_{in} + R_{out})} \\ T_{surf,j} = \dfrac{T_{surf,j-1}}{(a+1)} + \dfrac{a}{(a+1)} * (Q_{int} * R_{out} + T_{BTMS}) \end{cases} \tag{60}$$

Hence surface temperature depends on its preceding value, on some thermal parameters, on the BTMS temperature and on the internal heat formed because of chemical reactions occurring in the battery. This very last parameter changes with the squared current intensity I_{batt} value and can be found through the following system of equations.

$$\begin{cases} U_{ocv} = U_{ocv,cell} * m \\ R_{eq} = R_{cell} * m/n \\ U_{t,j-1} = 0.5 * (U_{ocv} + \sqrt{(U_{ocv}^2 - 4 * P_{batt,j-1} * R_{eq})} \\ I_{batt,j-1} = \dfrac{P_{batt,j-1}}{U_t} \\ Q_{int} = \dfrac{I_{batt,j-1}^2 * R_e}{n_{cell}} \end{cases} \tag{61}$$

Battery's overall open circuit voltage U_{ocv} and electric resistance R_{eq} depend on the single cell values extracted from the battery empirical data in [8], assuming 80% of SOC and they are equal to 2 V and 10 mΩ. The cells are divided in m modules with n cells per each and the total cells number n_{cell} is given by their multiplication.

The internal heat definition refers to the current intensity and to the battery power request of the previous timestep. R_e is an empirical electric resistance that gives rise to heat generation in the battery, and it is equal to 11.4 mΩ.

The overall heat is divided by the total number of cells n_{cell} since the surface temperature computations are carried on for a single battery cell.

The external temperature determines which kind of air is sent to the battery for heating and cooling purposes. For temperatures between 10 °C and 20°C external air is used, and the only electrical consumption is constituted by the fan's 0.1 kW [8] needed to head air towards the battery.

$$T_{BTMS} = T_o \tag{62}$$

$$P_{BTMS} = P_{fan,batt} \tag{63}$$

For colder and hotter weathers cabin air is used for battery thermal management although it needs to be furtherly heated or cooled before operating in order to be effective.

Hence an additional thermal load is included in the BTMS' consumption definition because of the extra climatization required by cabin air devoted to the battery. This additional climatization results in a temperature increase ΔT_{add} that is set as constant to reach a goal temperature.

Goal temperature for battery surface is set to 17 °C for winter condition and approximately to 25 °C for battery cooling. Core temperature is almost 3 °C higher than surface temperature [29] and therefore 17 °C is thought as goal temperature for heating purposes since brings the battery core temperature at 20 °C. This value is the lower limit of the range for battery core temperature previously defined, hence is acceptable. The choice of 25 °C as surface goal temperature for cooling (28°C as core one) is instead the result of a trade-off between battery functionality and cooling requirements. Cooling the battery until the ideal lower limit of 20 °C for core temperature is thought unnecessary since even 28 °C is an acceptable temperature and does not affect operations.

The air volumetric flow rate is equal to 1000 CFM [8] and the additional thermal load needed to reach the required T_{BTMS} is:

$$Q_{add} = v_{air,batt} * \rho_{air} * c_{air} * \Delta T_{add} \tag{64}$$

And the required electric power is then calculated as in the HVAC unit:

$$P_{BTMS} = P_{fan,batt} + \frac{Q_{add}}{COP} \tag{65}$$

This table synthetize all the reference variables exposed in this subheading:

Table 17: BTMS parameters

variable	value	u.o.m.
Battery specific heat	77.7	J/K
Thermal internal resistance	3.39	K/W
Thermal external resistance	9.08	K/W
Electric core resistance	11.4	mΩ
Cell electric resistance	10	mΩ
Cell open circuit voltage	2	V
Battery volumetric flow	1000	CFM
Battery core temperature range	[20;35]	°C

The BTMS unit is an unavoidable auxiliary for the BEB and tak good care of the battery integrity is of paramount importance in the buses' management. The electric demand coming from this unit strongly depends on how much battery is stressed and how rigid external temperature is. It is often considered joined with the HVAC and in extreme temperature condition, like 40 °C it can constitute one third of the overall HVAC plus BTMS consumption.

4 Results

Once the informatic tool is developed with all the different formulas and procedures to find each unit consumption in different scenarios the testing phase starts. This part of the thesis job has paramount importance in order to demonstrate how accurate the tool is, which information can provide and how many different simulations can it run. The results process is divided into two different moments:

- The validation process, where the tool's accuracy is tested to assess its reliability
- The sensitivity and scenarios simulation, where the main parameters are varied assessing the impact on the output variables of the tool

4.1. Validation process

Validation of a proposed model can be carried on by confronting its outputs with the one coming from another predictive tool or by looking at the datasets of a measurement champaign on real life experiment. The validation process for this thesis undertakes the first choice and the results in terms of average power requests and total consumption are confronted with their equivalent in the H. Basma et al. [8] paper.

The generated results for this paper are:

1. Two images showing the average power request for the thermal units: HVAC and BTMS. These tests are performed on Manhattan Bus driving cycle with 30 passengers on board and varying the external temperature between -10 °C and 40 °C.

2. Two graphs allowing a precise definition of the energy consumption of the propulsion and auxiliaries' units tested for the different driving cycle with 30 passengers' occupancy. The paper states that tests are performed with an external temperature of 20 °C but temperature does not affect in any way these consumptions.

3. Three different heat maps matching the units' outputs with some varying parameters affecting them, that made possible to simulate different conditions in terms of driving cycle, external temperatures, and passengers' occupancy. The first one shows the total propulsion's consumption with varying number of passengers and average speed, that allows to change the analyzed driving cycle. The HVAC power request including the BTMS contribution is reported and the parameters that can be switched are the occupancy and the external temperature. Finally, the auxiliaries are expressed as an average power request varying with average speed and average deceleration.

Three validation trials are conceived in order to test the model:

1. Validation on the HVAC and BTMS average power request to the battery for MB driving cycle and 30 passengers, confronting the results with the one taken down from the first graphical outcome of the paper.
2. Validation on the overall energy consumption of the MB driving cycle at -10 °C and 40 °C with 30 passengers on board. The energy consumption of the HVAC and BTMS, propulsion and auxiliaries are derived from the second type of outputs described
3. Validation on the overall energy consumption of different driving cycle, simulating different external temperature and occupancy couples. The results are derived, knowing the average speeds and the average decelerations of the driving cycles and fixing the desired temperature and passengers' number.

The following validations relied on the knowledge of each driving cycle specifics that are summarized in Table 18 for the tested ones.

Table 18: Driving cycles specifics. [7]

Driving cycles	stops	time [s]	distance [km]	average speed [km/h]	average deceleration [m/s²]	aggressiveness [m/s²]
MB	21	1089	3.32	10.98	-0.185	0.295
NYB	12	600	0.99	5.91	-0.143	0.422
OCTA	31	1909	10.55	19.89	-0.214	0.238
BRAU	30	1740	10.88	22.49	-0.215	0.234
UDDS	16	1372	11.99	31.44	-0.199	0.185
CBD	14	560	3.29	21.13	-0.223	0.187
CSHV	13	1700	10.76	22.77	-0.147	0.177
NYC	19	1029	4.04	14.11	-0.15	0.242

4.1.1. Validation on HVAC and BTMS

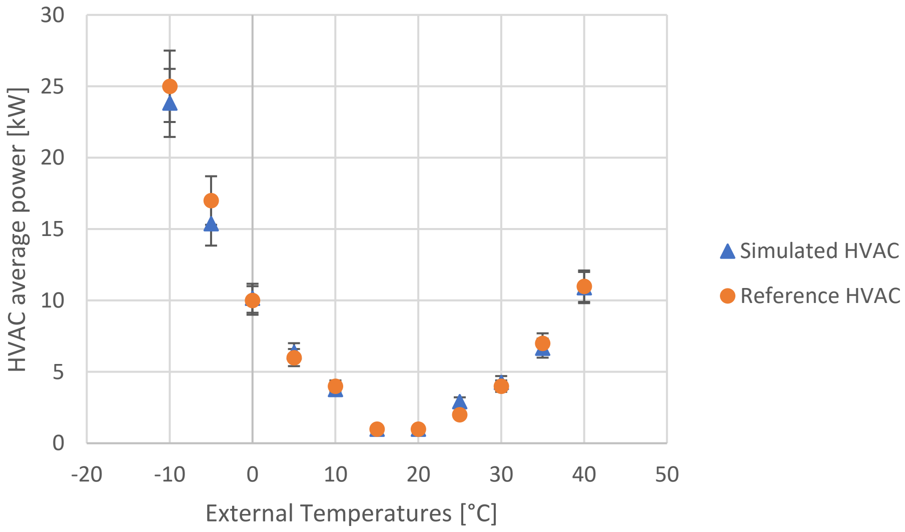

Figure 16: HVAC average power validation for Manhattan Bus with different external temperatures and 30 passengers.

For the HVAC unit, the simulated average power request follows the same trend as the reference values taken from [8] although the values are not exactly the same. In the graph it is underlined the range of ±10% error on each value plotted and simulated values fall always within the arms of the error bars of the reference ones.

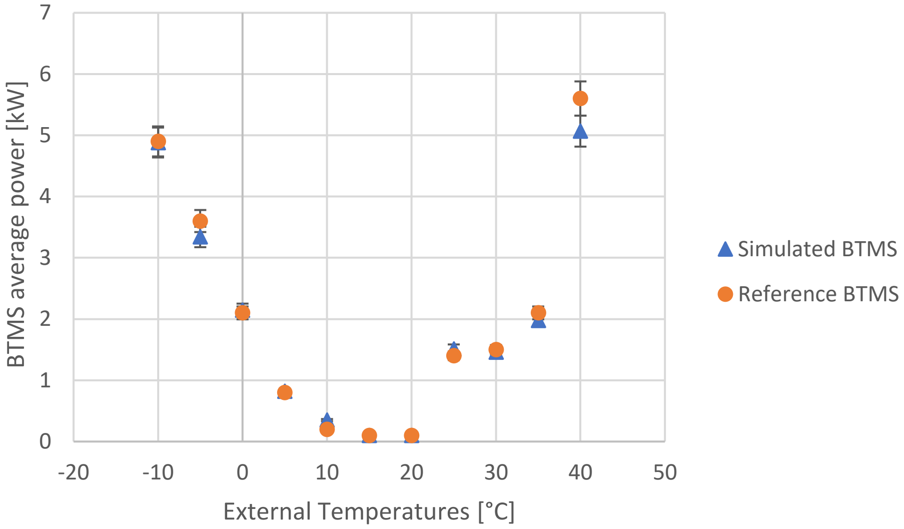

Figure 17: BTMS average power validation for Manhattan Bus with different external temperatures and 30 passengers.

The same kind of validation is carried on the BTMS and overall, the model correctly simulates the variation of the power average request varying the external temperature. The simulated value for 40 °C extreme warm condition is the further one from its respective reference one and falls outside the 10% error bars as shown in Figure 17.

Hence this first validation is considered successful since, although it refers to a single driving cycle and occupancy couple, it has proven to be solid to the variation of an interesting range of external temperatures.

4.1.2. Total consumption validation

The second kind of results can be transformed from HVAC and BTMS average power demand into an energy consumption expressed in terms of kWh/km like the traction and auxiliaries' units. This transformation allows to have an overall energy consumption for the MB driving cycle with 30 passengers at -10 °C and 40 °C. The simple mathematics of the switch of average power into energy specific consumption expressed in kWh/km is here reported. It relies on the knowledge of the kilometers travelled and the time duration of the route, equal to 3.32 km and 1089 seconds for MB.

For example, HVAC and BTMS power for -10 °C are equal to 25 kW and 4.9 kW then:

$$Thermal\ Consumption = 29.9 * \frac{1089}{3600*3.32} = 2.724\ kWh/km \tag{66}$$

The overall consumption is then easily found by summing the thermal one with the ones coming from auxiliaries and traction for the MB1 simulation:

$$Total\ Consumption = 2.724 + 2.040 + 0.100 = 4.864\ kWh/km \tag{67}$$

These calculations considering an external temperature of 40 °C result in a total consumption of 3.653 kWh/km for MB2.

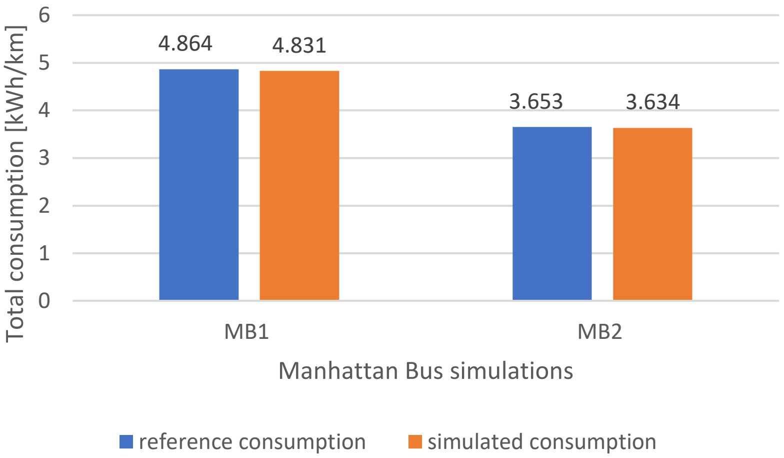

Figure 18: Total consumption validation for Manhattan Bus and 30 passengers: MB1 is performed at -10 °C while MB2 at 40 °C.

The simulations happen to be very closer to the reference values as can be seen in Figure 18 . The percentage error characterizing the two tests is calculated as in Equation 68 and it is reported in Figure 19, underlining that the simulation on the driving cycle at 40 °C is slightly better.

$$err_{\%} = \frac{model_{cons} - real_{cons}}{real_{cons}} \tag{68}$$

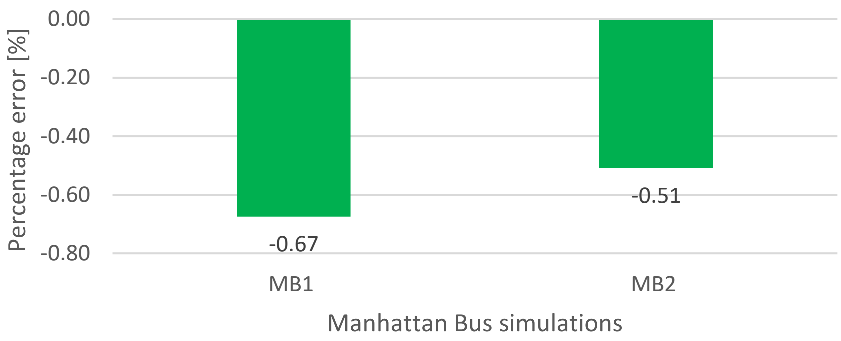

Figure 19: Total consumption error percentage for Manhattan Bus and 30 passengers: MB1 is performed at -10 °C while MB2 at 40 °C.

4.1.3. Total consumption validation for different external conditions

Starting from the driving cycle specifics in Table 18 and setting the passengers' occupancy and the external temperature, other ten different total consumptions are found and are utilized as reference values for the tool's validation.

These values are expressed again in kWh/km and are calculated from the heat maps of [8] as this example for NYC at -5 °C and 55 passengers shows:

Heat maps must be read fixing parameters at:

- -5 °C external temperature
- 55 passengers
- 14.11 km/h average speed
- -0.15 m/s^2 average deceleration

Propulsion consumption is 2 kWh/km, while thermal and auxiliaries power requests are 20 kW and 0.7 kW respectively.

$$Thermal + AUX\ Consumption = 20.7 * \frac{1029}{3600 * 4.04} = 1.465\ kWh/km \tag{69}$$

$$Total\ Consumption = 2.000 + 1.465 = 3.465\ kWh/km \tag{70}$$

The purpose of this part of the validation is to show how solid the model is to parameters variation and that's why the parameters are combined in order to form the more disparate conditions as reported in the following table. The two simulations of the previous validation are included in Table 19 for confront.

Table 19: Validation run parameters.

Driving cycles' run	passengers	To [°C]	Reference consumption [kWh/km]
MB1	30	-10	4.864
MB2	30	40	3.653
NYB1	20	0	4.943
NYB2	50	30	4.418
OCTA1	45	40	2.704
OCTA2	10	25	1.902
BRAU1	25	15	1.893
BRAU2	5	-5	2.533
UDDS	5	40	2.009
CBD	35	35	2.275
CSHV	5	-10	2.313
NYC	55	-5	3.472

The maximum capacity of the bus is 55 passengers, simulating a packed condition within the cabin and with an important addition to vehicle weight. On the other hand, the two extreme weather situations are set to -10 °C for very cold temperature and 40 °C for very warm climate.

MB, NYB, OCTA and BRAU driving cycle are tested with two different couple of passengers and external temperatures while UDDS, CBD, CSHV and NYC are run in just a single combination.

The results of this validation phase are summed up in Figure 20 and Figure 21 showing the total consumption comparison between simulated and reference total consumption values and the percentage error for each of the test. The data labels on top of the columns refer to the simulated consumptions.

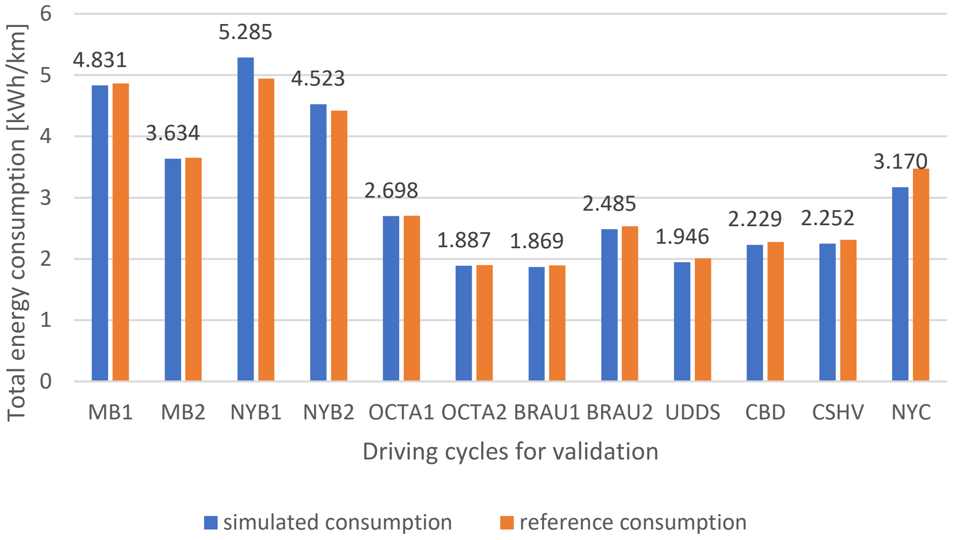

Figure 20: Total consumption validation for different driving cycles and different external conditions.

Figure 20 underlines how the simulated values follow the reference consumptions in very different scenarios and with different intensities of consumption.

The model provides results for low occupancy tests like UDDS with a percentage error of -3.13% and in packed conditions like NYB where that value is +2.38%. But also, for different climate for example CSHV test at -10 °C has a percentage error of -2.65 % and OCTA1 test at 40 °C happens to have the lowest error of all with a very interesting -0.22 % error. The worst error is found in the NYC test with maximum occupancy and very low temperature (-5°C) but it is still under 10 % and it can be considered acceptable. All the percentage error outcome are reported in Figure 21.

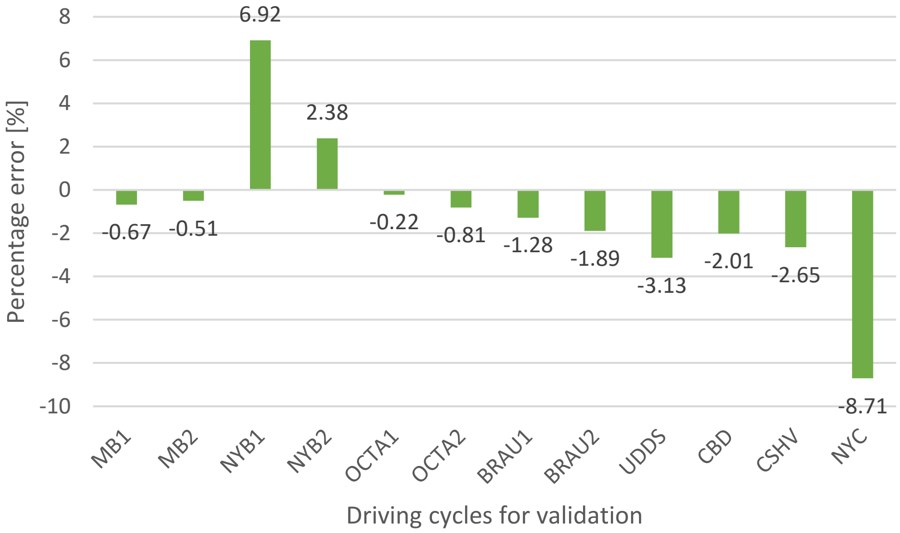

Figure 21: Percentage error in total consumption validation for different driving cycles and different external conditions.

The simulated values generally stand below the reference values taken and only the two tests performed on NYB driving cycle appear to break this "rule". The percentage error is never higher than 10 % and for 10 tests out of 12 it happens to be even lower than 5 % which is very much promising.

4.1.4. Infeasibility computation

Part of the timesteps composing the driving cycles have a request from the motor, P_{motor}, higher than the maximum power available of 157 kW. This can be addressed to the fact that road grade is set constant to 0 for all the routes while some of the power peaks observed during validation may be due to some favourable descending pendency. Moreover, the limit to the power is set to 157 kW through reasonable assumptions as reported in 2.2 subheading, but no precise reference for this value is available in [8]. Having said that, infeasibility is taken into account for the tested driving cycles and is calculated as the percentage of timesteps over the total time where the request from the motor P_{motor} is higher than the maximum power P_{max}.

The results from these calculations are shown in Figure 22 for each of the total consumption analysis performed in the validation phase.

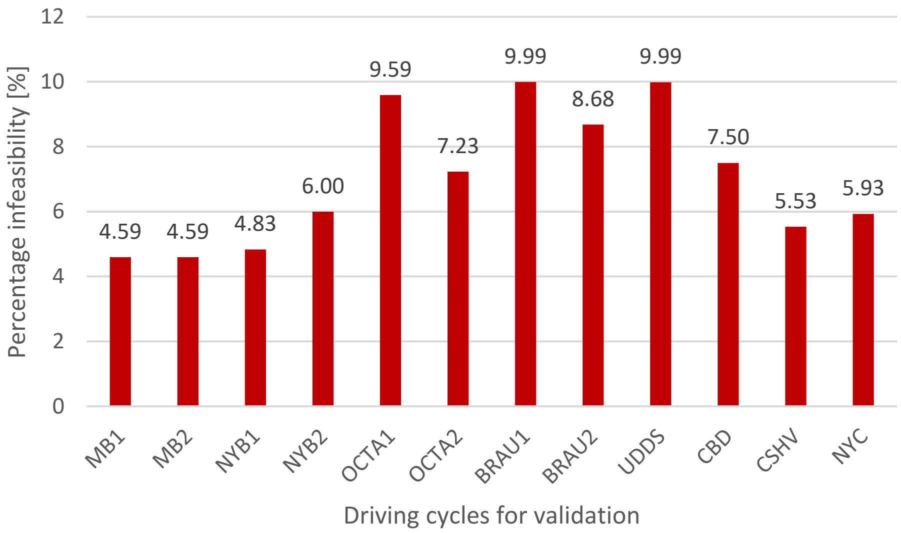

Figure 22: Infeasibility percentage in total consumption validation for different driving cycles and different external conditions

As a desirable feature, infeasibility should be nearest as possible to 0%, but as can be seen, the lowest value is 4.59% for the MB and for driving cycles like OCTA1, BRAU1 and UDDS it almost reaches 10% as the worst possible value experienced.

The logical limit for which the unfeasibility is thought to be ruining the data output is then set to 10%. This may seem a high threshold, but it needs to be understood that the amount of exceeding timesteps is not that high in absolute values. For example, the high unfeasibility percentage for the OCTA1 driving cycle results in an absolute unfeasibility of ~183 timesteps for an almost full occupancy scenario.

Arterial and Commuter driving cycles, are analyzed but are not included in the validation results since their registered unfeasibility percentage is higher than 10%.

4.2. Scenario and sensitivity analysis

The model validation allows to dive into the core part of the overall thesis job: utilising the validated tool to understand how different parameters impact on its output variables.

The developed tool is able to provide both total and single units consumption guaranteeing an overview on each condition that is analysed. This phase is very important in order to provide guidelines for further development of this tool or to exploit these results to orient investment in the different part of the bus.

Where it is not differently made explicit the radiation parameters are set as in Table 20.

Table 20: Baseline radiation parameters.

Radiation Parameter	symbol	value	u.o.m.
day	g	201	d
time	τ	12	h
longitude	long	-2	°
latitude	lat	48	°
central meridian of the time zone longitude	fu	-15	°

Results phase wants to underline the impact of:

- External temperature
- Passengers' occupancy
- Comfort temperature
- Road grade
- Driving cycle's aggressiveness
- Average deceleration and speed
- Geographical and temporal collocation

Most of the tests are performed on MB since it is the driving cycle with the best validation's results, considering the combination of a low percentage error on the total consumption (-0.67% and -0.51%) and the lowest infeasibility percentage (4.59%).

4.2.1. External temperature

The consumption coming from the thermal management of a bus throughout its route can be very impactful on the overall consumption of the bus. During extreme conditions, that fortunately are not that common, the HVAC and BTMS average power request is several times higher than the one at mild weather. In order to assess how external temperature can influence the requests coming from these two units and the total consumption, MB driving cycle with a fixed 30 passengers' occupancy is analysed. The choice of the geographical and temporal collocation is not specified but it is equal to the baseline case reported in Table 20. It may be stated that choosing a day of July (g=201) for analysing winter conditions is a mistake, but since radiation load is not considered for external temperatures lower than 21 °C this is acceptable. The trend for HVAC unit average power is reported in Figure 23.

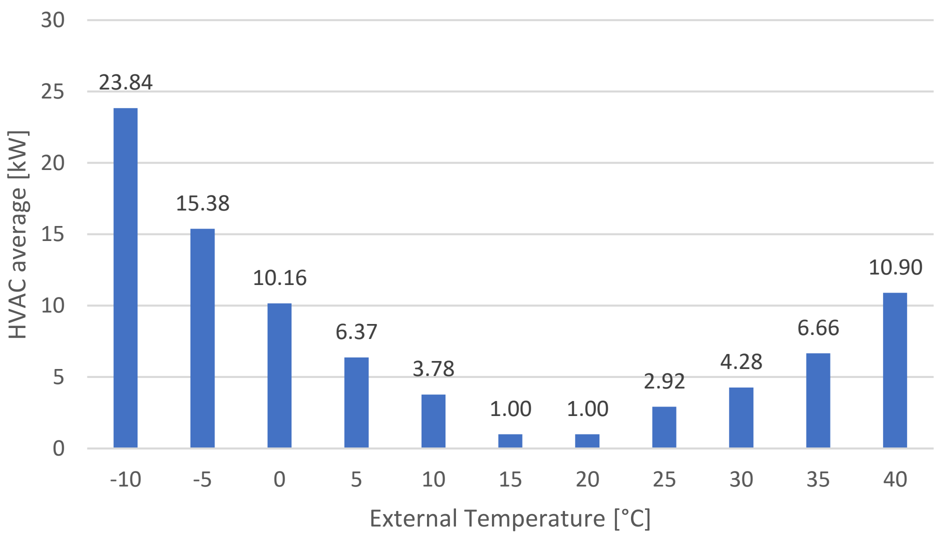

Figure 23: HVAC average power request for Manhattan Bus with different external temperatures and 30 passengers.

Varying external temperature between -10 °C and 40 °C, a specular behaviour between the heating and cooling mode can be observed. 15 °C and 20 °C behave as the centre of symmetry, where the HVAC is considered off and ventilation only is accounted for.

This pattern is not that precise since the cooling side has a less pronounced increase with the external temperature moving from the comfort temperature of 25 °C compared to the increase in heating mode with temperature decrease from 21 °C. During colder conditions the effect of temperature is more intensive especially for temperatures that are very far from the comfort temperature set to 21 °C. To heat the cabin with the freezing external temperature of -10 °C the request to the battery experiences a growth of more than 50 % of the previous value at -5 °C. This means that a deterioration of weather conditions, with temperatures becoming more rigid is worst for heating mode than for cooling. This is also due to the fact that the maximum distance experienceable between external temperature and comfort temperature is considerably higher in heating mode, with 31 °C for -10 °C and almost the half, 15 °C for 40 °C.

On the other hand, considering the distance from the comfort temperature as the basis for comparison, the average request for 35 °C that is 10 °C far from comfort is 6.66 kW while the equivalent for heating at 10 °C and 11 °C from the comfort is almost the half of it, 3.78 kW. This finds its explanation on the negative effect of radiation load, which is a constant penalty applied to all the timesteps of the cooling scenario and for the analysed geographical and temporal collocation accounts for 2.55 kW.

Taking into account the variation of the BTMS request over temperature in Figure 24, a similar trend to the one for HVAC can be seen but with the more extreme conditions having comparable values. BTMS request for heating has an almost linear growth with an important pendency between 10 °C and -10 °C with values ranging from 0.35 kW to 4.88 kW.

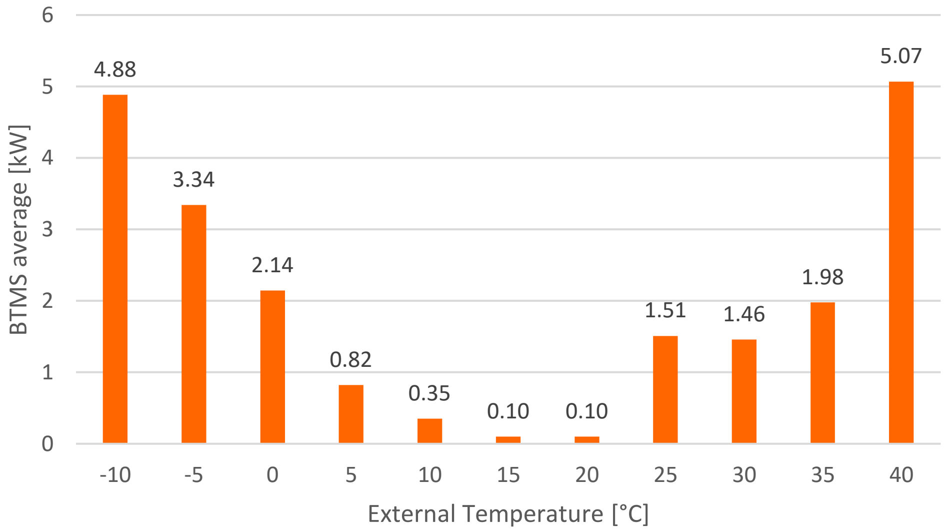

Figure 24: BTMS average power request for Manhattan Bus with different external temperatures and 30 passengers.

The cooling BTMS request experiences a great increase of 3 kW between 35 and 40 °C, while the values are similar between 25 and 35 °C. It can be noticed a slighter decrease after 25 °C, from 1.51 kW to 1.46 kW. The goal temperature for 25 °C of external temperature is set to 21.5 °C instead of the higher external temperatures where it is 25 °C. This is done in order to perform a reasonable cooling instead of keeping the battery at the same temperature as a result of a little temperature increase because of battery's operation and convection heat exchange with cabin air at ~25 °C. The additional temperature change ΔT_{add} is set at 7.5 °C like at 30 °C and the COP at 25 °C is 2.5 against 2.11 at 30 °C. The battery surface temperature in the two scenarios reaches the goal temperatures (which are different) in two similar timesteps, around 680 seconds. The BTMS power for each timestep where battery surface temperature is higher than the goal temperature is lower for 25 °C, ~1.835 kW against ~2.155 kW. These two aspects may lead to think that the second one should be higher on average, but it is not. The reason behind this slight difference is that once the goal temperature is reached less timesteps are needed where the BTMS is active for the 25 °C external temperature scenario, because when it works it pushes back the temperature to lower values. This more intense push keeps battery temperature lower than 21.5 °C for a higher number of timesteps once it has been reached once. So, BTMS power for active timesteps is higher for 30 °C case, but it has a lower number of active timesteps overall, and this results in a lower average BTMS power compared with the one of 25 °C of external temperature.

The effect of HVAC and BTMS average power changes on the total consumption of the driving cycle result in a more homogeneous graph with a more precise symmetry around the "ventilation only" centre, reported in Figure 25. The higher total consumption is detected at -10 °C and it is more than two times higher than the consumption at 15-20 °C. Then, for buses working at very cold climates, operating with the reversible heat pump configuration could not be the best available solution and choices with less penalty between ventilation only and rigid weather conditions must be thought. There is an important jump in terms of total consumption between -10 °C and -5 °C, with 4.83 kWh/km and 3.89 kWh/km respectively, and this is due to the sum of two similar behaviour in the HVAC and BTMS average power requests combined.

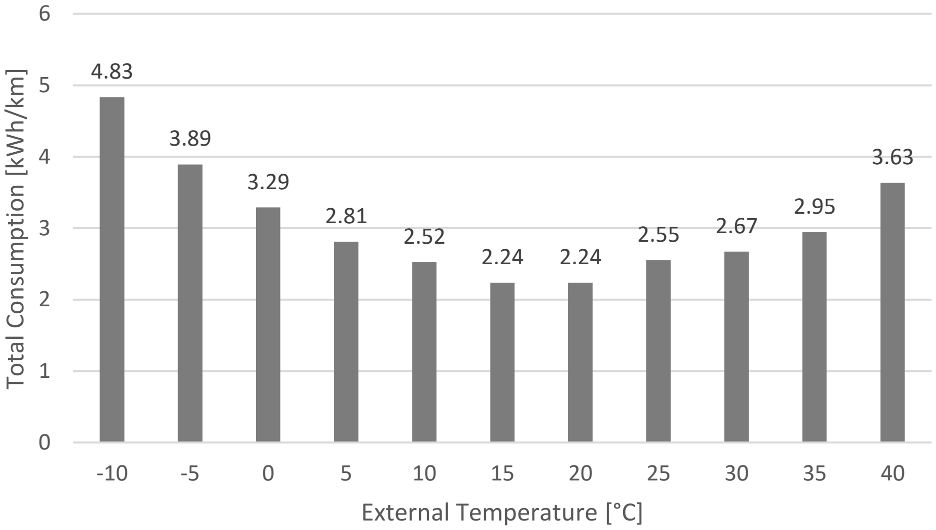

Figure 25: Total consumption for Manhattan Bus with different external temperatures and 30 passengers.

The thermal management effect on the consumption of the bus is not negligible and it has a paramount importance in the thermal comfort of the passengers, and then on the functionality of the public transport. On the other hand, the average power found out with our model are the worst possible one since cabin and battery initial temperature are set to the external temperature as the bus is operating at the start of the day or after a long pause standing still.

4.2.2. Passengers' occupancy

The number of passengers have an effect on different units of the bus, since it alters both the overall weight of the vehicle, affecting propulsion and auxiliaries, and the metabolic load contributing to the change of the HVAC energy consumption. The impact of different passengers' occupancy on the BTMS unit is negligible since the cabin temperature's transitory is almost the same between different passengers' level and then the BTMS energy consumption is similar. The variation of this parameter is analysed for 3 different levels of occupancy for the MB driving cycle:

- Low: 5 passengers
- Medium: 30 passengers
- Maximum: 55 passengers

Moreover, it is tested in different temperature conditions: -10 °C, 20 °C and 40 °C.

Starting from freezing conditions, the three varying contributions are shown in Figure 26

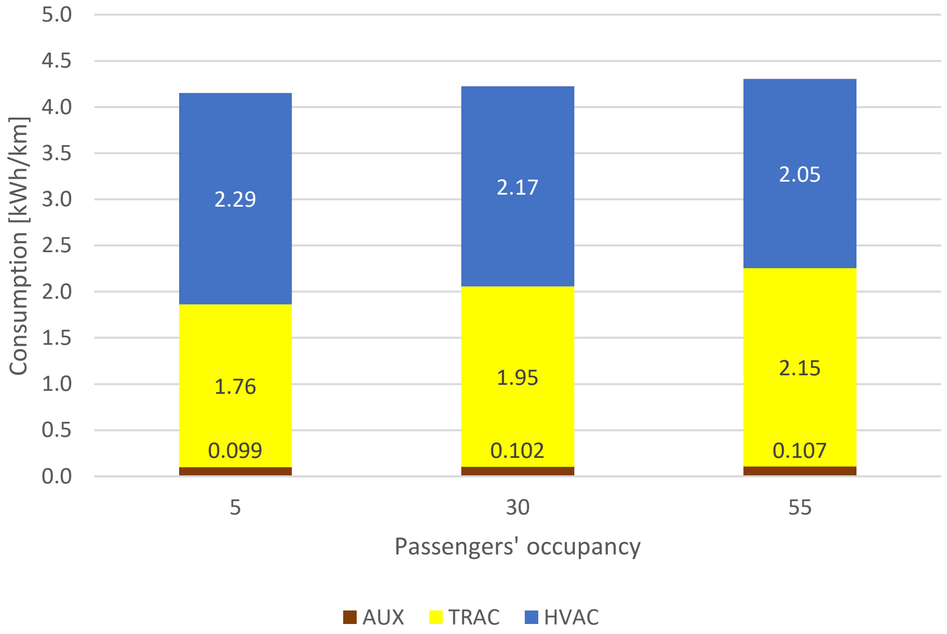

Figure 26: Units' consumption for Manhattan Bus with different passengers' occupancy at -10 °C.

Vehicle overall weight moves from 17.4 tons for 5 passengers to 20.8 tons for the highest passengers' level.

Auxiliaries consumes a negligible higher energy quantity of energy, and the increase is due to a higher mechanical braking power for heavier bus resulting in a bigger consumption for the air compressor. Their energy consumption moves from 0.099 kWh/km to 0.107 kWh/km which doesn't affect the overall consumption of the bus.

Traction contribution rises from 1.76 kWh/km to 2.15 kWh/km from low to high passengers' occupancy, which means an impressive increase of almost one fourth of the initial value. Vehicle weight is contained in all the power composing the traction power, excluded the drag one and this is the reason why it influences so much the final total consumption. The traction bars show the sum of the positive propulsion energy request and the negative brake energy recovery, which both grows with vehicle weight, but the positive one grows faster since an overall energy growth is experienced. Concerning the HVAC unit, the energy consumption decreases significantly from low to high occupancy because of the growing contribution of metabolic load. Hence this load helps reducing the overall positive AC to be furnished to the cabin since part of the heating is produced by the passengers themselves. For this reason, a higher presence of passengers on the bus is an advantage for HVAC energy consumption. The effect prevailing on the final consumption is the increase on the traction unit since it's more than one and a half times higher than the decrease in HVAC unit, 0.39 kWh/km against 0.24 kWh/km.

The resulting contributions for the analysis at mild temperature are shown in Figure 27.

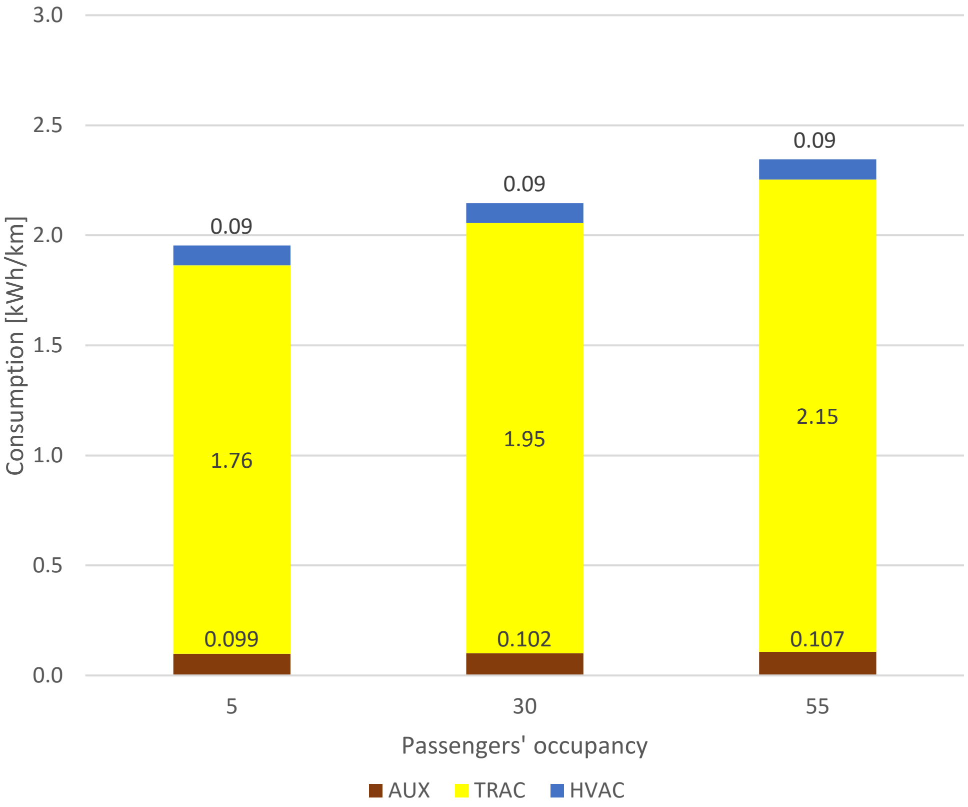

Figure 27: Units' consumption for Manhattan Bus with different passengers' occupancy at 20 °C.

For mild temperatures the HVAC is off and then has no influence on the overall consumption since it is fixed to ventilation only consumption for all the passengers' level. The behaviour of traction and auxiliaries is not influenced by temperature and then the way consumption changes, increasing the number of passengers, is the same for all the weather conditions. Since HVAC keeps constant in this scenario, there is no doubt that the energy consumption increases for higher passengers' number.

The final scenario analysed is at extremely hot temperature and reported in Figure 28.

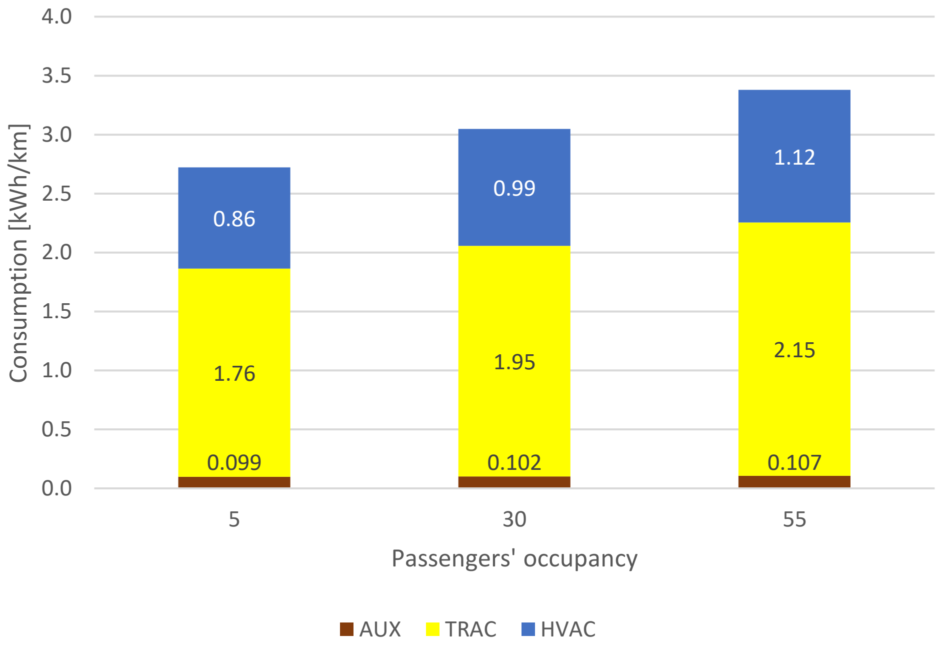

Figure 28: Units' consumption for Manhattan Bus with different passengers' occupancy at 40 °C.

The traction and auxiliaries behave in the same way as the other temperature levels, while HVAC changes in the opposite manner of the cold temperature case. The increase of passengers on board results in a higher metabolic load as previously but, in this scenario, it is a downside. This increasing contribution make the negative AC load rise since there is an additional heat produced in the cabin that needs to be removed. HVAC energy consumption switches from 0.86 kWh/km to 1.12 kWh/km in a 30% increase over its initial value.

This is the worst possible scenario since all the units consume more energy moving towards higher levels of occupancy and the overall worsening in the consumption of these 3 units of ~24% with respect to their initial sum.

Then, as a conclusion of this impact analysis we can state that the influence of passengers' increase is worsening the overall energy consumption for all the temperatures. At the same time the worst increase is experienced during cooling mode, because of the worsening in the energy consumption of all of the units.

4.2.3. Comfort temperature

The comfort temperature is the final goal that the climatization process has to persecute and for this reason its characterization is very important. The thermal comfort within the cabin affects the experience of the passengers riding the bus and the selected comfort temperatures for cooling and heating are taken inside two defined range as stated in 3.5:

- 21 °C for the 19-23 °C range
- 25 °C for the 23-27 °C range

The scope of this analysis is to understand how much the consumption for thermal units varies by shifting the comfort temperature whether to the upper or to the lower limits of the range both for cooling and heating, compared to the baseline case. These tests are performed on MB driving cycle, with 30 passengers and an external temperature of 40 °C for cooling and -10 °C for heating mode.

Starting from the cooling mode, the effect of shifting the comfort temperature to 23 °C produce an increase from 10.90 kW of the baseline case to 11.74 kW, due to the higher distance between the objective temperature and the starting point. Then, only 4 °C between the lower and upper limit of the range of comfort temperature produce a difference in terms of average needed power of ~1.7 kW.

The BTMS power request follows an opposite trend because the transitory has an average lower temperature for the lower limit and then it requires less power to cool down the cabin internal temperature for battery cooling purposes. This decrease is less intense than the increase in the HVAC, with less than one kW difference between the extremes. The graph in Figure 29 provides evidence of this.

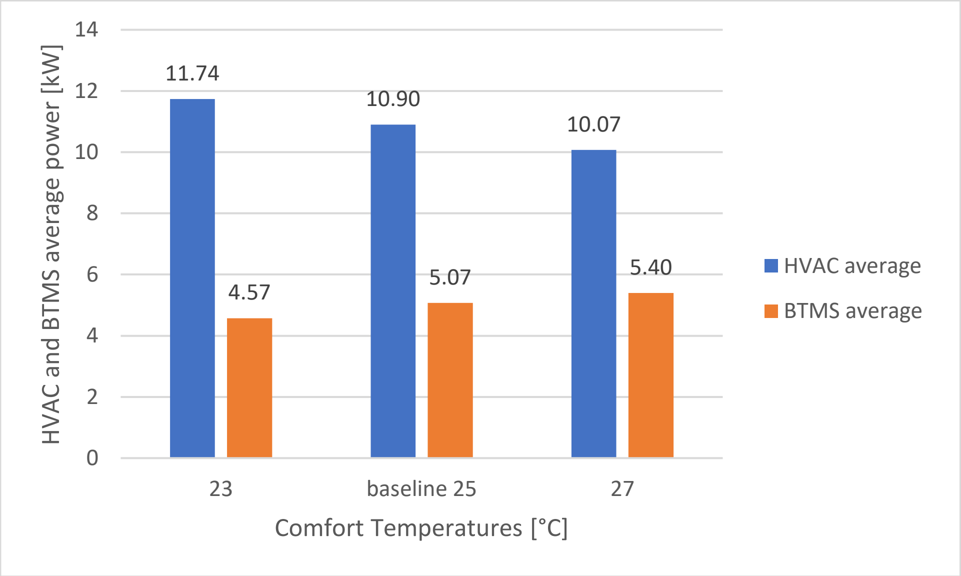

Figure 29: Thermal units' average power request for Manhattan Bus and 30 passengers with different comfort temperatures at 40 °C.

These opposite behaviours result in a decrease of the total energy consumption by more than 0.08 kWh/km by choosing the upper limit of the comfort temperature 27 °C as Figure 30 proves. This is interesting because by setting a goal temperature which is still part of a comfortable range, it can be experienced a ~2% reduction of the consumption with respect to the lower limit case.

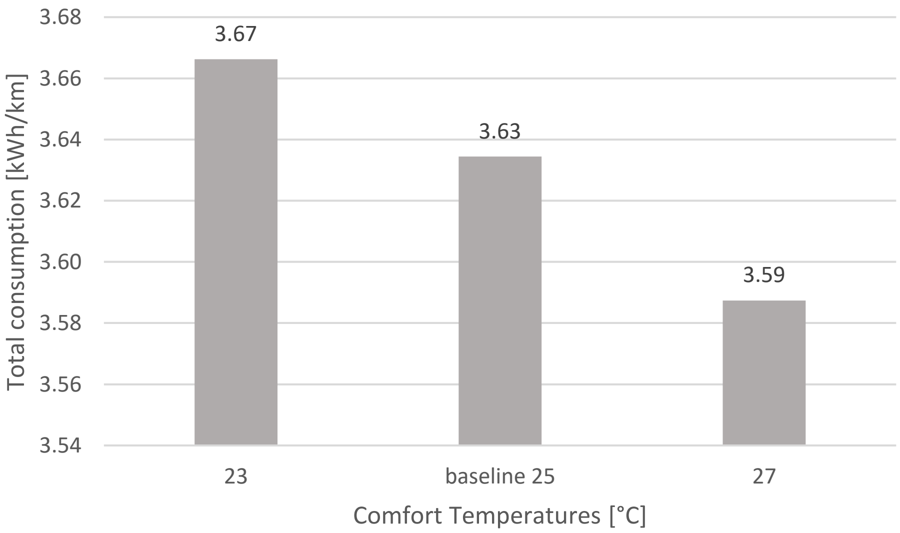

Figure 30: Total consumption for Manhattan Bus and 30 passengers with different comfort temperatures at 40 °C.

Considering the heating scenario, instead, the trend for HVAC is just the other way round as shown in Figure 31.

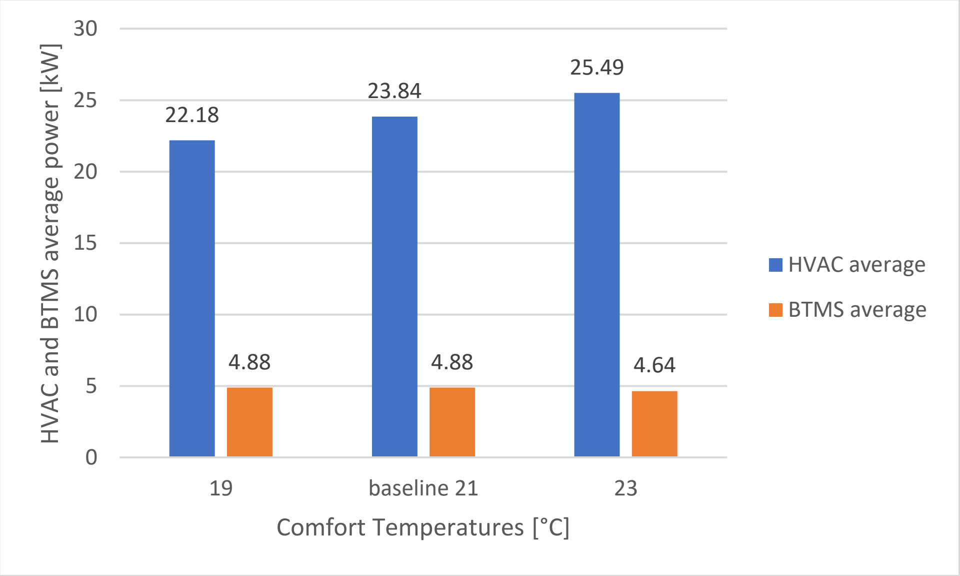

Figure 31: Thermal units' average power request for Manhattan Bus and 30 passengers with different comfort temperatures at -10 °C.

A higher comfort temperature corresponds to a longer path for the cabin temperature to reach it, hence a bigger average power request to the HVAC. The difference between the two limit scenarios is not negligible and is equal to 3.31 kW, two times higher than its equivalent in the cooling case. This is because heating mode requires more power in the extreme temperature scenario compared to the cooling one, and then the difference in absolute terms is higher. BTMS average power is the same for 19 °C and the baseline case because neither of the two battery surfaces temperature reaches the goal temperature of 17 °C before the end of the driving cycle. For 23 °C as comfort temperature the request is lower, and this is because the goal temperature is reached and then the active steps where BTMS actually works are less, reducing the average power of the BTMS. The values for BTMS power are very similar, hence there is no marked effect in changing the comfort temperature like in the cooling mode.

Moving from the lower to the upper limit of the range provides an increase in the total consumption of 0.28 kWh/km, that is higher in absolute terms of the cooling mode. This is due to the fact that BTMS power keeps being almost the same instead of reducing part of the effect on HVAC like in the cooling mode. The reduction percentage of the shift towards lower consumption is ~5.6% of the value for 23 °C comfort temperature. Total consumption's variation is reported here in Figure 32.

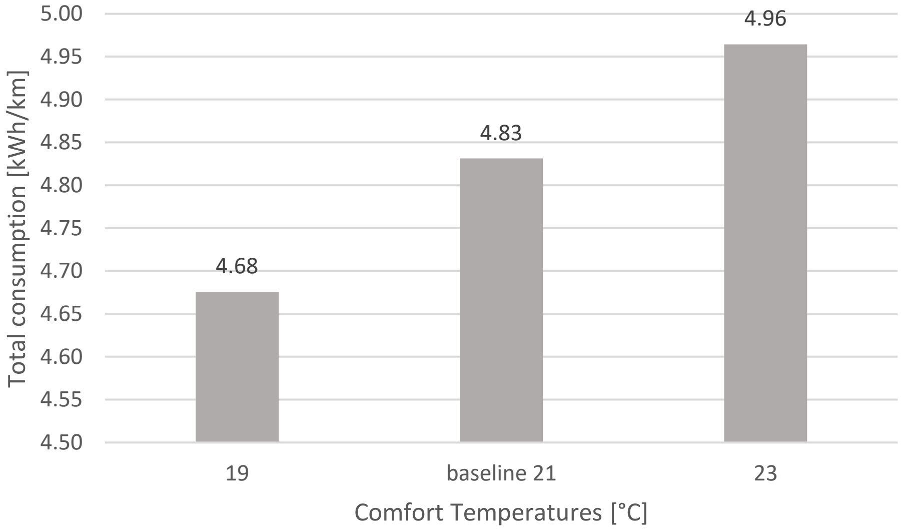

Figure 32: Total consumption for Manhattan Bus and 30 passengers with different comfort temperatures at -10 °C.

These can be seen as insignificant gains, but they are not since they are reached without sacrificing passengers' comfort or bus functionality. For this reason, moving towards less energy consuming comfort temperatures, hence higher for cooling and lower for heating, should be considered as a possibility to reduce overall energy consumption at zero price.

4.2.4. Road grade

During the validation testing and for all the different impact analysis performed in this section the road grade is kept constant and equal to zero. This is done because the information on the road grade for each timestep during all the analysed driving cycle is not available. In order to understand the effect of this parameter on the consumption of the bus, 5 different scenarios with a constant road grade are analysed: -1.5%, -1%, 0%, +1% and +1.5%. The chosen driving cycle is MB, with 30 passengers on board and at 20 °C. The assumption of a fixed road grade applied on every timestep is thought acceptable because the duration of the driving cycle, 600 seconds, that is short enough to think that the test is conducted on a realistic constant pendency path.

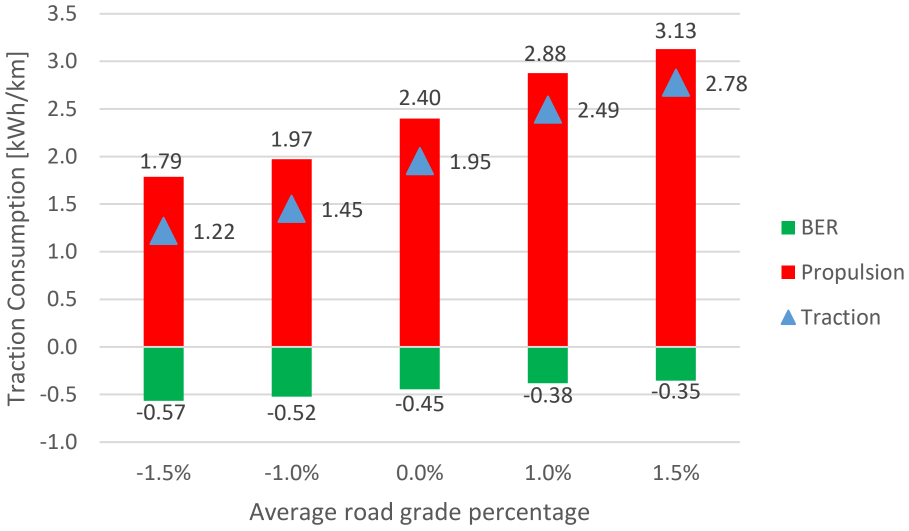

Figure 33: Propulsion and BER for Manhattan Bus and 30 passengers with different road grade at 20 °C.

Figure 33 shows the trend of the positive propulsion and negative brake energy recovery over pendency, including the baseline case at 0% road grade. It can be seen that the two series behave in two separate manners and the reason relies on the definition of two contribution to the traction power, both if it is propulsive and recuperative.

- Rolling power which depends on the cosine of the road grade angle
- Body power which is a function of the sine of the road grade angle

These powers are applied on every timestep and analysing their values on a random instant allows to understand why the propulsive energy trend is ascending.

The cosine of the road grade is equal for the positive and negative grade with the same absolute value, and it is positive for angles within the -90 ° and +90 ° range. Hence the rolling power is always an additional positive power for the traction power which is null only for the 0-road grade baseline. The highest value of rolling power is applied to the ± 1.5% road grade, and then the reason why the propulsion increases over pendency is not due only to rolling power trend, which has two peaks on the first and last tested scenario.

The sine of the road grade is negative for the negative pendency and vice versa for their positive equivalent. The most negative value is coupled with -1.5%, the most positive is with +1.5%, while is again 0 for the baseline case. The negative power of the body power contribution to -1.5% and -1% reduce the positive rolling power added and make them smaller than their positive equivalent. The baseline case is not affected by these powers' addition or detraction and then it keeps the baseline traction power and the consequent energy consumption. The +1.5% case results to be the most highly consuming because it receives only additional power by both the rolling power and the body power.

The mathematical explanation for brake energy recovery trend is the vice versa of the propulsive energy consumption one here reported. Intuitively speaking can be stated that the prevailing effect overall is the gravity that tends to push the bus in the opposite direction of the ascending route and favours its movement in the descending ones. The consequences of this effect are the increasing needed energy to move the bus uphill and the decreasing needed energy in order to break it, and consequently less energy recovered through the generator in the positive road grade scenarios.

The change in pendency from -1.5% to +1.5% produces an increase in the propulsion by ~75% of its initial value, while a ~39% decrease is experienced for BER.

The overall traction energy over pendency shows a prevalence of the propulsion increase over the BER decrease, since its trend is increasing.

The auxiliaries are influenced by the BER decrease because of the compressor presence and then, the compressor consumption decreases over pendency and the lowest value is in +1.5% road grade. The energy consumption of the compressor is almost split in half moving from the most descending road pendency to the most ascending one, having an important influence on the overall auxiliaries' consumption as Figure 34 proves.

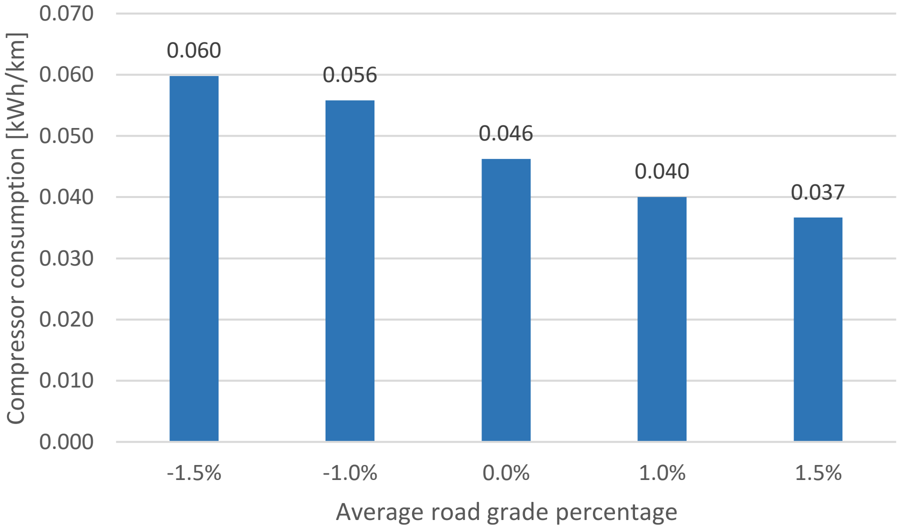

Figure 34: Compressor consumption for Manhattan Bus and 30 passengers with different road grade at 20 °C.

The impact of the road grade on the total consumption is impressive if compared to the most common urban road grade equal to none. A positive pendency of +1.5% gives rise to a worsening in the total consumption of almost one third of the plane road scenario one as shown in Figure 35.

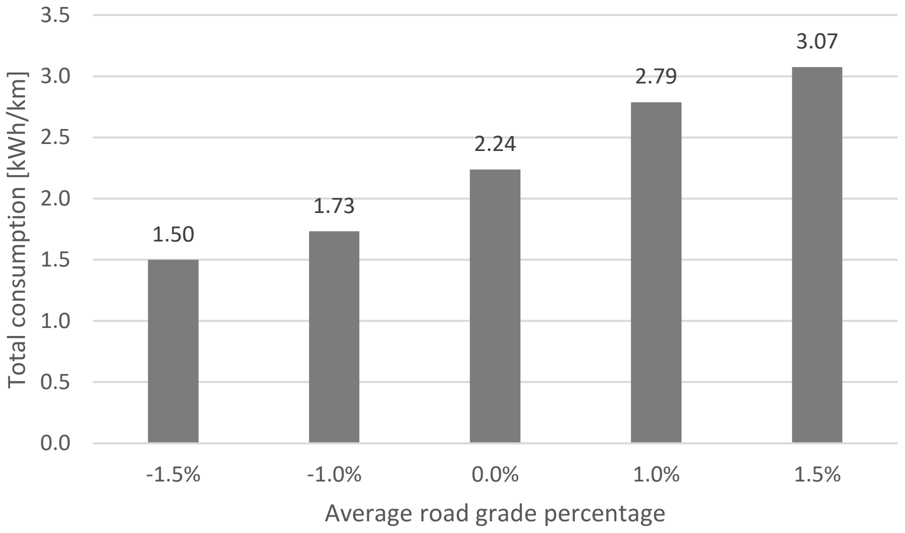

Figure 35: Total consumption for Manhattan Bus and 30 passengers with different road grade at 20 °C.

As a final statement, can be said that knowing precise road grade for every timestep can lead to a better definition of the total consumption and avoid considering unfeasible peaks during the driving cycle.

4.2.5. Aggressiveness

The different driving cycles are characterized by many factors like the average speed, the average deceleration and the idle time (the time where the bus is not moving). Besides all these parameters there is one that accounts for the way driving occurs during the route: aggressiveness. This parameter, calculated as follows, considers the impact of positive acceleration over the total distance. The + subscripts in the formula underline that only positive accelerations and their corresponding velocities are accounted. The aggressiveness is dimensionally equal to an acceleration.

$$A = \frac{\sum a_{+} * v_{+} * ts}{d_{tot}} \tag{71}$$

The analysed driving cycles during validation phase have different characteristics and they can be tested, with 30 passengers and at 20 °C, in order to detect the impact of the aggressiveness on their traction, auxiliaries and overall consumption. The route’s aggressiveness is strictly correlated with the number of stops, since positive accelerations are very frequent and intense where multiple restarts are performed. Moreover, a shorter route have a lower denominator and then, have a bigger consumption in terms of kWh/km if compared to a driving cycle consuming the same amount of energy but with more kilometres travelled.

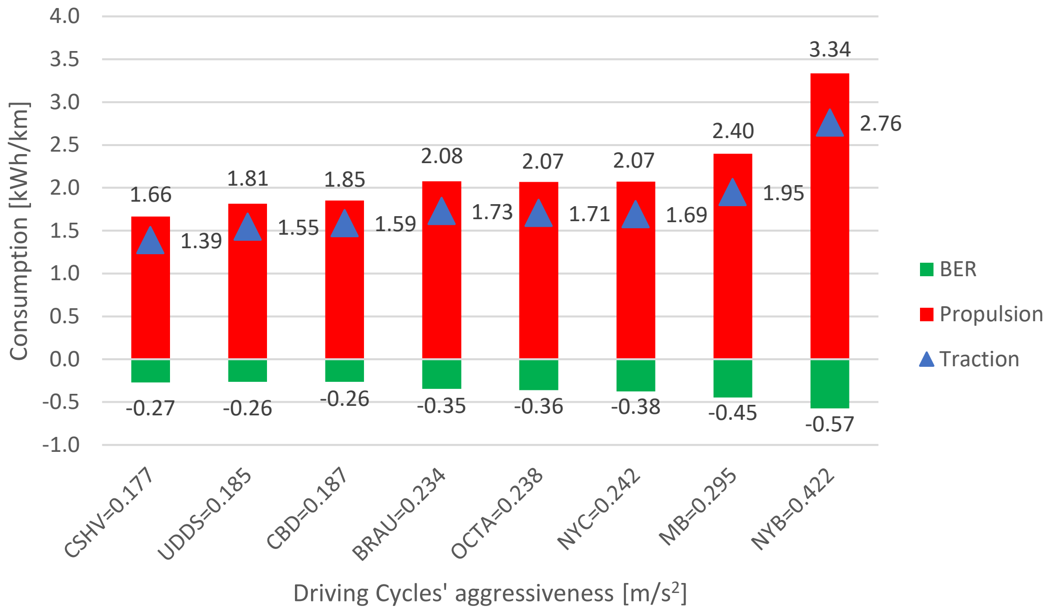

Figure 36: Propulsion and BER for different driving cycles and 30 passengers at 20 °C.

Figure 36 underlines the composition of the traction energy consumption, divided into positive propulsion and negative brake energy recovery, for different driving cycles with their aggressiveness reported.

At a first glance can be seen that there seems to be a correlation between driving cycle’s aggressiveness and energy consumption in kWh/km, with the highest value detected for New York Bus. Moreover, similar aggressiveness result in very near energy consumption also for routes with very different travelled kilometres. For example, UDDS and CBD have an almost equal aggressiveness and consumption composition but they have respectively 11.99 km and 3.29 km as distance parameter. This allows to understand that driving cycle aggressiveness sets the type of drive and its range of consumption, independently by the number of kilometres travelled.

It is true also for a higher level of aggressiveness, as can be seen for the triplet of driving cycles: BRAU, OCTA and NYC. They have comparable aggressiveness, and this can be recalled in an almost equal energy consumption for the traction, although the first two travel ~11 km and the third one only 4.04 km.

The impact of aggressiveness is particularly evident if confronting the lowest consuming driving cycle, that has the lowest aggressiveness, CSHV, with the highest consuming route with the highest aggressiveness NYB. CSHV has less than the half of NYB aggressiveness and this reflects in an almost perfect half of its consumption, 1.39 kWh/km against 2.76 kWh/km. Of course, an increase in the propulsive energy is accompanied by a higher energy recovered during the route, and this is due to the fact that frequent positive accelerations are often forerun by decelerations, where BER comes into action. The results on the impact of aggressiveness on the auxiliaries consumption are outlined in Figure 37.

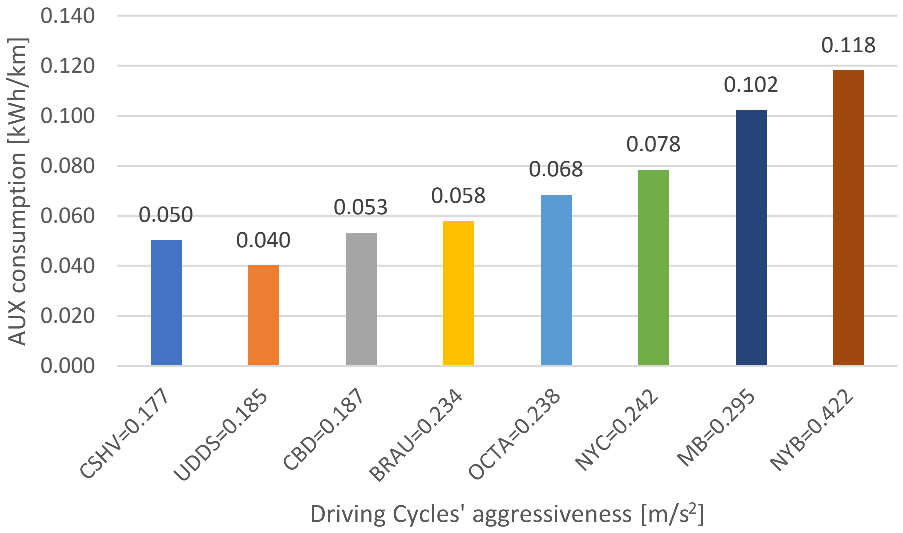

Figure 37: Auxiliaries consumption for different driving cycles and 30 passengers at 20 °C.

Concerning the auxiliaries overall consumption, the correlation still stands, since the largest contribution is due to air compressor, which is dependent on the braking of the bus. Hence, the growing of the brake energy recovered shifting towards higher aggressiveness is also an index of an increasing brake energy to be handled by the mechanical brake. As the graph shows, higher driving cycles' aggressiveness results in a higher consumption from the auxiliary side. This general rule is not respect by the initial values for CSHV and UDDS, even though the values are acceptably low. A possible explanation for this observation is that auxiliary consumption is very low and then the fact that UDDS travels ~1 km more than CSHV can have an impact on the consumption expressed in kWh/km, although CSHV has a higher aggressiveness. The highest consumption for the auxiliaries is again the one related to the NYB driving cycle, just like it is for the traction. In this field, the proportion between the most consuming driving cycle (NYB) and the least one (UDDS), is even more marked, since it is almost four times higher.

This analysis grants a proven correlation between the pervasiveness of positive acceleration within the driving cycle and the consumption of the traction of the bus. Aggressiveness can be reduced by shaping differently the route in terms of number of passengers' stops, allowing less starts and stops, having important impact on the overall bus consumption. It can be especially true for urban driving cycles where a consistent number of additional stops may rise during congested traffic situation, that are unavoidable.

4.2.6. Auxiliaries consumption composition

Another interesting focus is carried on auxiliaries' unit for a better understanding of the influencing parameters of bus's consumption. The way this unit consumes is often neglected, setting a constant value of power requested throughout the driving cycle in any condition. The goal of this thesis is a more accurate definition of every consuming component and for this reason, analysing the output of each auxiliary for the different driving cycle is an on-point examination. The auxiliaries are not influenced by external temperature and the driving cycle are tested with 30 passengers on board.

Figure 38 here reported shows how much the auxiliaries' consumption can vary from one route and another and each overall value is shown on top of each stacked column. The single consumption of each auxiliary is not reported for the sake of clarity of the graph but a clear understanding of the proportion between them and an approximative idea of their dimensions can be grasped.

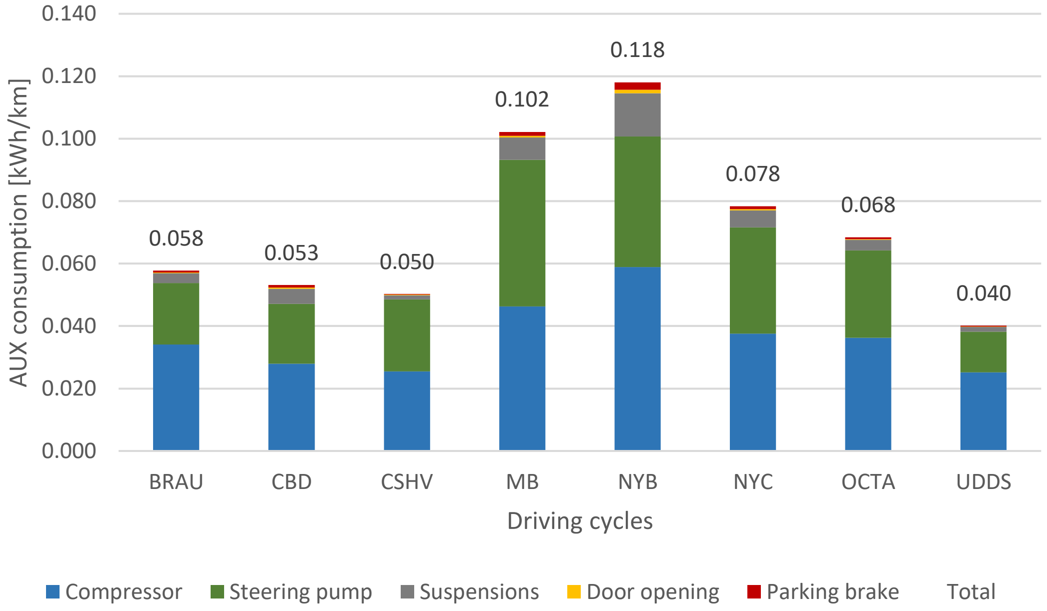

Figure 38: Auxiliaries consumption composition for different driving cycles and 30 passengers at 20 °C.

In 4.2.5 has already been shown the total consumption of the auxiliaries for each driving cycle, but it is interesting to understand that the prevailing contributions to that value are the one coming from the compressor and the steering pump. These two consumptions are almost in a 1 to 1 ratio between them for all the driving cycle a part for some exception where the compressor is slightly predominant. The other three auxiliaries are all related to the bus stops' operation: the suspensions, the parking brake and the doors' opening. The most consuming between these three are suspensions since the amount of vehicle weight that have to lift is considerable. Each of these auxiliaries consume the same amount of energy for each of the bus stop, throughout the route and this is why they have the same proportion between them for all the different driving cycles. Their sum, hence, the contribution they provide to the total consumption depends on the number of bus stops per kilometre that characterize the driving cycle. The proof of this dependency can be found in Figure 38, the largest contribution for these three components is the one of the NYB, while the lower one is for BRAU. The first one performs 12 stops for ~1 km of route travelled, while the second one, even though has a similar number of stops, 13, has 1.208 stops/km, and this 10 times difference is evident in the bus stops' consumption.

Aggressiveness has proven to have a clear influence on the consumption of the auxiliaries and for this reason another two analysis are performed in order to find similar correlations for other driving cycles' characteristics.

First of all, the compressor consumption is confronted with the growing average deceleration characterizing the driving cycles as outlined in Figure 39.

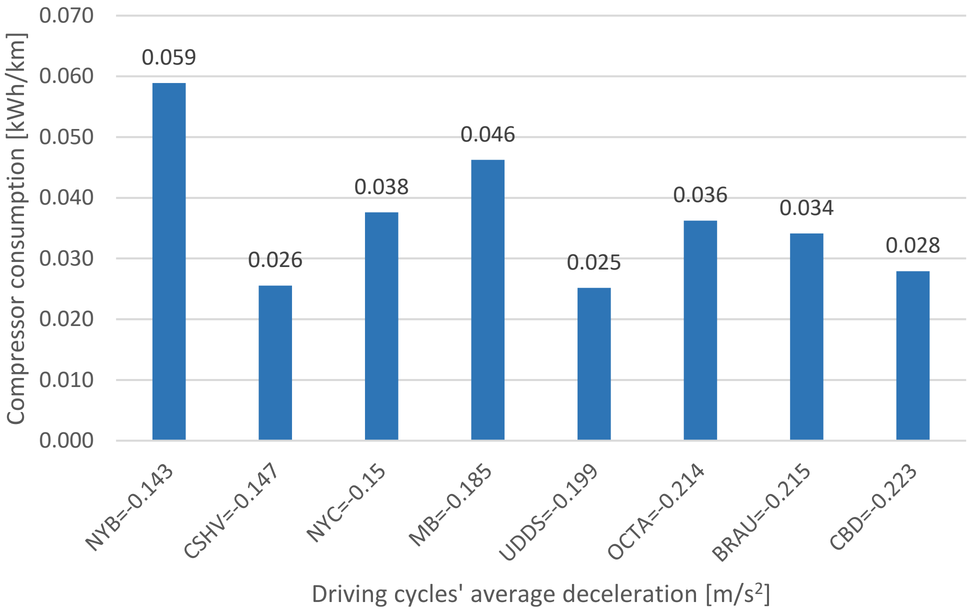

Figure 39: Compressor consumption for different average deceleration and 30 passengers at 20 °C.

The average deceleration range is not that wide and moves from 0.143 m/s^2 for the NYB and the 0.223 m/s^2 of the CBD route. A sort of general rule can be seen: the compressor's consumption decreases with the increase of the average deceleration. The reason behind this general rule is that driving cycle with higher average deceleration happens to have less frequent stops, and then when the bus performs one, starts from higher velocities and needs to break more. This results in lower consumptions of the compressor since braking occupies less time of the overall driving cycle and with less intensity. For NYB instead the high number of stops per km involves a continuous use of the brake with low average deceleration and this explains why it is the most consuming one. On the other hand, CSHV, NYC and UDDS driving cycles seems to not follow the general rule, hence, can't be undeniably stated that there is a correlation between the average deceleration and compressor consumption.

Concerning the steering pump consumption, a possible dependency from the average velocity is searched, because of the way this auxiliary has been defined in 3.3.2.

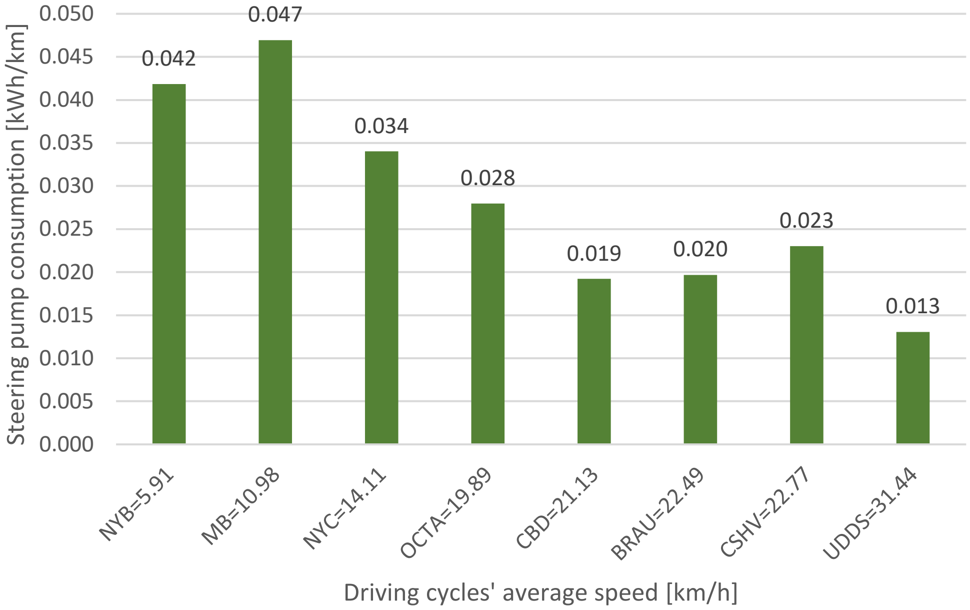

Figure 40: Steering pump consumption for different average speed and 30 passengers at 20 °C.

The average speed has an important span since it varies from 5.91 km/h for NYB to 31.44 km/h for UDDS, showing very different type of driving cycles. Just as in the previous analysis, a descending trend in the steering pump consumption with the increase of the average speed can be detected in Figure 40, but few tests do not follow it.

This trend finds its origin on the fact that steering pump is defined in order to consume more during the part of the path where the velocity is close to zero. At the same time, the average velocity is calculated considering also the timesteps when the bus is still, and speed is 0 and then the steering pump consumption is null. This is the reason why the searched link is not universally valid.

Having a wider look to this analysis, it shows that driving cycles are a complex instrument and it is difficult to characterize them by referring to just one variable. The whole information must be possessed in order to provide more precise answers on the dependency between driving conditions and the output variables of the model.

Concluding this focus can be said that, generally speaking, urban driving cycles with very high number of stops per km, fragmented drive style and a low number of km travelled tend to be very much penalized in the auxiliaries’ consumption with respect to other kind of routes.

4.2.7. Geographical and temporal collocation

The model presented a detailed determination of the radiation load, with the possibility to insert different time of the day, different day of the year and different geographical location. For this reason, the last scenario analysis performed intends to understand the importance of the radiation load in the total consumption definition and how impactful the variation of its settable parameters is. The analyses are carried on with the same methodology for the three varying parameters, keeping the other ones fixed and showing: the radiation load, the HVAC average power request and the total consumption in all the different cases.

First of all, the influence of the time of the day is searched by testing the MB driving cycle, at 30 °C with 30 passengers on board and at the baseline geographical and temporal location. Five different moments of the day are tested: the night-time, the morning at 8, the middle of the day at 12, the afternoon at 16 and the evening at 20. The results for the radiation load are shown in Figure 41.

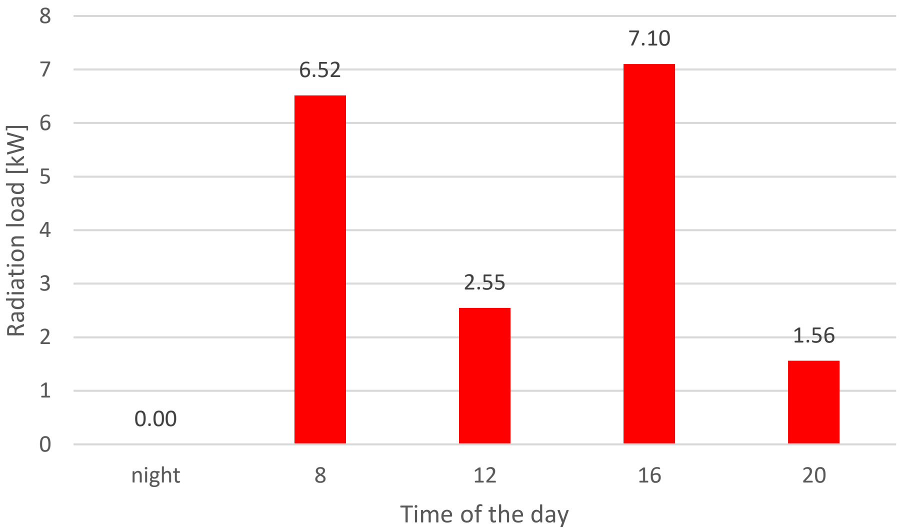

Figure 41: Radiation load for Manhattan Bus and 30 passengers at 30 °C over different time of the day.

Of course, the load during night-time is null, since no radiation is present, while the evening one is low since the sun is very low on the horizon. The radiation contributions during afternoon and morning are comparable and that is because the majority of the sun rays hit the sides of the bus which have very similar ratio in terms of material composition between them. It may seem surprising that the radiation at midday is lower than during afternoon and morning, but it depends on the definition of the radiation load. In facts, during midday, the radiation hits prevalently the roof of the bus, that is made of vehicle body only and then has 0-

trasmittance. The 2.55 kW radiation load is made by the part of the radiation hitting the rest of the opaque sides of the bus.

Figure 42 underlines how this difference in radiation load impacts the HVAC average power request for the five different moments.

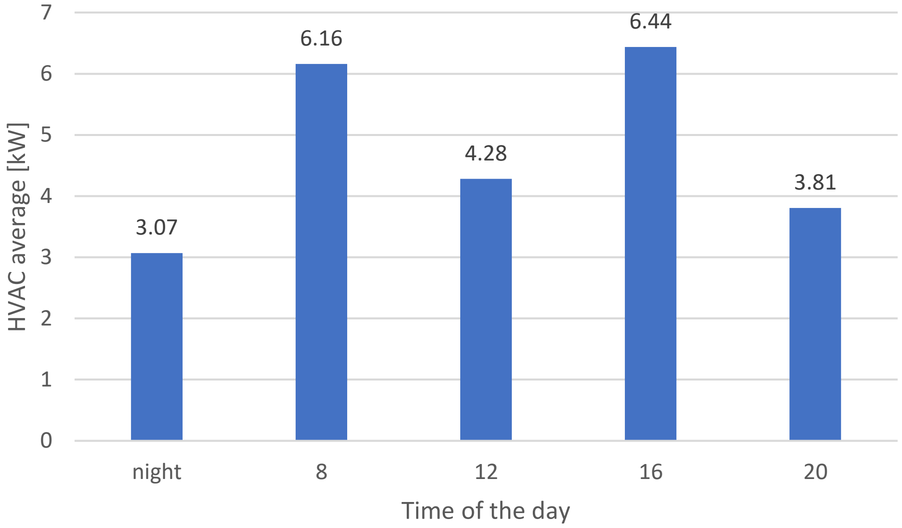

Figure 42: HVAC average power for Manhattan Bus and 30 passengers at 30 °C over different time of the day.

The lowest value is experienced, of course, during night-time, where the penalty due to the radiation is not present. The similar radiation load couples, 8 and 16, and 12 and 20, reflects in a similar power of the HVAC unit as predictable. The worsening effect due to radiation consist in more than doubling the average power request as can be seen by confronting the lowest case, 3.07 kW during night, and the highest one, 6.44 kW for the afternoon.

The core of this analysis is to understand how, setting the correct time of the day, influence the total consumption, since it is the final prediction of the tool and the most interesting one. The answer to this question is synthetized in Figure 43.

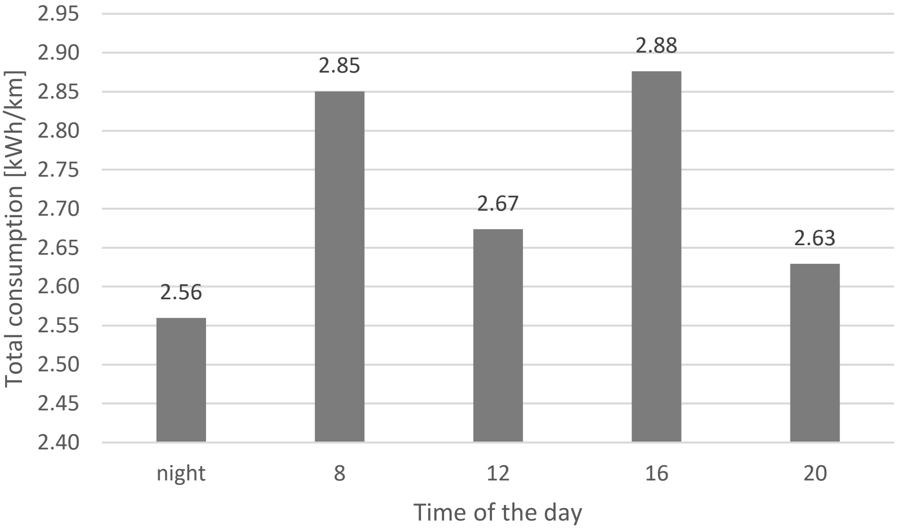

Figure 43: Total consumption for Manhattan Bus and 30 passengers at 30 °C over different time of the day.

The total consumption for the different time of the day stands between 2.56 kWh/km, and 2.88 kWh/km, meaning that a ~13% variation is experienced in confronting the highest consuming time of the day and night-time, that is the equivalent of not considering the radiation. This variation is similar even if confronting the lowest consuming moment of the daytime at 20, with a ~10% increase in the consumption. Then, neglecting radiation load or setting an incorrect time of the day value can lead up to a maximum ~10% error, which acceptability depends on how precise the prediction wants to be.

Radiation has different intensity over the year, and a clearer understanding of how impactful this difference is, on the output variables of the tool is at the basis of the second analysis performed.

Concerning the time of the year, keeping all the other parameters equal during the analysis is impossible, since different seasons are characterized by different average temperatures. The testing is carried on, considering four days, at midday, with the same passengers' occupancy equal to 30, and for the same baseline location.

The days are accompanied by a typical temperature in order to perform a realistic HVAC definition for the season selected. The typical days are summed up in Table 21.

Table 21: Typical days.

Season	**g**	**To [°C]**	**label**
Winter	21	5	W5
Spring	111	15	S15
Summer	201	30	SU30
Autumn	291	10	A10

The radiation load value, at midday, ranges between 2.06 kW for Autumn and 2.83 kW for Winter, entailing a ~37% variation moving towards the highest value. The analysis aims also at detecting the impact of not considering radiation for the temperature under 20 °C. Hence, for Winter, Autumn and Spring seasons, the null value for radiation load is reported also in the graph. The radiation contribution is not considered in the baseline model because of the high quantity of cloudy days during seasons other than Summer, but Figure 44 shows how relevant radiation can be, considering the analysed day as sunny.

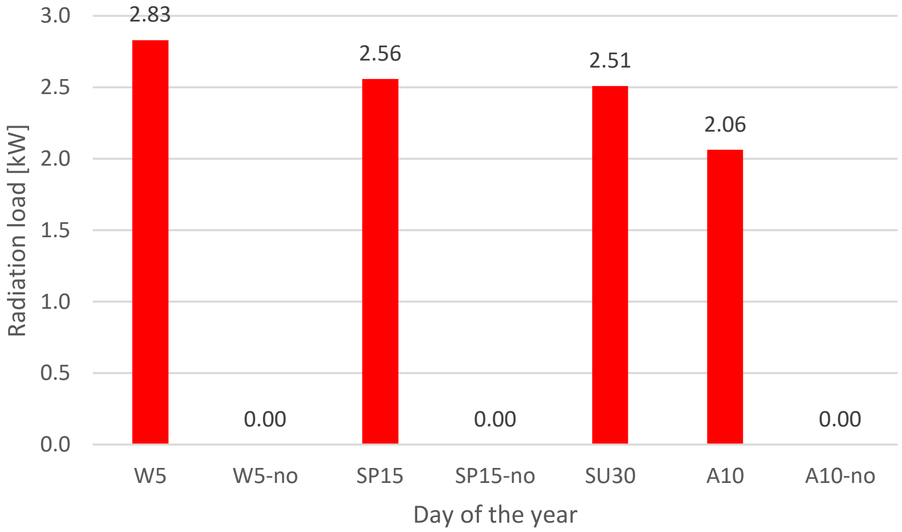

Figure 44: Radiation load for Manhattan Bus and 30 passengers over different days.

The seasonal effect of radiation load, joined with the external temperature characterizing the tests, gives rise to the HVAC average power distribution reported in Figure 45. The interesting aspect is that since temperatures are lower than 20 °C, not considering radiation consists in a penalty for the HVAC, since there is no radiation load introduced reducing the amount of heat to be furnished to the cabin.

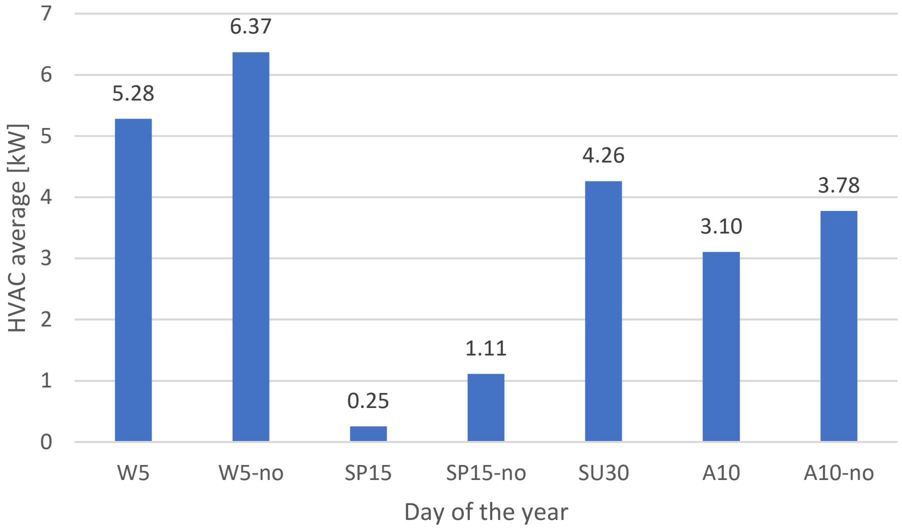

Figure 45: HVAC average for Manhattan Bus and 30 passengers over different days.

The HVAC average power is mainly influenced by the external temperature, but it can be appreciated how impactful the radiation neglection can be on its outcome. For example, HVAC average power for Spring is more than four times higher without considering the help from radiation in SP15-no against SP15.

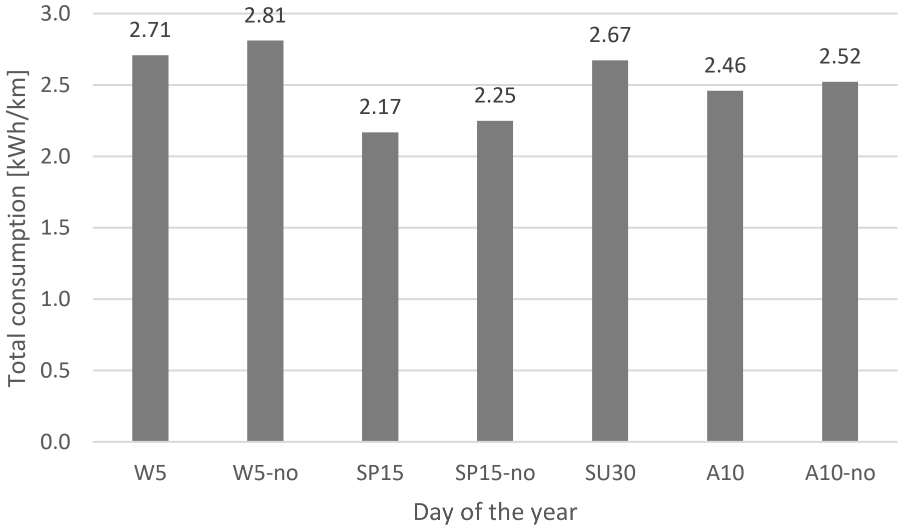

Figure 46: Total consumption for Manhattan Bus and 30 passengers over different days.

The seasonal effect on radiation load, and the impact of considering radiation, loses part of its intensity by looking at the total consumption for the different typical days in Figure 46. The values switches between 2.81 kWh/km for the worst case, W5-no and 2.06 kWh/km for SP15. But this difference is due to the external temperature difference and this analysis has already been performed in 4.2.1. Concerning the impact of not considering the radiation, the maximum change in absolute value is the one for winter, 0.10 kWh/km, which is the season above all, where the sun is less likely to be present.

In light of these considerations, not considering radiation load for temperature lower than 20 °C, typical of the season other than summer, is an acceptable assumption, and knowing the exact time of the year, to have a precise radiation load definition is not impactful on the final outcomes of the software.

Another changeable parameter is the geographical collocation of the place where the tool is tested, by setting its coordinates. The tests are performed on MB driving cycle, with 30 passengers on board, at 30 °C and the location is changed simulating six different cities: Paris, Amsterdam, Milano, Oslo, Roma and Tripoli reported in Table 22.

The simulations are performed keeping the same hour of the same day, τ=12 and g=201, in order to have comparable conditions for all the analysed cities.

Table 22: Cities' coordinates.

City	Longitude	Latitude
Paris	-2.32	48.86
Amsterdam	-4.89	52.37
Milano	-9.19	45.47
Oslo	-10.75	59.9
Roma	-12.48	41.91
Tripoli	-13.18	32.89

As in the previous analyses the first step consists in having a look at the different radiative loads for the different conditions, shown in Figure 47.

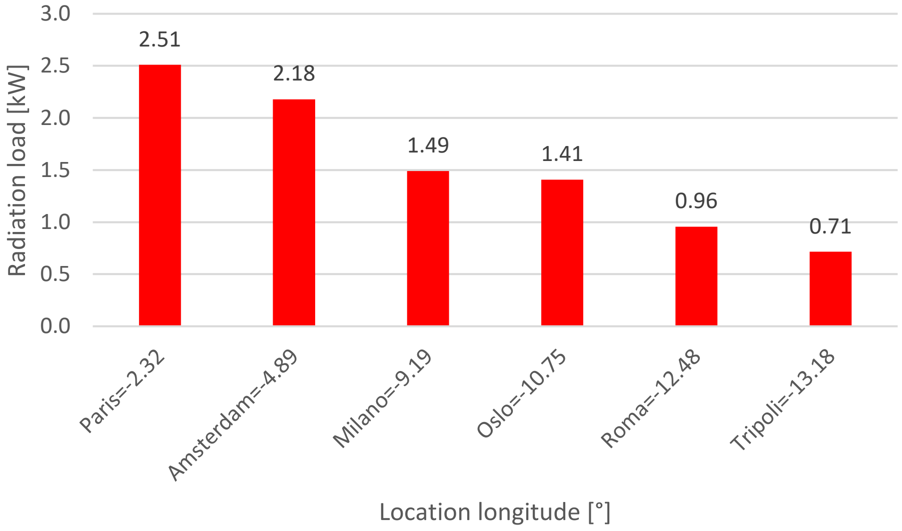

Figure 47: Radiation load for Manhattan Bus and 30 passengers over different locations.

A precise correlation between the location's longitude and the radiation load can be detected, with the highest radiation load for Paris being 2.51 kW and the lowest for Tripoli at 0.71 kW. This means that in terms of radiation load, an almost 2 kW error can be committed in not considering the place's coordinates.

This mistake reflects in a HVAC average power request of 4.26 kW for Paris against a 3.41 kW one for Tripoli, as reported in Figure 48.

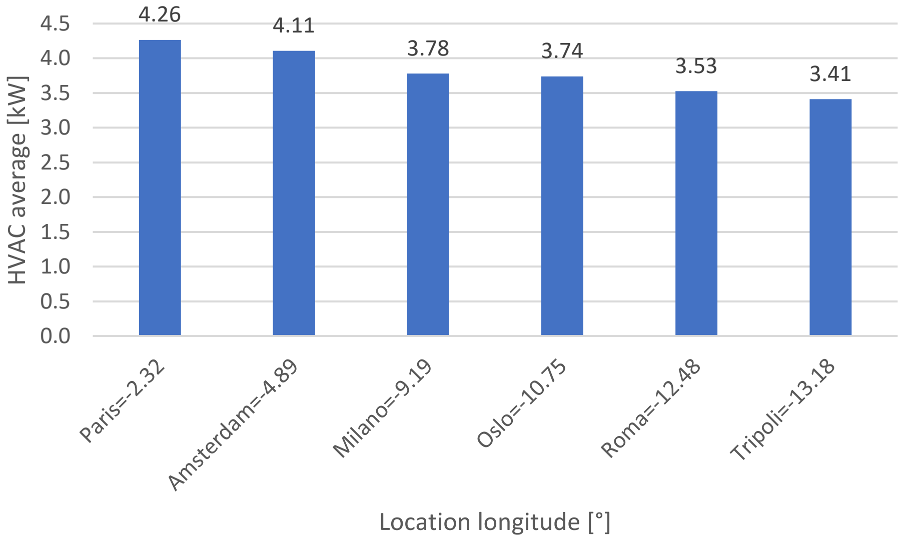

Figure 48: HVAC average power for Manhattan Bus and 30 passengers over different locations.

The final outcome of this analysis is the effect of the varying parameter, in this case, coordinates, on the final consumption. The highest consumption for Paris is 2.67 kWh/km, while the lowest for Tripoli is 2.59 kWh/km, resulting in a worst-case scenario error of 3%.

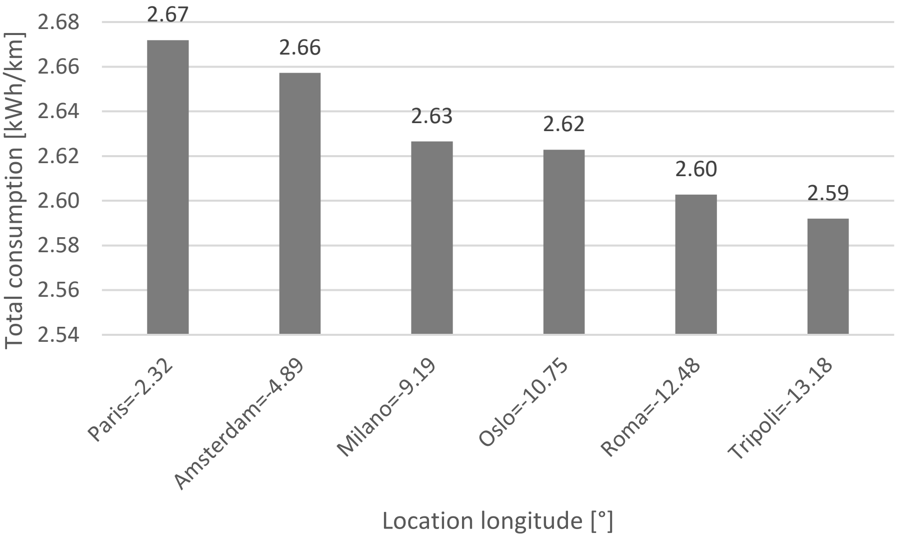

Figure 49: Total consumption for Manhattan Bus and 30 passengers over different locations.

Taking into consideration the different locations is not impactful on the total consumption definition, also because the radiation load follows the same pattern for all the different cities, just not at the same time of the day.

5 Conclusions

The activities carried out in this thesis consisted in the extension of an already existing Lumped Parameters' Model (LPM) conceived for estimating passenger car consumption to electric buses. The model covers electric vehicle powertrains enriching the software by all those components and systems buses are equipped with.

The consumption simulation tool is modular and is mainly consisting in four different blocks and it deals with vehicle's longitudinal dynamics, heat and ventilation air conditioning (HVAC), auxiliaries and battery thermal management system (BTMS). As an input for the model can be reported the specifications of the vehicle and of its additional components, the driving cycles to be examined, the external temperature, the desired comfort temperature and the solar radiation parameters (time of the day, day of the year and place in the world). The outcome of the model contains the consumption of each single component concurring to the final energy consumption as well as the overall one, each of them expressed in kWh/km.

The starting point in order to reach the goal was the analysis of the existing models to understand where the state-of-the-art stands and which possible methodological choices could be taken. The literature review process' findings were that most of the models had the same backward facing approach concerning the longitudinal dynamics and that many of them did not provide specifications on the auxiliaries and thermal units sides. The possibility to offer a complete consumption overview was sacrificed for the sake of a reduced complexity in these papers. The impact of temperature on HVAC and BTMS and of the driving conditions on the auxiliaries were neglected. A fixed average power with different values for each paper was set under the voice of "auxiliaries" instead.

The chosen methodology for the proposed model followed the literature concerning the vehicle dynamics, with a backward facing approach, accounting also for the motor/generator variable efficiency and fixing a limit to recoverable energy from braking. Thermal transitory modelling was persecuted for the HVAC system, with a Heat Balance Method approach to find all the concurring thermal loads. BTMS was shaped as an additional consumption to the HVAC, aiming at a final goal temperature for the battery surface. Auxiliaries was considered as a mix of fixed and variable contributions to the final consumption instead. The researched level of complexity and completeness allows to the simulation tool to be flexible and able to shape multiple scenarios. by changing some of the input parameters. On one hand, a possible downside of this model is the high number of variables needed as can be clear from 3. On the other hand, these variables are very similar for each of the electric bus operating in the public transport, contrastingly with what happens in the automotive industry. Then, the complexity in the input's determination of the tool is an annoying but manageable aspect but allows a completeness level of the outputs that is not available in this field's literature. The second part of this thesis followed the guidelines undertaken to develop the model in Python language.

After the model was created, it needed to be validated, in order to be considered reliable and scientifically reasonable. The validation was carried on comparing the total consumption and average power request of the HVAC and BTMS units of different driving cycles taken from the National Renewable Energy Laboratory website. The outputs of the tool were confronted with the results' graphical representation coming from the Basma et al. [8].
The tests were performed with different levels of both passengers' occupancy and external temperature in order to have a model validated for different conditions.
This process was successful both on HVAC and BTMS validation, and on the total consumption ones. The percentage errors experienced in the validation of the thermal units were always under the 10% limit except for two cases. The worst one is the average power request for BTMS at 10 °C, where the percentage error is 75% but the actual difference is only 0.15 kW.
The validation for the total consumption was even better since no percentage error higher than 10% was detected and the worst error found was the 8.71% for the NYC driving cycle in the extreme conditions of 55 passengers and -5 °C.
The model demonstrated to be solid to temperature and passengers' variation and it performed well in all the analysed driving cycles with the majority of the detected percentage errors below 5% threshold.

The last phase of this work contains the scenario and sensitivity analysis where the possibility of changing the input parameters of the model were exploited in order to determine their impact.
First of all, the external temperature was proven to have a massive impact on the total consumption of the bus with the output at -10 °C being more than two times higher than the HVAC off scenarios at 15-20 °C.
The passengers' occupancy influence was examined at three different levels of temperature, and besides all three of them resulted in an increase of the final consumption with the increase of this parameter, the worst scenario was detected

for 40 °C of external temperature. This is due to the fact that, not only traction consumption is increasing but also HVAC's one because of the growth in the metabolic load to be expelled from the cabin.

Comfort temperature variation was varied within its acceptable range and a 2% and 5.6% reduction in the final consumption shifting between the two limit temperatures, respectively for the Cooling and Heating mode. These may seem negligible gains, but they become interesting since the comfort of the passengers wasn't sacrificed to reach them.

Road grade impact was tested with positive, null and negative pendency, and the total consumption predicted at +1.5% is double with respect to the one at -1.5%. By the way, is improbable to have a constant pendency in the city but this scenario analysis was helpful in order to state that very different output in consumption may rise with different road grade for each timestep and then its knowledge is key for a correct consumption prediction.

The driving cycles' aggressiveness resulted in having a clear correlation with both traction and auxiliaries' consumption, with the NYB driving cycle being the most aggressive and the most consuming one for both of these units.

A similar correlation was tried to be find between average deceleration and compressor consumption, and between average velocity and steering pump's one. This search was unsuccessful apart from a timid general rule, and this allows to understand that driving cycles are a complex set of numbers and is hard to find a single characteristic describing them universally.

The tool was developed with a particular attention to the radiation load participating to the HVAC consumption and for this reason the impact of its parameters was analysed. The impact of the time of the day resulted in a ~10% variation comparing the lowest total consumption at 20 with highest one at 16. The seasonal effect on the radiation load was negligible and not considering this load for the season other than summer, turned out to be an acceptable assumption. Finally, the impact of the coordinates was searched, and no particular influence was found since the worst difference experienced was ~3% on the total consumption between two distant localities, Paris and Tripoli.

The possible future development of this predictive model must persecute the reduction of approximation, introducing a precise heat pump functioning and giving the possibility to analyse the BTMS of different kind of batteries different from Lithium-Ion ones. Moreover by, changing few parts of the code, this model could run consumption analysis on different kind of alternative powertrains, like Fuel Cell Electric Bus (FCEB) and Plug-in Hybrid Electric Bus (PHEB).

Acronyms

AC	Air Conditioning
APS	Announced Pledges Scenario
BEB	Battery Electric Bus
BER	Brake Energy Recovery
BRAU	Braunschweig driving cycle
BTMS	Battery Thermal Management System
CBD	Central Business District driving cycle
CFM	Cubic Feet per Minute
COP	Coefficient of Performance
CSHV	City Suburban Heavy Vehicle driving cycle
DTM	Deep Thermal Mass
EU	European Union
FCEB	Fuel Cell Electric Bus
FD	Final Drive ratio
GHG	Greenhouse gas
GR	Gear ratio
HP	Heat Pump
HVAC	Heat and Ventilation Air Conditioning
IEA	International Energy Agency

LPM	Lumped Parameters Model
MB	Manhattan Bus driving cycle
NDC	Nationally Determined Contribution
NREL	National Renewable Energy Laboratory
NYB	New York Bus driving cycle
NYC	New York Composite driving cycle
NZE	Net Zero Emissions
OCTA	Orange County Transit Authority driving cycle
OCV	Open Circuit Voltage
PHEB	Plug-in Hybrid Electric Bus
PKM	Passengers Kilometres
PP	Polypropylene
PTC	Positive Temperature Coefficient
SOC	State of Charge
STEPS	Stated Policies Scenario
TS	Timestep
UDDS	Urban Dynamometer Driving Schedule driving cycle
VB	Vehicle Body
W	Windows
WH	Waste Heat recovery

Bibliography

[1] «4.1 – Transportation and Energy | The Geography of Transport Systems», 1 agosto 2019. https://transportgeography.org/contents/chapter4/transportation-and-energy/

[2] «World Energy Outlook 2021 – Analysis - IEA».

[3] «Reducing CO_2 emissions from heavy-duty vehicles». https://ec.europa.eu/clima/eu-action/transport-emissions/road-transport-reducing-co2-emissions-vehicles/reducing-co2-emissions-heavy-duty-vehicles_en.

[4] «Understanding WEO Scenarios – World Energy Model – Analysis - IEA». https://www.iea.org/reports/world-energy-model/understanding-weo-scenarios

[5] «Transport Energy Consumption Trends | ODYSSEE-MURE». https://www.odyssee-mure.eu/publications/efficiency-by-sector/transport/energy-consumption.html

[6] «Emission Test Cycles».

https://dieselnet.com/standards/cycles/index.php#eu-hd

[7] «NREL Drive Cycle Analysis Tool». https://www.nrel.gov/transportation/drive-cycle-tool/index.html

[8] H. Basma, C. Mansour, M. Haddad, M. Nemer, e P. Stabat, «Comprehensive energy modeling methodology for battery electric buses», *Energy*, vol. 207, pag. 118241, set. 2020, doi: 10.1016/j.energy.2020.118241.

[9] O. A. Hjelkrem, K. Y. Lervåg, S. Babri, C. Lu, e C.-J. Södersten, «A battery electric bus energy consumption model for strategic purposes: Validation of a proposed model structure with data from bus fleets in China and Norway», *Transportation Research Part D: Transport and Environment*, vol. 94, pag. 102804, 2021.

[10] D. Göhlich, T.-A. Fay, D. Jefferies, E. Lauth, A. Kunith, e X. Zhang, «Design of urban electric bus systems», *Design Science*, vol. 4, 2018.

[11] O. Czogalla e U. Jumar, «Design and control of electric bus vehicle model for estimation of energy consumption», *IFAC-PapersOnLine*, vol. 52, n. 24, pagg. 59–64, 2019.

[12] H. Basma, C. Mansour, M. Haddad, M. Nemer, e P. Stabat, «Energy consumption and battery sizing for different types of electric bus service», *Energy*, vol. 239, pag. 122454, 2022.

[13] N. Kammuang-lue e J. Boonjun, «Simulation and Comparison on Energy Consumption between Electric and Diesel Buses: Feasibility Study on Electric Rubber-Tire Bus Potential in Chiang Mai», in *2019 IEEE 10th International Conference on Mechanical and Aerospace Engineering (ICMAE)*, lug. 2019, pagg. 490–496. doi: 10.1109/ICMAE.2019.8880940.

[14] K. R. Mallon, F. Assadian, e B. Fu, «Analysis of on-board photovoltaics for a battery electric bus and their impact on battery lifespan», *Energies*, vol. 10, n. 7, pag. 943, 2017.

[15] «Novel Electric Bus Energy Consumption Model Based on Probabilistic Synthetic Speed Profile Integrated With HVAC | IEEE Journals & Magazine | IEEE Xplore». https://ieeexplore.ieee.org/abstract/document/8998578?casa_token=ofL7uBubmOQAAAAA:8YfKea95xbGknPKclWyYkx6uDNaW8Ff4qDGvfOcWWCDAonrKAKMDWWj3OjDFhD5-swvfvPg

[16] H. Basma, C. Mansour, M. Haddad, M. Nemer, e P. Stabat, «Comprehensive energy assessment of battery electric buses and diesel buses», Wroclaw, Poland, giu. 2019. https://hal.archives-ouvertes.fr/hal-02169856

[17] M. A. Fayazbakhsh e M. Bahrami, «Comprehensive modeling of vehicle air conditioning loads using heat balance method», *SAE technical paper*, vol. 2013, pag. 1507, 2013.

[18] J. P. Vale, P. G. Alves, S. F. Neves, L. Nybo, A. D. Flouris, e T. S. Mayor, «Analysis of the dynamic air conditioning loads, fuel consumption and emissions of heavy-duty trucks with different glazing and paint optical properties», *International Journal of Sustainable Transportation*, pagg. 1–14, 2021.

[19] L. Porta, «Iveco Urbanway 12 m», pag. 2.

[20] «Vascat 145kW (195HP) 1500RPM AC Vector Motor, IP23, B35, 200 Frame - AC Motors (Vector)». https://inverterdrive.com/group/Motors-AC-Vector/Square-Frame-AC-Vector-Motor-150kW-200HP-1500RPM/

[21] P. Iora e L. Tribioli, «Effect of ambient temperature on electric vehicles' energy consumption and range: Model definition and sensitivity analysis based on nissan leaf data», *World Electric Vehicle Journal*, vol. 10, n. 1, pag. 2, 2019.

[22] F. Sanvito, M. Ferraro, R. Mereu, e E. Colombo, *Improving electric vehicle consumption representation in energy system modelling: the impact of temperature in all European countries*. 2020. doi: 10.13140/RG.2.2.26325.35046.

[23] C. Andersson, *On Auxiliary Systems in Commercial Vehicles*. 2016. https://portal.research.lu.se/ws/files/5907461/716038.pdf

[24] R. A. Haddad, H. Basma, e C. Mansour, «Modeling and control of heat pump system for battery electric buses», *Proceedings of the Institution of Mechanical Engineers, Part D: Journal of Automobile Engineering*, pag. 09544070211069465, gen. 2022, doi: 10.1177/09544070211069465.

[25] S. In-Soo, L. Minyoung, K. Jedok, T. O. Sang, e W. Jong-Phil, «Design and experimental analysis of an efficient HVAC (heating, ventilation, air-conditioning) system on an electric bus with dynamic on-road wireless charging».

[26] A. Lajunen, «Energy efficiency and performance of cabin thermal management in electric vehicles», SAE Technical Paper, 2017.

[27] F. Brèque e M. Nemer, «Cabin thermal needs: Modeling and assumption analysis», in *Proceedings of the 12th International Modelica Conference, Prague, Czech Republic, May 15-17, 2017*, 2017, n. 132, pagg. 771–781.

[28] «Approfondimenti Radiazione Solare». https://architettura.unige.it/did/l2/architettura/terzo0708/fisicatecnica/capitoli/cap3_II.pdf

[29] Q. Wang, B. Jiang, B. Li, e Y. Yan, «A critical review of thermal management models and solutions of lithium-ion batteries for the development of pure electric vehicles», *Renewable and Sustainable Energy Reviews*, vol. 64, pagg. 106–128, 2016.

[30] C. Forgez, D. V. Do, G. Friedrich, M. Morcrette, e C. Delacourt, «Thermal modeling of a cylindrical LiFePO4/graphite lithium-ion battery», *Journal of Power Sources*, vol. 195, n. 9, pagg. 2961–2968, 2010.

[31] X. Lin *et al.*, «Online parameterization of lumped thermal dynamics in cylindrical lithium ion batteries for core temperature estimation and health monitoring», *IEEE Transactions on Control Systems Technology*, vol. 21, n. 5, pagg. 1745–1755, 2012.

List of Figures

Figure 1: CO2 emissions trend by mode and final consumption prevision by fuel. [2] 5

Figure 2: Share of alternative fuels and electric vehicles in the subsectors. [2] 5

Figure 3: Share of investments in transports in 2016-2020 period and future scenarios. [2] 7

Figure 4: Cost-competitiveness in the road transport sector. [2] 8

Figure 5: Transport sector overall energy consumption trend in the EU. [5] 9

Figure 6: : Transport sector energy consumption by mode in the EU. [5] 10

Figure 7: Passengers' transport consumption growth composition. [5] 10

Figure 8: Intensity of consumption for the main transports. [5] 11

Figure 9: BRAU driving cycle. [7] 14

Figure 10: UDDS driving cycle. [7] 14

Figure 11: E-bus's units schematization. [8] 23

Figure 12: Reference public transport bus. [19] 24

Figure 13: Electric Power-Speed trend for hydraulic steering pump. [23] 34

Figure 14: COP values for different external temperatures [26] 39

Figure 15: Battery cell's simplified thermal equivalent circuit. [30] 48

Figure 16: HVAC average power validation for Manhattan Bus with different external temperatures and 30 passengers. 53

Figure 17: BTMS average power validation for Manhattan Bus with different external temperatures and 30 passengers. 54

Figure 18: Total consumption validation for Manhattan Bus and 30 passengers: MB1 is performed at -10 °C while MB2 at 40 °C. 55

Figure 19: Total consumption error percentage for Manhattan Bus and 30 passengers: MB1 is performed at -10 °C while MB2 at 40 °C. 56

Figure 20: Total consumption validation for different driving cycles and different external conditions. 58

Figure 21: Percentage error in total consumption validation for different driving cycles and different external conditions. 59

Figure 22: Infeasibility percentage in total consumption validation for different driving cycles and different external conditions 60

Figure 23: HVAC average power request for Manhattan Bus with different external temperatures and 30 passengers. 62

Figure 24: BTMS average power request for Manhattan Bus with different external temperatures and 30 passengers. 63

Figure 25: Total consumption for Manhattan Bus with different external temperatures and 30 passengers. 65

Figure 26: Units' consumption for Manhattan Bus with different passengers' occupancy at -10 °C. 66

Figure 27: Units' consumption for Manhattan Bus with different passengers' occupancy at 20 °C. 67

Figure 28: Units' consumption for Manhattan Bus with different passengers' occupancy at 40 °C. 68

Figure 29: Thermal units' average power request for Manhattan Bus and 30 passengers with different comfort temperatures at 40 °C. 70

Figure 30: Total consumption for Manhattan Bus and 30 passengers with different comfort temperatures at 40 °C. 70

Figure 31: Thermal units' average power request for Manhattan Bus and 30 passengers with different comfort temperatures at -10 °C. 71

Figure 32: Total consumption for Manhattan Bus and 30 passengers with different comfort temperatures at -10 °C. 72

Figure 33: Propulsion and BER for Manhattan Bus and 30 passengers with different road grade at 20 °C. 73

Figure 34: Compressor consumption for Manhattan Bus and 30 passengers with different road grade at 20 °C. 74

Figure 35: Total consumption for Manhattan Bus and 30 passengers with different road grade at 20 °C. 75

Figure 36: Propulsion and BER for different driving cycles and 30 passengers at 20 °C. 76

Figure 37: Auxiliaries consumption for different driving cycles and 30 passengers at 20 °C. 77

Figure 38: Auxiliaries consumption composition for different driving cycles and 30 passengers at 20 °C. 79

Figure 39: Compressor consumption for different average deceleration and 30 passengers at 20 °C. 80

Figure 40: Steering pump consumption for different average speed and 30 passengers at 20 °C. 81

Figure 41: Radiation load for Manhattan Bus and 30 passengers at 30 °C over different time of the day. 82

Figure 42: HVAC average power for Manhattan Bus and 30 passengers at 30 °C over different time of the day. 83

Figure 43: Total consumption for Manhattan Bus and 30 passengers at 30 °C over different time of the day. 84

Figure 44: Radiation load for Manhattan Bus and 30 passengers over different days. 85

Figure 45: HVAC average for Manhattan Bus and 30 passengers over different days. 86

Figure 46: Total consumption for Manhattan Bus and 30 passengers over different days. 86

Figure 47: Radiation load for Manhattan Bus and 30 passengers over different locations. 88

Figure 48: HVAC average power for Manhattan Bus and 30 passengers over different locations. 88

Figure 49: Total consumption for Manhattan Bus and 30 passengers over different locations. 89

List of Tables

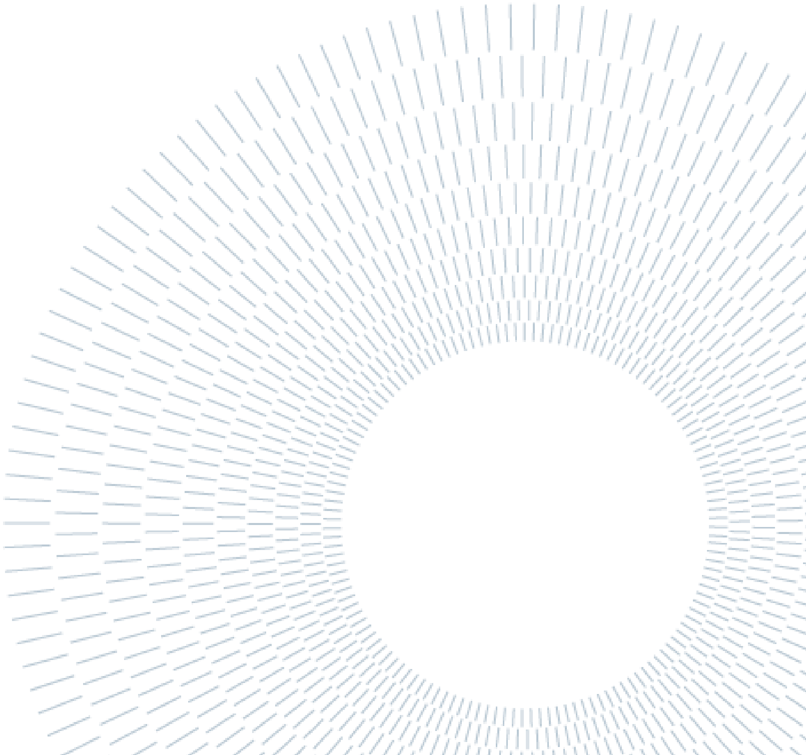Table 1: Longitudinal dynamics parameters. 16
Table 2: Powertrain specifications. 18
Table 3: Surfaces composition. 24
Table 4: Materials' properties. [17] 25
Table 5: Vehicle overall weight definition's parameters. [8], [14] 25
Table 6: Electric machine' efficiencies. 28
Table 7: Longitudinal dynamics' parameters. [8] 31
Table 8: Electric auxiliaries' parameters. [8] 32
Table 9: Hydraulic suspensions' parameters. [8], [23] 33
Table 10: Steering pump power levels and speed windows. [23], [24] 34
Table 11: Pneumatic brakes' parameters. [8], [23] 36
Table 12: Cabin thermal mass' estimation parameters [7]. 38
Table 13: COP heating. 39
Table 14: COP cooling. 40
Table 15: Ventilation load parameters. 42
Table 16: Surfaces' orientation. 43
Table 17: BTMS parameters 50
Table 18: Driving cycles specifics. [7] 53
Table 19: Validation run parameters 57
Table 20: Baseline radiation parameters. 61
Table 21: Typical days. 85
Table 22: Cities' coordinates. 87